



HAL
open science

Novel Approaches in Functional Electrical Stimulation for Rehabilitation: Development, Analysis, and Optimization

Ehsan Jafari

► **To cite this version:**

Ehsan Jafari. Novel Approaches in Functional Electrical Stimulation for Rehabilitation : Development, Analysis, and Optimization. Physics [physics]. Ecole normale supérieure de lyon - ENS LYON, 2024. English. NNT : 2024ENSL0008 . tel-04680555

HAL Id: tel-04680555

<https://theses.hal.science/tel-04680555>

Submitted on 28 Aug 2024

HAL is a multi-disciplinary open access archive for the deposit and dissemination of scientific research documents, whether they are published or not. The documents may come from teaching and research institutions in France or abroad, or from public or private research centers.

L'archive ouverte pluridisciplinaire **HAL**, est destinée au dépôt et à la diffusion de documents scientifiques de niveau recherche, publiés ou non, émanant des établissements d'enseignement et de recherche français ou étrangers, des laboratoires publics ou privés.



THESE

en vue de l'obtention du grade de Docteur, délivré par
l'ECOLE NORMALE SUPERIEURE DE LYON

Ecole Doctorale N° 52
Physique et Astrophysique de Lyon (PHAST)

Discipline : Physique

Soutenue publiquement le 10/06/2024, par :

Ehsan JAFARI

Novel Approaches in Functional Electrical Stimulation for Rehabilitation: Development, Analysis, and Optimization

Nouvelles Approches de la Stimulation Électrique Fonctionnelle pour la Rééducation : Développement, Analyse et Optimisation

Devant le jury composé de :

AMBROSINI Emilia	Prof.	Politecnico di Milano	Rapporteur
MASANI Kei	Prof.	University of Toronto	Rapporteur
HAUTIER Christophe	Prof.	Université Claude Bernard - Lyon 1	Examinateur
METAHNI Mohamed Amine	IR	ENS de Lyon	Examinateur
PEDROCCHI Alessandra	Prof.	Politecnico di Milano	Examinatrice
BERGERON Vance	DR	ENS de Lyon	Directeur de thèse

Acknowledgments

From the bottom of my heart, I extend my deepest gratitude to my supervisors at Kurage and Physics Laboratory at École Normale Supérieure de Lyon: Dr. Lana Popović-Maneski, Dr. Amine Metahni, and Dr. Vance Bergeron. Beyond the roles of academic supervisors, they have been my mentors, my pillars, and, indeed, my family away from home. They have skillfully balanced granting me intellectual autonomy with providing crucial direction, offering not just academic advice but also personal encouragement that has significantly shaped my career's trajectory. As I look towards the horizon of my future career, I'm filled with a profound sense of readiness, a gift from their unwavering belief in me.

A wave of warmth and appreciation goes out to my Kurage family. The past three years have been a transformative journey, touching the soul of research and development in neurorehabilitation, all thanks to their encouragement and support. Special thanks to Mr. Rudi Gombauld, Kurage's indefatigable CEO, whose leadership through storms and calm has been nothing short of inspirational.

To my dear friend and colleague, Dr. Petar Kajganić, thank you for the gift of your friendship. Your kindness, sincerity, and unwavering professional excellence have not only enriched our work together but have also brought joy and laughter to my days.

My journey at Kurage was brightened by the camaraderie and support of my friends and colleagues—Amina, Barbara, Baptiste, Bruno, Guillaume, Hassen, Hugo, Louisiane, Louise, Maël, Marwan, Maxime, Nicolas, Romaric, Solene, and Youssef. Our lunchtime chats, filled with laughter and shared dreams, have been a source of joy and strength.

I owe immense gratitude to Minoo and Adam for their exceptional illustrations that sig-

nificantly elevated the quality of my work. A heartfelt thank you also goes to the dedicated staff at the ANTS association—Mathilde, Maëlle, and Martin. Additionally, my deepest appreciation to the subjects who participated in our studies, offering their time and trust, with a special mention of Julien’s invaluable contribution.

Outside the lab, I have friends “better than the running brook,” as Sohrab beautifully penned. Ali, Elham, Saadi, and Shabnam, thank you for helping us settle down in Lyon and for sharing countless joyful moments far from our beloved homeland, Iran.

To Maryam, my rock, my love—your boundless love, attention, and sacrifice have been the light guiding me through the challenges of this Ph.D. journey. Your support is the wind beneath my wings, and for that, I am eternally grateful.

And to my beloved family—my parents, Farideh and Mohsen, and my sister, Sarina—your endless ocean of love, support, and belief in me has been my anchor. Your sacrifices have paved the path I walk on today.

Contents

Acknowledgments	i
Abstract	vii
Résumé	ix
List of Tables	xi
List of Figures	xiii
List of Abbreviations	xvii
Chapter 1 Introduction	1
1.1 Nervous System	2
1.1.1 Neuron	2
1.1.2 Neuronal Communication	4
1.1.2.1 Intraneuronal Communication	5
1.1.2.2 Interneuronal Communication	7
1.2 Skeletal Muscle	8
1.2.1 Structure	9
1.2.2 Mechanism of Excitation and Contraction	10
1.3 Volitional Muscle Contraction: From Motor Cortex to Skeletal Muscle . . .	11
1.4 Motor Neuron Lesion	15

1.4.1	Upper Motor Neuron Lesion	15
1.4.2	Lower Motor Neuron Lesion	16
1.4.3	Spinal Cord Injury	16
1.5	Electrical Stimulation	20
1.5.1	Physiological Basis	20
1.5.2	Applications	21
1.5.3	Stimulation Parameters	23
1.5.4	Lower-limb FES Cycling	26
1.5.5	Limitations of FES	27
1.6	Thesis Objectives	30
1.7	Thesis Outline	31
 Chapter 2 Textile versus Hydrogel Electrodes: Comfort, Consistency, and Efficiency		 34
2.1	Introduction	35
2.2	Methods	40
2.2.1	Participants	40
2.2.2	Instrumentation	40
2.2.3	Experimental Protocol	43
	2.2.3.1 Comfort, Consistency, and Efficiency Tests	43
	2.2.3.2 Electrical Impedance Spectroscopy Test	45
2.2.4	Data Analysis and Statistics	46
2.3	Results	48
2.3.1	Comfort, Consistency, and Efficiency Tests	48
	2.3.1.1 Comfort	48
	2.3.1.2 Temporal Consistency	50
	2.3.1.3 Efficiency	51
2.3.2	Electrical Impedance Spectroscopy Test	53
2.4	Discussion	54

2.5	Conclusion	58
Chapter 3	Efficacy of High versus Moderate-Intensity SDSS in Subjects with Spinal Cord Injury – an Isometric Study	60
3.1	Introduction	61
3.2	Methods	63
3.2.1	Participants	63
3.2.2	Instrumentation	64
3.2.3	Electrode Configuration	65
3.2.4	Experimental Protocol	67
3.2.5	Data Analysis and Statistics	69
3.3	Results	70
3.3.1	Experiment 1	70
3.3.2	Experiment 2	75
3.4	Discussion	80
3.5	Conclusion	83
Chapter 4	SDSS Applied to the Paralyzed Quadriceps Muscles while Performing Motor-assisted FES Cycling – a Case Series	84
4.1	Introduction	85
4.2	Methods	86
4.2.1	Participants	86
4.2.2	Instrumentation	87
4.2.3	Electrode Configuration	89
4.2.4	Stimulation Parameters	91
4.2.5	Experimental Protocol	92
4.2.6	Data Collection and Analysis	94
4.3	Results	95
4.3.1	Overall Outcomes	95

4.3.2	Individual Cases	95
4.3.2.1	Case 1	95
4.3.2.2	Case 2	97
4.3.2.3	Case 3	99
4.3.2.4	Case 4	101
4.4	Discussion	103
4.5	Conclusion	106
Chapter 5 Optimization of Seating Position and Stimulation Pattern in Functional Electrical Stimulation Cycling: a Simulation Study		107
5.1	Introduction	108
5.2	Methods	110
5.2.1	Model of Skeletal Muscle	110
5.2.2	Model of Stationary Cycle	111
5.2.3	Optimization	114
5.2.4	Constraints	115
5.3	Results	116
5.4	Discussion and Conclusion	120
Conclusion and Future Prospects		123
Bibliography		128

Abstract

This thesis aims to overcome the limitations of functional electrical stimulation (FES) through a multifaceted novel approach that concentrates on developing transcutaneous electrodes, stimulation strategies, and biomechanical optimization perspectives. The first study investigates the effectiveness of garment-embedded textile electrodes, used with a moisturizing lotion, against conventional self-adhesive hydrogel electrodes. The evaluation encompasses aspects such as stimulation comfort, temporal consistency, efficiency, and electrical impedance behavior under isometric conditions. Participants in the study underwent tests with both electrode types, evaluating parameters like motor threshold intensity, burning sensation intensity, and maximum tolerable intensity. The results indicate that textile electrodes, when supplemented with lotion, perform comparably to hydrogel electrodes in terms of comfort, consistency, and efficiency. The next study investigates the impact of spatially distributed sequential stimulation (SDSS) at high and moderate intensities on reducing fatigue in individuals with spinal cord injury. The study, focusing on the quadriceps muscle group, found that moderate-intensity SDSS is significantly more effective than high-intensity SDSS. Additionally, a case study was conducted to assess the differences in power generation and fatigue levels between FES cycling using SDSS and a single electrode setup. This involved stimulating the paralyzed quadriceps muscles of four participants over multiple days during motor-assisted FES cycling. The results indicated that SDSS not only generated more power compared to the single electrode setup but did so without significantly impacting fatigue levels. The last study focuses on the optimization of the cycling biomechanical properties and stimulation pattern to achieve maximum

output power with minimum applied stimulation. In this work, an easy-to-use and precise muscle model in conjunction with Jacobian-based torque transfer functions was adopted to determine the optimal seating position, trunk angle, crank arm length, and stimulation intervals. Furthermore, the impact of muscle force-velocity factor in finding the optimal seating position and stimulation intervals was investigated. The simulation models showed the trivial effect of the force-velocity factor on the resulting optimal seating position of six healthy simulated subjects. We believe that the contributions of this thesis will increase the efficacy of FES as a rehabilitation technique.

Keywords: Functional electrical stimulation (FES), Cycling, Fatigue, Textile electrode, Spatially distributed sequential stimulation (SDSS), Optimization

Résumé

Cette thèse vise à surmonter les limites de la stimulation électrique fonctionnelle (SEF) grâce à une approche novatrice et multimodale, qui explore aussi bien le développement d'électrodes transcutanées, que les stratégies de stimulation, ainsi que les perspectives d'optimisation biomécanique. Une première étude compare l'efficacité des électrodes textiles intégrées dans les vêtements, utilisées avec une lotion hydratante, par rapport aux électrodes conventionnelles à hydrogel auto-adhésives. L'évaluation porte sur des aspects tels que le confort de la stimulation, la cohérence temporelle, l'efficacité, et le comportement de l'impédance électrique dans des conditions isométriques. Les participants à l'étude ont effectué des tests avec les deux types d'électrodes, nous permettant d'évaluer des paramètres tels que les intensités minimales générant une contraction musculaire ou une sensation de brûlure, et l'intensité maximale tolérable. Les résultats indiquent que les électrodes textiles, lorsqu'elles sont complétées par une lotion, sont comparables aux électrodes à hydrogel en termes de confort, de consistance et d'efficacité. Une seconde étude examine l'impact de la stimulation séquentielle distribuée spatialement (SSDS) à intensité moyenne ou haute, sur la réduction de la fatigue chez les personnes souffrant d'une lésion de la moelle épinière. L'étude révèle que la SSDS est significativement plus efficace à moyenne intensité. En outre, une étude de cas a été réalisée pour évaluer les différences de puissance et fatigue produites lors d'un exercice de cyclisme électrostimulé utilisant la SSDS. Il s'agissait de stimuler les quadriceps de quatre participants paraplégiques moteurs complets. L'étude a montré que la SSDS génère non seulement plus de puissance que la configuration à une seule électrode, mais également sans avoir d'impact significatif

sur le niveau de fatigue. La dernière étude se concentre sur l'optimisation des propriétés biomécaniques du cyclisme et de la séquence de stimulation afin d'obtenir une puissance de sortie maximale avec une stimulation appliquée minimale. Un modèle musculaire précis et facile à utiliser, associé à des fonctions de transfert de couple basées sur le Jacobien, a été adopté pour déterminer la position assise optimale, l'angle du tronc, la longueur du bras de manivelle et les séquences de stimulation. En outre, l'impact de la fonction force-vitesse du muscle sur la détermination de la position assise optimale et des séquences de stimulation a été étudié. Les modèles de simulation ont montré un effet insignifiant de la fonction force-vitesse sur la position assise optimale de six sujets sains simulés. Nous pensons que les contributions de cette thèse augmenteront l'efficacité de la SEF en tant que technique de rééducation fonctionnelle.

Mots-clés: Stimulation électrique fonctionnelle (SEF), Cyclisme, Fatigue, Électrode textile, Stimulation séquentielle distribuée spatialement (SSDS), Optimisation

List of Tables

1.1	ASIA Impairment scale.	19
2.1	Demographic characteristics of the participants.	41
2.2	Coefficients of linear regression model of Average Torque [%MVIC] = a + B*Intensity [mA] for each electrode.	53
2.3	Analysis of variance of linear regression models of Average Torque [%MVIC] = Intensity [mA] * Electrode Type.	53
3.1	Demographic characteristics of the participants.	64
3.2	The summary of the results from each subject from Experiment 1 con- ducted on the quadriceps muscle group.	75
3.3	The summary of the results from each subject from Experiment 1 con- ducted on the quadriceps muscle group.	80
4.1	The demographic and clinical characteristics of participants with the spinal cord injury.	87
4.2	The demographic and clinical characteristics of the subject with multiple sclerosis.	87
4.3	Summary of the results for power produced and the fatigue index of each experimental session along with the overall mean power produced by each subject during both experimental sessions with SDSS and SES stimula- tions.	96

4.4	Stimulation intensity and stimulation patterns measured for subject P1 for each experimental session and the results of each stimulation phase presented in chronological order.	97
4.5	Stimulation intensity and stimulation patterns measured for subject P2 for each experimental session and the results of each stimulation phase presented in chronological order.	99
4.6	Stimulation intensity and stimulation patterns measured for subject P3 for each experimental session and the results of each stimulation phase presented in chronological order.	100
4.7	Stimulation intensity and stimulation patterns measured for subject P4 for each experimental session and the results of each stimulation phase presented in chronological order.	102
5.1	Summary of the characteristics of the subjects.	116
5.2	The Muscle model parameters of averaged subjects [139].	117
5.3	Summary of optimized variables using Method 1 and Method 2 at 35 rpm and 50 rpm for all subjects.	118
5.4	Summary of the difference in total generated torque over a crank cycle (%) between optimized variables from Method 1 and Method 2 at 35 rpm and 50 rpm for all subjects.	118
5.5	The difference between the normalized muscle optimization functions of both methods (δ_m^1 and δ_m^2) for the optimal variables derived from Method 2 at 35 rpm and 50 rpm, evaluated across three muscle groups and all subjects.	120
5.6	Stimulation intervals measured from normalized muscle optimization functions (δ_m^1 and δ_m^2) greater than threshold value of 0.5 for the optimal variables derived from Method 2 at 35 rpm, and 50 rpm.	121

List of Figures

1.1	Simplified structure of a motor neuron	4
1.2	Voltage-time diagram of an action potential	7
1.3	Illustration of a chemical synapse.	9
1.4	Illustration of the structure of the skeletal muscle.	10
1.5	Illustration of cross-bridge formation.	12
1.6	Simplified motor pathway from motor cortex to skeletal muscle.	13
1.7	Illustration of spinal cord segments and paralysis level.	17
1.8	Therapeutic applications of electrical stimulation.	22
1.9	Common waveforms utilized in FES	25
1.10	Parameters of biphasic electric pulse utilized in FES	26
1.11	Strength-duration curve of sensory, motor, and pain fibers.	29
2.1	Stretchable pants embedded with textile electrodes.	42
2.2	Illustration of the experimental setup for the isometric knee extension task using pants embedded with textile electrodes.	43
2.3	Torque as a percentage of maximum voluntary isometric contraction (%MVIC) across multiple repetitions at different time intervals from the commencement of the test for one participant (P1)	48
2.4	Box-and-whisker plots of (a) average burning sensation intensity (BSI) for each participant (n = 10) and (b) maximum tolerated intensity (I_{MAX}) (n = 9) using both hydrogel electrodes and textile electrodes with lotion.	49

2.5	Linear regression models of burning sensation intensity (BSI) points (n = 5) for each participant (n = 10) across multiple repetitions at different time intervals from the commencement of the test utilizing (a) hydrogel electrodes and (b) textile electrodes with lotion.	50
2.6	Box-and-whiskers plots of the slope of BSIs regarding electrode types. . . .	51
2.7	a. Box-and-whisker plots of average minimum intensity required to evoke torque (I_{min}) for each participant (n = 10) using hydrogel electrodes (blue) and textile electrodes with lotion (red). b. Linear regression models of Average Torque [%MVIC] = a + B*Intensity [mA] for hydrogel electrodes (blue) and textile electrodes with lotion (red) extracted from the final trial (after 40 minutes). The number of data points for each electrode type is equal (n = 84).	52
2.8	Average absolute impedance values (k Ω) for tests conducted on one participant with hydrogel electrodes (blue), textile electrodes without lotion (green), and textile electrodes with lotion (orange) at various frequencies (20, 40, 60, 80, 100, and 1000 Hz).	54
3.1	Illustration of the experimental setup for performing isometric muscle contractions to assess muscle fatigue using SDSS and SES electrode configurations.	65
3.2	Illustration of the experimental setup for performing isometric muscle contractions to assess muscle fatigue using SDSS and SES electrode configurations.	67
3.3	Measurements conducted on subject P3 of the force produced by the quadriceps muscle group (Experiment 1) stimulated with a) moderate electrical stimulation intensity (80 mA) and b) high electrical stimulation intensity (130 mA).	71

3.4	Summary of the results from Experiment 1 of %TTF _{Difference} values for the entire study group under moderate (colored blue) and high (colored red) electrical stimulation intensity conditions.	72
3.5	Summary of the results from Experiment 1 of %MPF _{Difference} values for the entire study group under moderate (colored blue) and high (colored red) electrical stimulation intensity conditions.	73
3.6	Summary of the results from Experiment 1 of %APF _{Difference} values for the entire study group under moderate (colored blue) and high (colored red) electrical stimulation intensity conditions.	74
3.7	Measurements conducted on subject P5 of the force produced by the vastus lateralis muscle stimulated with a) moderate electrical stimulation intensity (60 mA) and b) high electrical stimulation intensity (100 mA).	76
3.8	Median %TTF _{Difference} values for the entire study group for moderate and high electrical stimulation tests conducted on the vastus lateralis muscles (Experiment 2) are provided.	77
3.9	Summary of the results from Experiment 2 of %MPF _{Difference} values for the entire study group under moderate (colored blue) and high (colored red) electrical stimulation intensity conditions.	78
3.10	Summary of the results from Experiment 2 of %APF _{Difference} values for the entire study group under moderate (colored blue) and high (colored red) electrical stimulation intensity conditions.	79
4.1	Illustration of the experimental setup for the assessment of the power output and fatigue-reducing properties of SDSS versus SES applied to the paralyzed quadriceps muscles of subjects performing motor-assisted FES cycling.	88
4.2	An illustration of the electrode configuration used for both SDSS and SES.	90
4.3	An illustration of the experimental protocol.	94

4.4	Power produced by the subject’s P1 left leg (blue) and right leg (red) during each stimulation phase of (a) the first experimental session and (b) the second experimental session.	97
4.5	Power produced by the subject’s P2 left leg (blue) and right leg (red) during each stimulation phase of (a) the first experimental session and (b) the second experimental session.	98
4.6	Power produced by the subject’s P3 left leg (blue) and right leg (red) during each stimulation phase of (a) the first experimental session and (b) the second experimental session.	100
4.7	Power produced by the subject’s P4 left leg (blue) and right leg (red) during each stimulation phase of (a) the first experimental session and (b) the second experimental session.	102
5.1	Skeletal model of stationary cycling.	112
5.2	Normalized muscle optimization function (δ_m) of gluteal, quadriceps, and hamstrings over a whole crank cycle using optimal seating position resulted from Method 1 (blue solid line) and Method 2 (red dashed line) for (a) S1 and (b) S5.	119

List of Abbreviations

Abbreviation	Description
AC	Alternating Current
ADP	Adenosine Diphosphate
AFU	Anti-Fatigue Unit
ACh	Acetylcholine
APF	Average Produced Force until Fatigue
ASIA	American Spinal Injury Association
ATP	Adenosine Triphosphate
BSI	Burning Sensation Intensity
CNS	Central Nervous System
cm	Centimeter
ECG	Electrocardiography
EDSS	Expanded Disability Status Scale
EEG	Electroencephalography
EMD	Electromechanical Delay
EMG	Electromyography
ES	Electrical Stimulation
FES	Functional Electrical Stimulation
FI	Fatigue Index
FTI	Force-Time Integral
GABA	γ -Aminobutyric Acid

Abbreviation	Description
GTO	Golgi Tendon Organ
HI	High Intensity
Hz	Hertz
ICU	Intensive Care Unit
IQR	Interquartile Range
L	Power Produced in the Last 30 seconds
LMN	Lower Motor Neuron
LMNL	Lower Motor Neuron Lesion
MFP	Muscle Force Profile
MHz	Megahertz
MI	Moderate Intensity
MS	Multiple Sclerosis
MU	Motor Unit
MVIC	Maximum Voluntary Isometric Contraction
N	Newton
N.m	Newton-meter
NMES	Neuromuscular Electrical Stimulation
NMJ	Neuromuscular Junction
P	Power Produced Only by the Electrical Stimulation
PA	Pulse Amplitude
Pi	Inorganic Phosphate
PNS	Peripheral Nervous System
PW	Pulse Width
Q1	First Quartile
Q2	Second Quartile (Median)
Q3	Third Quartile
QF	Quadriceps Femoris

Abbreviation	Description
R	Resistance
RF	Rectus Femoris
RMS	Root Mean Square
SDSS	Spatially Distributed Sequential Stimulation
SCI	Spinal Cord Injury
SES	Single Electrode Stimulation
SR	Sarcoplasmic Reticulum
TA	Tibialis Anterior
TENS	Transcutaneous Electrical Nerve Stimulation
TTF	Time to Fatigue
UMN	Upper Motor Neuron
UMNL	Upper Motor Neuron Lesion
VL	Vastus Lateralis
W	Watt
X	Reactance
kg	Kilogram
mA	Milliampere
mV	Millivolt
ms	Milliseconds
nAChRs	Nicotinic Acetylcholine Receptors
rpm	Revolutions per Minute
μ s	microseconds
I_{MAX}	Maximum Tolerable Intensity
I_{min}	Minimum Intensity Required to Evoke Torque
P_F	Power Produced in the First 30 seconds
P_L	Power Produced in the Last 30 seconds
P_m	Mean Power

Chapter 1

Introduction

Abstract

This chapter aims to establish the neurophysiological foundation for the subsequent sections of the thesis and set the stage for addressing the challenges at hand. It commences with the human nervous system and its complex communication mechanisms. Subsequently, it examines the structure of skeletal muscles before delving into the fundamental, yet pivotal inquiry of how voluntary muscle contraction occurs. The discussion then turns to various types of neurological lesions that impede voluntary muscle contraction, categorizing them systematically. Following this, the chapter elaborates on the electrical stimulation method, exploring its extensive applications. It places particular emphasis on functional electrical stimulation (FES) as a rehabilitation technique for individuals with neurological lesions, addressing how they can benefit based on their specific lesion category. Lower-limbs FES cycling will be described particularly to provide the necessary details required for the subsequent chapters. The benefits and limitations of FES are thoroughly examined. Finally, the abstract outlines the goal of this thesis regarding the current limitations of FES and how it aims to address them.

1.1 Nervous System

The nervous system serves as the controlling and coordinating system of the human body, continuously monitoring, processing, and responding to both internal and external stimuli. This intricate network oversees a wide range of physiological functions, ranging from basic reflexes to higher-order cognitive functions, such as memory and thinking.

The nervous system is organized into two main subdivisions: the central nervous system (CNS) and the peripheral nervous system (PNS). The CNS, comprising the brain and spinal cord, acts as the central processing unit, receiving sensory input from the PNS, processing it, and generating appropriate responses based on past experiences and current conditions. The PNS, comprising nerves that lie outside the CNS, including cranial and spinal nerves, acts as a communication relay. It transmits sensory information to the CNS and conveys motor commands from the CNS to muscles and glands, controlling both voluntary and involuntary actions [1], [2].

1.1.1 Neuron

The human nervous system comprises two main cell types: neurons and glial cells. Neurons are the fundamental units of neural communication, tasked with generating and transmitting electrical impulses, the essential currency of nerve signaling. Glial cells provide support, nutrition, and insulation for neurons, and are essential for maintaining the stability and integrity of the nervous system.

Neurons can be classified into three functional types based on their role in the nervous system: sensory (or afferent), motor (or efferent), and interneurons. Sensory neurons are specialized for detecting a wide range of stimuli from both external and internal environments (e.g., temperature, touch, and pain), converting them into electrical signals, and transmitting them to the CNS. They are the first step in the process of sensory perception.

Motor neurons, also known as motoneurons, are specialized nerve cells that constitute the efferent arm of the nervous system. These neurons are responsible for transmitting

signals from the brain and spinal cord to effector organs, primarily muscles, and glands. Motor neurons play a fundamental role in the execution of voluntary and involuntary motor functions by translating neural signals into precise and coordinated muscular contractions. The activation of motor neurons is essential for the regulation of skeletal muscle activity involved in purposeful movements, posture maintenance, as well as the orchestration of autonomic functions (e.g., breathing) vital for various physiological processes.

Interneurons, also known as associative or internuncial neurons, are specialized nerve cells within the CNS that serve as intermediaries in neural pathways. They function to relay and integrate signals between sensory neurons, motor neurons, or other interneurons (e.g., inhibitory interneurons in the spinal cord), facilitating the processing and coordination of information within the CNS.

A typical motor neuron exhibits four distinct structural regions, each playing a crucial role in signal generation and communication (Figure 1.1):

1. **Soma (Cell body):** The metabolic powerhouse of the neuron, the cell body houses the nucleus, the repository of genetic information, and the endoplasmic reticulum, a labyrinthine network that orchestrates protein synthesis. It serves as the command center, integrating incoming signals and initiating action potentials, the electrical impulses that convey information throughout the neuron.
2. **Dendrites:** Branching like the outstretched branches of a tree, dendrites serve as the neuron's receptive antennae, absorbing incoming signals from other neurons. These signals, in the form of electrical impulses or chemical neurotransmitters, converge on the cell body, preparing the neuron for action. The branching network of dendrites allows neurons to receive inputs from a vast array of other neurons, enabling them to integrate information from multiple sources.
3. **Axon:** A slender and elongated extension that serves as the neuron's communication highway, transmitting signals to other cells, whether neurons or muscle fibers. Emerging from the cell body at a region known as the axon hillock, it extends over

considerable distances before branching into smaller terminal branches. This intricate structure allows for the efficient transmission of signals across the nervous system.

4. Presynaptic terminals: The final outposts of the axon, presynaptic terminals are specialized to release neurotransmitters, the chemical messengers that bridge the gap between two neurons called synapses. These neurotransmitters, like chemical bullets, carry information to the dendrites of neighboring neurons, inhibiting, or initiating a chain reaction of electrical impulses that propagates throughout the nervous system [3].

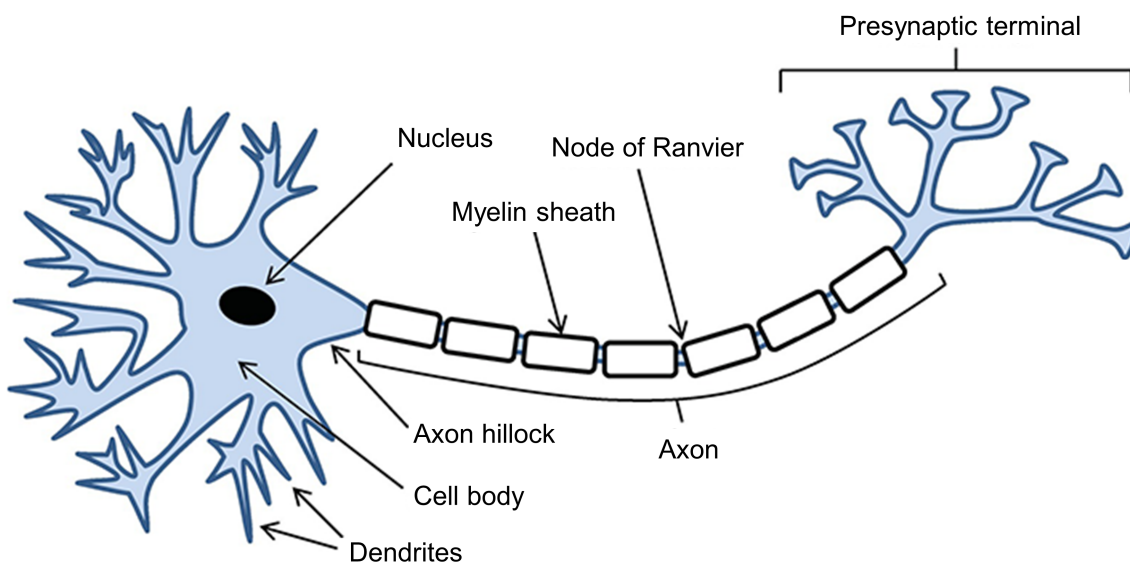


Figure 1.1: Simplified structure of a motor neuron (Adapted from [4]).

1.1.2 Neuronal Communication

The remarkable capability of neurons to communicate effectively is grounded in two fundamental characteristics: their pronounced morphological and functional asymmetry, and their dual electrical and chemical excitability. Morphological and functional asymmetry refers to the distinct structural design and specialized roles of different parts of a neuron,

such as dendrites for receiving signals and axons for transmitting them. The dual excitability of neurons encompasses their ability to propagate electrical signals in the form of action potentials within the neuron and to use chemical signals through neurotransmitters for communication between neurons. Action potentials are critical for intraneuronal signal transmission, while neurotransmitters facilitate interneuronal communication. Together, these mechanisms enable rapid and precise information relay within the nervous system [3].

1.1.2.1 Intraneuronal Communication

Action potential, an electrical charge that travels unidirectionally along the axon, is remarkable for its rapidity (occurs in milliseconds (ms)), and dichotomous nature (it either occurs fully or not at all). This all-or-none behavior consists of the following steps (Figure 1.2):

1. **Resting Membrane Potential:** In a non-excited or resting state, a cell maintains a stable membrane potential, called the resting membrane potential. For most neurons, this is typically around -70 millivolt (mV), meaning the inside of the cell is negatively charged relative to the outside. Stimuli received by a neuron's dendrites momentarily alter its membrane potential. When this potential reaches the threshold level of around -55 mV, it initiates an action potential. If the stimuli are below this threshold level, known as subthreshold stimuli, they fail to provoke an action potential. In such cases, the neuron eventually reverts to its resting potential.
2. **Depolarization:** At the threshold of around -55 mV, voltage-gated sodium channels open, allowing sodium ions (Na^+) to rush into the cell. This influx of positively charged Na^+ creates a rapid depolarization, causing the membrane potential to swing from approximately -55 mV to around +35 mV. This transient positivity, known as the overshoot, is the hallmark of the action potential.
3. **Repolarization:** The repolarization phase is initiated by the closing of voltage-gated sodium channels and the opening of voltage-gated potassium channels. As sodium channels close, the Na^+ influx subsides, and the membrane potential begins to move

back toward its resting state. Potassium channels, in contrast, remain open, allowing potassium ions (K^+) to exit the cell. This outward flow of K^+ further reverses the depolarization and eventually restores the membrane potential to its resting level of approximately -70 mV.

4. **Hyperpolarization:** Immediately after repolarization, the membrane potential briefly dips below the resting potential, reaching a hyperpolarized state. This hyperpolarization is caused by the continued outflow of K^+ through voltage-gated potassium channels. The hyperpolarized state serves to further stabilize the membrane potential and ensure that the neuron is refractory to further stimulation.
5. **Restoration of Resting Membrane Potential:** While the opening and closing of voltage-gated sodium and potassium channels play a crucial role in the depolarization, repolarization, and hyperpolarization phases of the action potential, it is the sodium-potassium pump that ultimately restores the neuron's resting membrane potential. This specialized membrane protein actively transports Na^+ out of the cell and K^+ into the cell, effectively reversing the ion imbalance caused by the action potential.

The speed of propagation depends on the axon's thickness and myelination. Thicker axons conduct action potentials faster due to their increased surface area, allowing for more efficient sodium channel activation. Myelination, the wrapping of the axon in a fatty sheath called myelin, further enhances conduction speed. Myelin acts as an insulator, preventing the loss of ions across the axon membrane. Saltatory conduction, a unique feature of myelinated axons, occurs when the action potential jumps from one myelinated segment to the next, called the node of Ranvier. This mechanism significantly increases the conduction speed of action potentials [3], [5], [6].

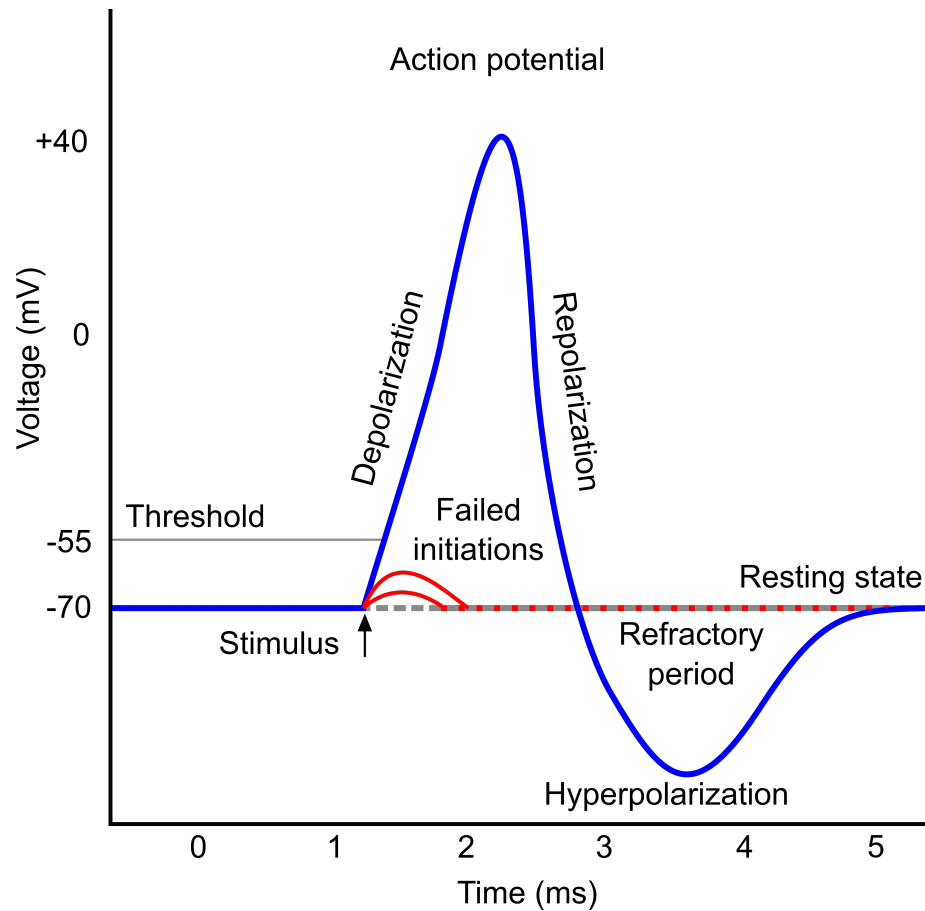


Figure 1.2: Voltage-time diagram of an action potential (Adapted from [6]).

1.1.2.2 Interneuronal Communication

Interneuronal communication occurs at synapses, where neurons exchange chemical or electrical signals. While many synaptic connections in the central and peripheral nervous systems exhibit remarkable specialization, all neurons employ either chemical or electrical synaptic transmission to convey information.

Chemical synapses are composed of three primary components (Figure 1.3): the presynaptic terminal at the axon's end of the presynaptic neuron where neurotransmitters are stored; the synaptic cleft, a small gap separating the presynaptic terminal and the postsynaptic neuron; and the postsynaptic terminal, which includes the dendrites or cell body of the postsynaptic neuron where neurotransmitters bind to receptors.

When an action potential reaches the presynaptic terminal, it causes voltage-gated cal-

cium channels to open. This allows calcium ions (Ca^+) to enter the terminal, triggering the release of neurotransmitters. Neurotransmitters are packaged into vesicles within the presynaptic terminal. When Ca^+ ions bind to receptors on the vesicle membrane, the vesicles fuse with the membrane and release their contents into the synaptic cleft. Neurotransmitters diffuse across the synaptic cleft and bind to receptors on the postsynaptic membrane. These receptors are specialized proteins that open or close ion channels in the postsynaptic membrane. The opening or closing of ion channels in the postsynaptic membrane causes a change in the membrane potential of the postsynaptic neuron. This change can be either excitatory (increases the likelihood of an action potential) such as glutamate, or inhibitory (decreases the likelihood of an action potential) such as γ -Aminobutyric Acid (GABA).

The interplay between excitatory and inhibitory neurotransmitters creates a delicate balance that influences the activity of the postsynaptic neuron. This dynamic dialogue shapes the overall function of the nervous system, enabling it to process information and control behavior e.g., movement. Electrical synapses are less common than chemical synapses, but they are found in a variety of tissues, including the brain, spinal cord, and heart. They consist of gap junctions, which are channels that directly connect the cytoplasm of the presynaptic and postsynaptic neurons. Compared to chemical synapses, electrical synapses are faster and transmit information in both directions [3], [7].

1.2 Skeletal Muscle

Muscle tissue assumes a pivotal role in the conversion of chemical energy into mechanical energy, thereby serving indispensable functions within the human body. Coordinated cycles of contraction and relaxation in muscles significantly contribute to body stabilization, movement facilitation, and the transport of internal substances. The three primary types of muscular tissue, i.e., skeletal, cardiac, and smooth, exhibit variations in anatomy, location, and activation mechanisms. While cardiac and smooth muscles are subject to involuntary regulation, skeletal muscles are primarily under voluntary control [9], [10]. This section

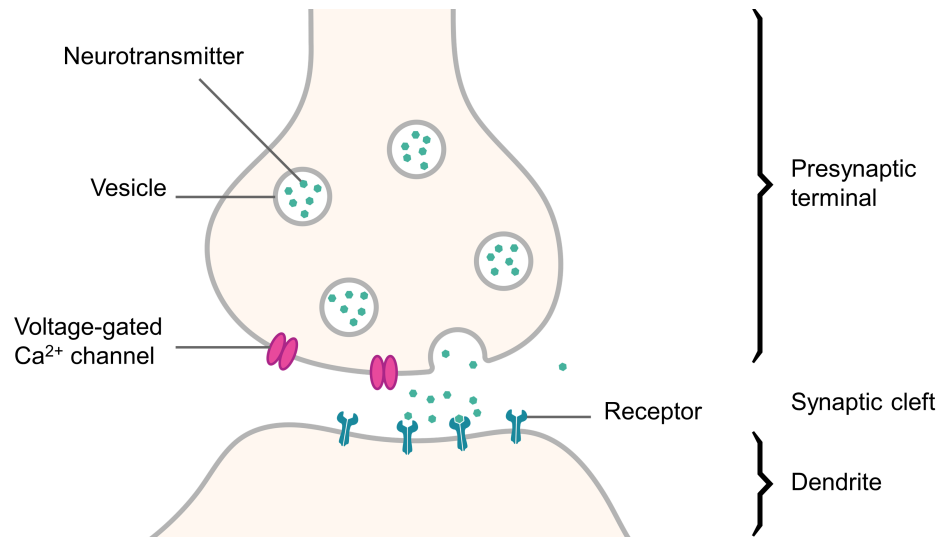


Figure 1.3: Illustration of a chemical synapse (Adapted from [8]).

focuses specifically on the intricate structure and function of skeletal muscles.

1.2.1 Structure

Skeletal muscle, connected to the corresponding bones through a primarily collagen-based tissue known as tendon, is composed of various components intricately working together to facilitate movement. Each muscle is encased in a layer of connective tissue known as the epimysium, which provides structural support and protection (Figure 1.4). Beneath the epimysium, the muscle is subdivided into bundles of muscle fibers called fascicles. These fascicles are surrounded by another layer of connective tissue called the perimysium, which helps to separate and cushion the muscle fibers. Within each fascicle, the individual muscle fibers, or cells of the muscle, are elongated and multinucleated, housing several nuclei crucial for cellular activities. Within each muscle fiber, myofibrils are densely packed. These myofibrils consist of connected sarcomeres, the primary sites where the sliding filament theory of muscle contraction, proposed by A. F. Huxley and H. E. Huxley, comes into play. This theory explains how the interaction of actin, a thin filament, and myosin, a thick filament, within the sarcomeres, is essential for muscle contraction [3], [11].

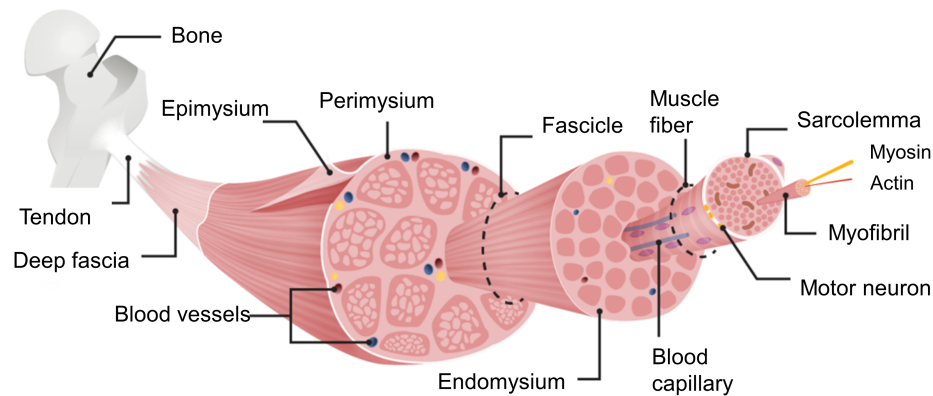


Figure 1.4: Illustration of the structure of the skeletal muscle (Adapted from [12]).

1.2.2 Mechanism of Excitation and Contraction

The communication between the axon of the motor neuron and the muscle fiber occurs at the neuromuscular junction (NMJ) (Figure 1.5). At the NMJ, the action potential triggers the release of acetylcholine (ACh), an excitatory neurotransmitter, from the terminal of the motor neuron. ACh, released across the synaptic cleft, diffuses towards the muscle fiber membrane, where it binds to nicotinic acetylcholine receptors (nAChRs). This binding event opens ion channels, allowing an influx of Na^+ ions into the muscle fiber, generating an electrical signal called a muscle action potential.

The muscle action potential, a rapid depolarization of the muscle fiber membrane, serves as the signal that initiates the process of muscle contraction. This intricate process, known as excitation-contraction coupling, involves a series of events within the muscle fiber itself. As the muscle action potential propagates along the T-tubules, triggering the release of Ca^+ ions from the sarcoplasmic reticulum (SR), a cascade of events ensues to initiate and regulate muscle contraction. Released Ca^+ ions bind to troponin, a protein complex situated on the actin filaments. This binding induces a conformational change in troponin, leading to the exposure of myosin-binding sites on actin, thereby facilitating the formation of cross-bridges (Figure 1.5).

The cross-bridge cycle, a pivotal process in muscle contraction, commences as myosin heads, part of the thick filaments, bind to the exposed sites on actin. In this low-energy

state, myosin is firmly attached to actin. The arrival of adenosine triphosphate (ATP) triggers the first stage of the cycle - the detachment of myosin from actin. The hydrolysis of ATP into adenosine diphosphate (ADP) and inorganic phosphate (Pi) provides the energy necessary for myosin detachment. ATP binding to the myosin head follows, energizing it and preparing it for the subsequent power stroke.

During the power stroke, ADP and Pi remain associated with the myosin head. This energized state prompts a conformational change in the myosin head, causing it to pivot and pull the actin filament towards the center of the sarcomere. This movement results in muscle contraction. Despite the power stroke, ADP persists on the myosin head, sustaining the attachment to actin.

The completion of the cross-bridge cycle requires the dissociation of ADP, paving the way for a new cycle. This step is facilitated by ATP binding to the myosin head, inducing detachment from actin and initiating a fresh cycle. This cyclic process continues as long as Ca^+ ions remain bound to troponin, ensuring the availability of active sites on actin for myosin binding. Once the muscle action potential subsides, the Ca^+ ions are pumped back into the SR by active transport pumps. This decrease in Ca^+ ions leads to the dissociation of the myosin cross-bridges from the actin filaments, resulting in muscle relaxation [13].

1.3 Volitional Muscle Contraction: From Motor Cortex to Skeletal Muscle

The human brain, comprising approximately 86 billion neurons and over 100 trillion synapses, stands as the most intricate structure known to science. It is broadly segmented into three main divisions: the cerebrum, cerebellum, and brainstem. The cerebrum, the largest portion of the brain, is bifurcated into the right and left hemispheres and is instrumental in executing higher functions, including the fine control of movement. Situated beneath the cerebrum, the cerebellum plays a pivotal role in the coordination of movements, maintaining posture and balance, as well as in motor learning. The brainstem, function-

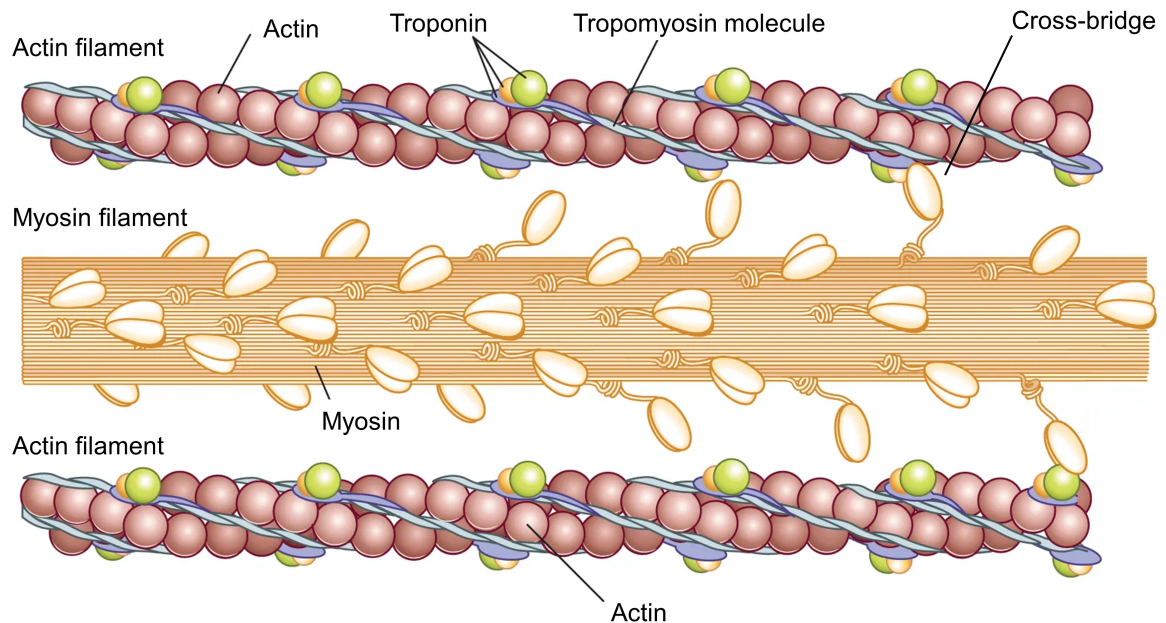


Figure 1.5: Illustration of cross-bridge formation (Adapted from [13]).

ing as a critical relay center, connects the cerebrum and cerebellum to the spinal cord and orchestrates several autonomic functions, such as respiration.

The cerebral cortex, the cerebrum's outermost layer, is predominantly composed of gray matter, which includes neuron cell bodies, dendrites, and unmyelinated axons, giving it a distinctive gray hue. Beneath this gray matter lies the white matter, consisting primarily of myelinated axons. These axons form intricate networks connecting various areas of gray matter both within the cerebrum and with other brain regions. The motor cortex, positioned in the frontal lobe of the cerebral cortex, is specifically tasked with the initiation and regulation of voluntary movements.

Upper motor neurons (UMNs) and lower motor neurons (LMNs) play crucial roles in the control of voluntary movements, operating collaboratively within a hierarchical system to regulate skeletal muscle activity of limbs (Figure 1.6). UMNs, pivotal in initiating and modulating voluntary movements of limbs, have their cell bodies situated in the motor cortex. The axons of these neurons primarily travel through the corticospinal tract, an essential anatomical pathway for transmitting movement-related information from the brain to the spinal cord. In the spinal cord, UMNs form synapses with interneurons and a specific

class of LMNs known as α -motoneurons. These α -motoneurons, with cell bodies located in the anterior horn of the spinal cord, are directly responsible for innervating skeletal muscle fibers. They play a central role in the actual contraction of these muscles [3], [14]. A muscle twitch is a single, brief contraction and relaxation cycle in a muscle fiber

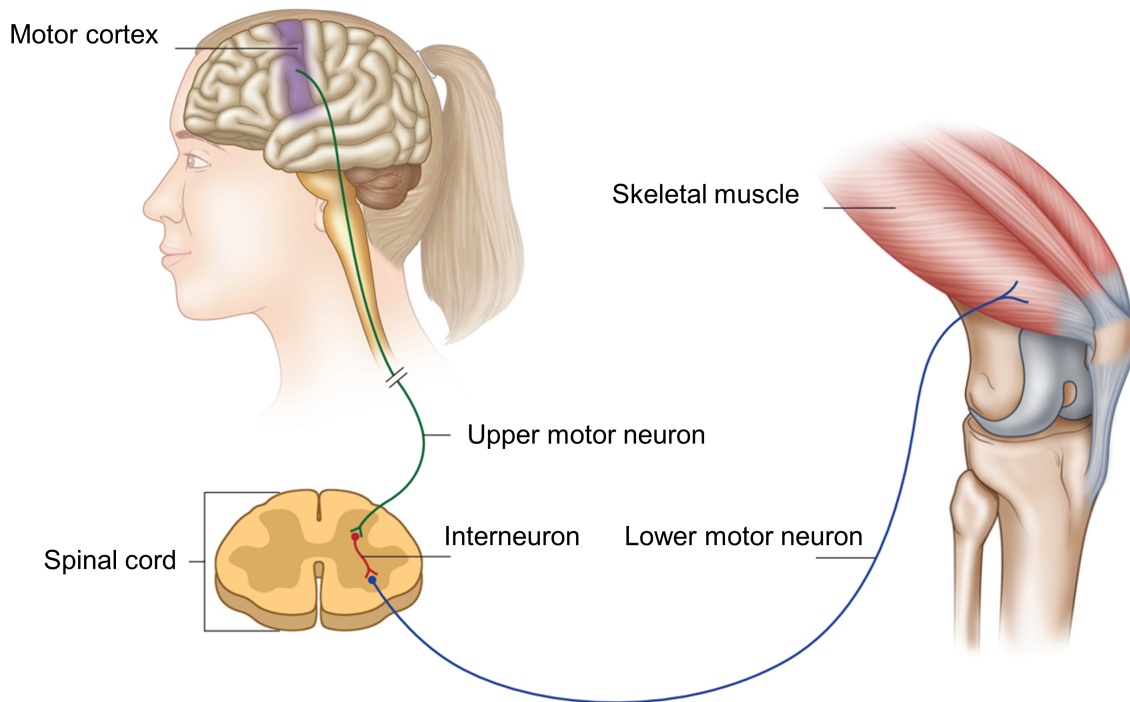


Figure 1.6: Simplified motor pathway from motor cortex to skeletal muscle (Adapted from [15]).

following a single action potential. In contrast, a tetanic contraction occurs when a muscle fiber is stimulated repeatedly at a high frequency, not allowing it to fully relax between stimuli, resulting in a sustained, forceful contraction.

Human skeletal muscle fibers are broadly classified as Type I, Type IIa, and Type IIb. Type I fibers are more resistant to fatigue and efficient for long-duration, low-intensity activities such as endurance sports. They produce muscle twitches that are less forceful but longer-lasting, suitable for sustained, aerobic activities. The slowness refers to the time it takes for these muscle fibers to generate force and contract after receiving an excitation input. Type II fibers are designed for short, high-intensity activities like sprinting or weightlifting. Type IIa fibers, also known as intermediate or fast oxidative fibers, are some-

what resistant to fatigue and can sustain activity for a moderate duration. They are a hybrid, possessing both the high-speed contraction of fast-twitch fibers and the endurance qualities of slow-twitch fibers. Type IIb fibers or fast glycolytic fibers, are the most powerful and fatigue quickly. They are ideal for short, explosive movements, generating powerful twitches that are brief but forceful [16], [17].

Each α -motoneuron connects to a distinct group of muscle fibers, forming what is known as a motor unit (MU). The extent of muscle fibers each α -motoneuron innervates correlates with its size, leading to motor units of varying sizes. Smaller motor neurons typically innervate slow-twitch (Type I) muscle fibers and larger motor neurons, on the other hand, innervate fast-twitch (Type II) fibers.

Based on the contractile speed and fatigability characteristics, motor units can be classified as type S (slow twitch, fatigue resistant), type FR (fast twitch, fatigue resistant), and type FF (fast twitch, fatigable) innervating Type I, Type IIa, and Type IIb muscle fibers, respectively [3], [17].

To adjust the force exerted by a particular muscle, the CNS employs two methods: recruitment, which activates more MUs, and rate coding, which enhances the firing rate of a specific MU. As excitatory synaptic input into an α -motoneuron pool increases, motor units are recruited sequentially, starting from the smallest (low-threshold) to the largest (high-threshold), adhering to Henneman's size principle [18]. In other words, the recruitment starts from Type I muscle fibers to Type II muscle fibers. Concurrently, an increase in synaptic input boosts the frequency of action potentials in specific neurons. Following what is termed the onion skin principle [19], smaller neurons, activated earlier, tend to discharge action potentials at higher frequencies than their larger counterparts.

The orchestration of coordinated movements is linked to proprioception, encompassing the awareness of limb position, movement, force, effort, and balance. Proprioceptive information is relayed to the CNS by sensory organs, prominently among them being muscle spindles and Golgi tendon organs (GTO). Muscle spindles, abundant in skeletal muscles, sense length changes in muscle fibers, relaying this information to the spinal cord through

Ia and II afferent nerves. This proprioceptive input, especially from Ia afferents forming monosynaptic connections with α -motoneurons, directly influences muscle activation and control. Simultaneously, GTOs, located at the musculotendinous junction, function as force sensors sensitive to muscle tension. Each GTO, innervated by Ib afferents, forms inhibitory connections with the α -motoneuron pool, contributing to the regulation of muscle force and preventing excessive tension. This sophisticated interplay between muscle spindles, GTOs, and their corresponding sensory fibers ensures precise proprioceptive feedback, fine-tuning voluntary muscle contractions for optimal motor control [14], [20].

1.4 Motor Neuron Lesion

A motor neuron lesion encompasses damage, injury, or impairment to motor neurons, arising from diverse factors such as trauma, neurodegenerative diseases, infections, or autoimmune conditions. The consequences of motor neuron lesions may manifest as compromised motor function, muscle weakness, atrophy, and difficulties in executing voluntary movements. The extent and location of damage within the motor neuron pathway influence the specific challenges and symptoms experienced [21] [22].

1.4.1 Upper Motor Neuron Lesion

UMN lesions denote impairments affecting motor neurons located within the motor cortex of the brain and the associated pathways transmitting impulses from the motor cortex to the spinal cord, notably the corticospinal tract. These neurons play a crucial role in the initiation and voluntary regulation of skeletal muscles governing the torso, upper limbs, and lower limbs.

The hallmark characteristics of UMN lesions encompass a loss of voluntary control over muscles. Despite this loss of control, individuals with UMN lesions often retain a certain degree of muscle bulk and tone. However, the nature of muscle tone is altered, displaying increased spasticity. Spasticity refers to a condition where muscles exhibit heightened,

involuntary contractions, leading to stiffness and resistance to movement. Additionally, reflex responses become exaggerated in the presence of UMN lesions. This means that the body's reflexes, such as the knee-jerk reflex, may be more pronounced than normal. These changes in muscle tone and reflex activity are indicative of the disruption in the communication between the motor cortex and the spinal cord caused by the UMN lesion [21]–[24].

1.4.2 Lower Motor Neuron Lesion

Lesions affecting LMNs involve damage to motor neurons situated in the anterior horn of the spinal cord or the cranial nerve nuclei within the brainstem. These motor neurons have the direct responsibility of innervating skeletal muscles, thereby exerting control over their movements and reflexes.

The distinctive features of LMN lesions include more pronounced manifestations of muscle weakness, atrophy, and a reduction in reflex activity. The muscle weakness observed in LMN lesions tends to be more evident and severe compared to UMN lesions. Atrophy, characterized by a decrease in muscle mass, is a consequence of the reduced neural input to the affected muscles. Furthermore, LMN lesions lead to diminished or absent reflex responses due to the disruption in the neural circuitry involving the LMNs. This contrasts with the exaggerated reflexes observed in UMN lesions [21]–[24].

1.4.3 Spinal Cord Injury

The spinal cord constitutes an intricate network of pathways facilitating the transmission of information and directives between the brain and the body. Within the spinal cord, distinct anatomical pathways play crucial roles in transmitting specific information. The corticospinal tract, for instance, is responsible for conveying information related to motor functions, while the spinothalamic tract and posterior columns serve as the primary sensory pathways. These sensory pathways exhibit differences in the types of sensations they convey; the posterior columns transmit information related to vibration, fine touch, and pro-

prrioception, while the spinothalamic tracts carry signals for pain, temperature, and coarse touch [3], [23]. Shielded by the vertebral column (Figure 1.7), the spinal cord is segmented into 8 cervical (C), 12 thoracic (T), 5 lumbar (L), and 5 sacral (S) vertebrae [25].

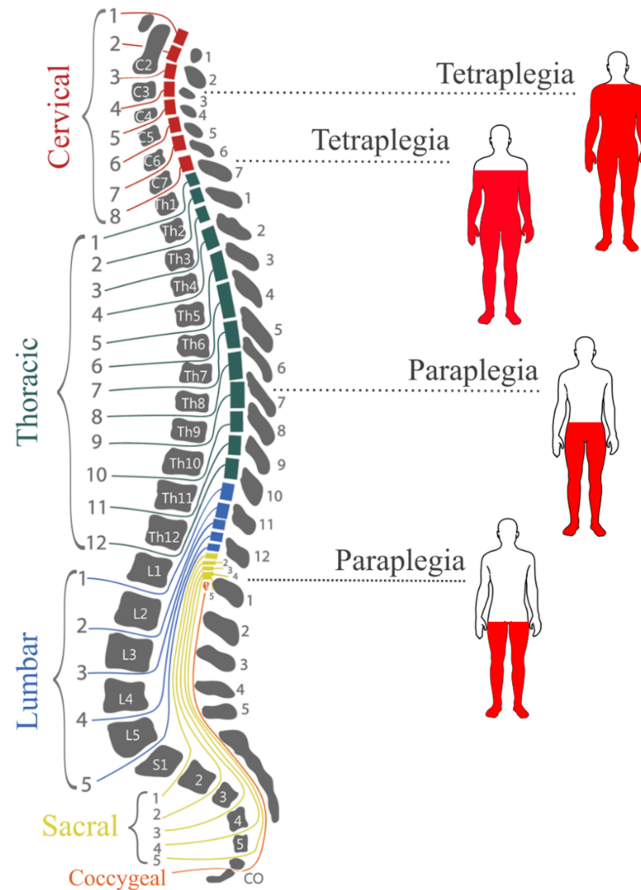


Figure 1.7: Illustration of spinal cord segments and paralysis level (Adapted from [26]).

Spinal cord injury (SCI) stands as a profound neurological condition, impacting between 250,000 and 500,000 individuals annually, with an estimated two to three million people worldwide living with disabilities resulting from SCI [27].

SCI is defined as damage to the spinal cord, causing temporary or permanent alterations in its function. This condition is categorized into traumatic and non-traumatic etiologies. Traumatic SCI arises from an external physical impact, such as motor vehicle accidents, falls, sports-related injuries, or violence, acutely damaging the spinal cord. On the other hand, non-traumatic SCI is the result of acute or chronic disease processes, such as tumors

or infections [28].

It is well documented that the pathophysiological progression of traumatic SCI unfolds in two distinct stages. The initial phase involves immediate mechanical injury, causing permanent or temporary compression and resultant spinal cord contusion. Subsequently, a secondary phase ensues, characterized by destructive and self-propagating biochemical alterations in neuronal and glial cells. These changes lead to escalating dysfunction, culminating in cell death over a span of hours to weeks following the initial insult [27].

The cervical portion of the spinal cord stands as the most frequently affected site in traumatic SCI, constituting approximately 60% of all cases, followed by lumbar and thoracic regions. Thoracic cord injuries are comparatively less frequent due to the augmented biomechanical support offered by the thorax in this segment of the cord [27].

Contingent on the location, SCI can lead to either paraplegia or tetraplegia. Paraplegia typically involves dysfunction or loss of motor and/or sensory capabilities in the thoracic, lumbar, or sacral spinal segments, affecting the lower limbs and abdomen. Conversely, tetraplegia involves similar impairments in the cervical spinal segments, impacting all four limbs.

SCIs are classified based on severity as either complete or incomplete. A complete SCI is characterized by a total absence of conscious sensory and voluntary motor functions at the S4-S5 sacral segment. In contrast, an incomplete SCI allows for some sensory and/or motor functions below the injury site to remain intact. The majority of spinal cord injuries fall into the incomplete category [29]. The American Spinal Injury Association (ASIA) Impairment Scale is a widely recognized tool for categorizing the severity of SCIs into five distinct categories (Table 1.1).

The impact of SCI on motor neurons varies with the injury's location along the spinal cord. Injuries in the cervical or thoracic regions can disrupt the function of UMNs, which originate in the brain and traverse the spinal cord to synapse with LMNs at various levels. Such injuries typically result in spastic paralysis, marked by increased muscle stiffness and exaggerated reflex responses.

Table 1.1: ASIA Impairment scale.

A	Complete	No sensory or motor function is preserved in the sacral segments S4-S5.
B	Incomplete	Sensory but not motor function is preserved below the neurological level including sacral segments S4-S5.
C	Incomplete	Motor function is below the neurological level and more than half key muscles below the neurological level have a muscle grade less than 3.
D	Incomplete	Motor function is below the neurological level and more than half key muscles below the neurological level have a muscle grade greater than 3.
E	None	Normal motor and sensory function.

Injuries at the lumbar or sacral levels, or near the spinal cord's lower end, directly impact LMNs that exit the spinal cord at these sites. These neurons are responsible for innervating muscles in the lower limbs and pelvic area. LMN injuries in these regions often lead to flaccid paralysis, diminished or absent reflexes, and muscle atrophy. In certain cases, individuals with spinal cord injuries may exhibit symptoms of both UMN and LMN damage. This scenario can occur if the injury is in the cervical or thoracic region, causing UMN-related symptoms in the lower body, while also damaging nerves exiting the spinal cord at these levels, leading to LMN symptoms in the upper body [30].

The ramifications of SCI extend beyond the initial trauma, encompassing a heightened risk of developing secondary conditions that can be debilitating and, in some cases, life-threatening. These secondary conditions include but are not limited to cardiovascular disease, respiratory complications, urinary tract infections, chronic pain, pressure ulcers, muscle spasms, and osteoporosis.

Beyond the physical challenges, individuals with SCIs often face societal barriers that further hinder their ability to fully participate in society and contribute to exclusion from

education, employment, and overall social engagement. For instance, children with SCIs are less likely to start schooling and experience greater challenges in academic progress. Similar barriers persist into adulthood, limiting economic participation and perpetuating a global unemployment rate for individuals with SCIs that surpasses 60% [31].

Acute care, rehabilitation services, and ongoing health maintenance play crucial roles in managing the diverse array of conditions associated with SCI. However, there exist challenges and limitations related to the current rehabilitation techniques which necessitate the combination of engineering skills and neurophysiological background to enhance the effectiveness of these methods for SCI patients. This is the primary motivation behind this thesis.

1.5 Electrical Stimulation

Electrical stimulation (ES), involving the controlled application of electrical pulses to induce nerve or muscle activation, encompasses a broad spectrum of diagnostic and therapeutic techniques [32], [33]. Operating on the principle of cellular excitability, ES utilizes exogenous electrical currents to elicit action potentials in excitable tissues, including neurons and muscle fibers, thereby eliciting muscle contractions. These electrical pulses are generated by an external device called a stimulator and can be delivered through various methods, such as transcutaneous and subcutaneous approaches. While subcutaneous methods offer increased selectivity and precision, they are invasive and carry a risk of infections [32], [34], [35]. This study specifically focuses on transcutaneous applications of electrical stimulation.

1.5.1 Physiological Basis

Creating a potential difference between surface electrodes forms the foundation for inducing muscle contractions using transcutaneous electrical stimulation. The anode (the 'positive' terminal) draws in negatively charged ions while pushing away positively charged

ions towards the cathode (the 'negative' terminal). Simultaneously, the cathode attracts positive ions and repels negative ions. This activity establishes a directional current flow from the anode to the cathode, effectively transmitting an electrical charge to the nerve trunk. Modern stimulators typically operate on current regulation, unlike their voltage-regulated predecessors. This approach guarantees the delivery of a consistent quantity of electrical charge to the excitable tissues, independent of the impedance at the electrode-tissue interface.

Under normal conditions, nerve cells and muscle fibers have a resting membrane potential ranging approximately from -70 to -90 mV relative to the surrounding extracellular fluid. When electrical stimulation is applied to the nerve trunk or muscle fibers, it introduces an electrical charge near the external cell membrane. This alters the cell's resting membrane potential. Such a change in membrane potential can artificially trigger action potentials, leading to the generation of muscle contractions [36], [37].

1.5.2 Applications

In a diagnostic framework, ES can be employed as an instrumental tool to distinguish between UMN and LMN lesions. It is noteworthy that motor neurons possess a comparatively lower threshold for excitability than muscle fibers. The elicitation of effective muscle contraction via nerve stimulation necessitates the intactness of the LMN pathway. Thus, the absence of muscle contraction in response to ES applied on shallow nerve trunks indicates potential dysfunction within the LMN system. In such instances, the muscle is described as 'denervated,' signifying that contraction can only be achieved through direct stimulation of muscle fibers. Conversely, in the context of UMN lesions, the affected muscle is often characterized as 'paralyzed,' indicating that activation is feasible through nerve stimulation [33],[38].

From a therapeutic perspective, ES represents a diverse set of techniques used in pain management, rehabilitation, and muscle strengthening.

Transcutaneous electrical nerve stimulation (TENS) primarily aims at pain relief by

stimulating sensory nerves (Figure 1.8). In TENS therapy, the electrical currents specifically target sensory nerve fibers responsible for transmitting sensations of light touch ($A\beta$ fiber) and are less involved in pain transmission. When TENS activates these sensory fibers, it employs the gate control theory of pain, which posits that stimulating non-nociceptive (non-painful) fibers can inhibit the transmission of nociceptive (pain) signals. This interference primarily occurs at the level of the spinal cord, where inhibitory interneurons are activated as a result of $A\beta$ fiber stimulation. These interneurons then prevent the pain signals (carried by $A\delta$ fibers for sharp pain and C fibers for dull pain) from ascending to the brain through the dorsal horn of the spinal cord.

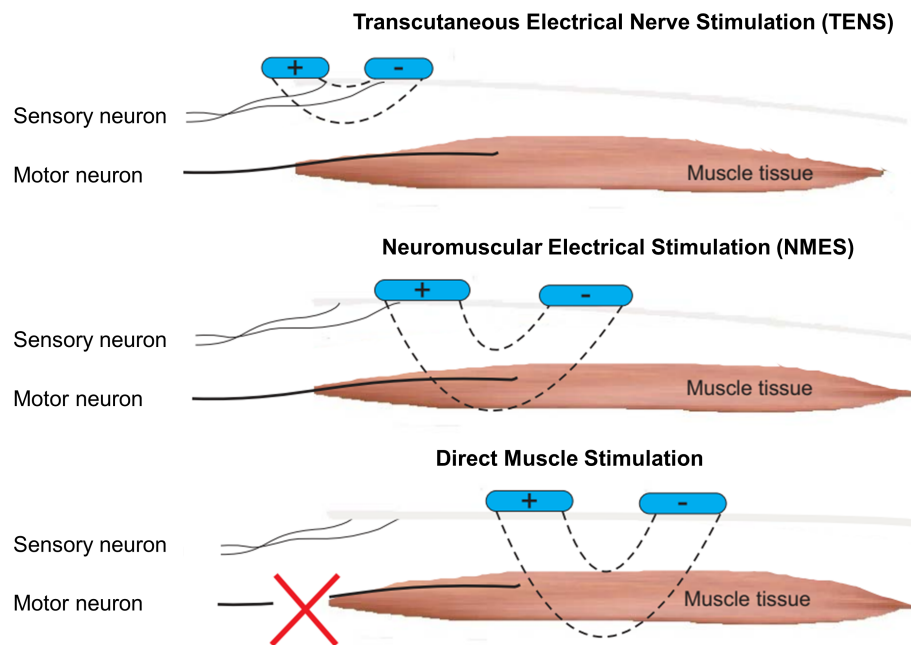


Figure 1.8: Therapeutic applications of electrical stimulation (Adapted from [39]).

Neuromuscular electrical stimulation (NMES) is designed to artificially induce muscle contractions by generating action potentials in the axons of LMNs (α -motoneurons) that innervate paralyzed muscles. Its primary aim is to stimulate these muscles for strengthening, re-education, and to prevent atrophy, thereby enhancing muscle performance. Functional electrical stimulation (FES) goes a step further by not only eliciting muscle contractions but also coordinating these contractions in a sequenced manner to replicate functional

movements such as walking, cycling, rowing, and grasping. While FES and NMES are sometimes used interchangeably, FES is distinctively focused on restoring or improving functional activities, utilizing a patterned stimulation approach to mimic natural movement sequences [34],[40].

FES facilitates the activation of paralyzed or weakened muscles, contributing to functional movement and promoting neural plasticity. Additionally, FES improves cardiovascular function through increased blood circulation, enhances respiratory functions, offers protection and rapid healing of pressure sores by promoting muscle contractions that facilitate changes in body positions, reduces the risk of osteoporosis and bone fractures, and diminishes muscle spasms. Altogether, these advantages contribute to an improved quality of life for individuals undergoing FES interventions in rehabilitation and healthcare settings [41], [42].

1.5.3 Stimulation Parameters

The effectiveness of FES depends on parameters such as electrode placement, size, current type, intensity, pulse duration, and frequency [34], [43].

Motor point refers to a specific area on the skin that corresponds to the underlying location where the motor nerve enters the muscle. At the motor point, the axons of the LMNs branch extensively to form a neuromuscular junction with numerous muscle fibers. This branching increases the density of synaptic connections, making the area highly sensitive to electrical stimuli. Consequently, at the motor point, electrical excitation is more effective due to this dense congregation of neuromuscular junctions. Motor points can be located using anatomical landmarks, palpation, and electrical stimulation devices with a pen electrode. Identifying the motor point is crucial for effective NMES, as it ensures maximum efficiency and response with minimal discomfort [32], [44].

The cathode is generally placed closer to the motor point. This placement is based on the physiological response of nerve and muscle tissue to electrical stimulation. The cathode emits negative charges and attracts positive charges. When placed close to the endplates

of the LMNs at the motor point, these electric charge migrations result in a local increase in positive ions in the extracellular environment. This phenomenon facilitates reaching the threshold for an action potential, requiring less additional stimulus to change the membrane potential to a level that triggers an action potential. In contrast, the anode tends to have the opposite effect, making the extracellular environment more negative. This can raise the threshold for firing an action potential, leading to the placement of the anode farther from the motor points.

Electrode size is a critical factor in electrical stimulation. The size of the electrode affects the current density, which is the amount of electric current per unit area of the electrode. Larger electrodes spread the current over a greater area, resulting in lower current density. Conversely, smaller electrodes concentrate the current over a smaller area, leading to higher current density. Smaller electrodes allow for more precise targeting of specific nerves or muscle fibers. Larger electrodes, due to their broader current spread, stimulate a wider area which may affect adjacent tissues. Sensory nerve endings (nociceptors) in the skin are sensitive to changes in electrical fields [45]. When the current density is high (as with smaller electrodes), the intensity of the electrical field at the skin's surface is higher. This increased intensity is more likely to exceed the threshold level at which nerve endings are stimulated, leading to stronger sensations [33].

In the domain of NMES, alternating current waveforms are utilized predominantly, characterized by their delivery of brief electrical impulses. Monophasic waveforms present certain drawbacks, notably the potential for electric charge accumulation in tissues during extended periods of electrical stimulation [46]. To mitigate this issue, symmetric biphasic impulses are employed. These impulses are designed to ensure that any residual electric charge within the tissues is effectively neutralized. A limitation of such pulses is that they induce muscle contractions under both the anode and cathode. To enhance specificity and control, advanced stimulation systems now frequently utilize asymmetric balanced biphasic impulses (Figure 1.9). This approach aims to concentrate muscle contractions predominantly under the cathode [46].

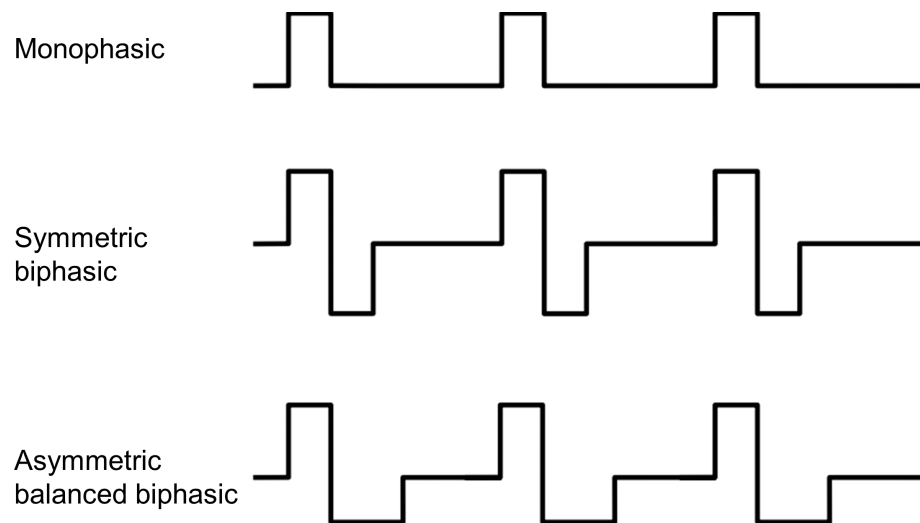


Figure 1.9: Common waveforms utilized in FES (Adapted from [35]).

The intensity of muscle contractions can be modulated by adjusting key parameters of the stimulating pulse: the pulse width (μs), pulse amplitude (mA), and pulse frequency (Hz) (Figure 1.10). Pulse width refers to the duration of each stimulation pulse and determines what kind of nerve fibers will be activated. Adequate pulse width is essential for the effective depolarization of nerve fibers, which in turn triggers muscle contraction. In FES clinical settings, the pulse width usually ranges from 200 to 500 μs . The pulse amplitude, or intensity of the stimulation, is directly associated with the depolarizing effect. Higher amplitudes lead to more potent depolarization effects. In FES applications, pulse amplitudes typically do not surpass 130 mA, although the precise values vary depending on several factors such as the size of the muscle, the dimensions of the stimulating electrodes, and the pulse width of the stimulation waveform. The product of pulse amplitude and width determines the charge delivered to the target tissue. Smaller muscles in the upper limbs usually necessitate smaller electrodes and lower electric charge for effective contraction. In contrast, larger muscles usually need larger electrodes and higher electric charges for effective contraction. The stimulation frequency modulates the quality of achieved muscle contraction, similar to the muscle contraction that originates from the CNS. Frequencies typically used in clinical applications of FES range from 20 to 50 Hz [34], [35].

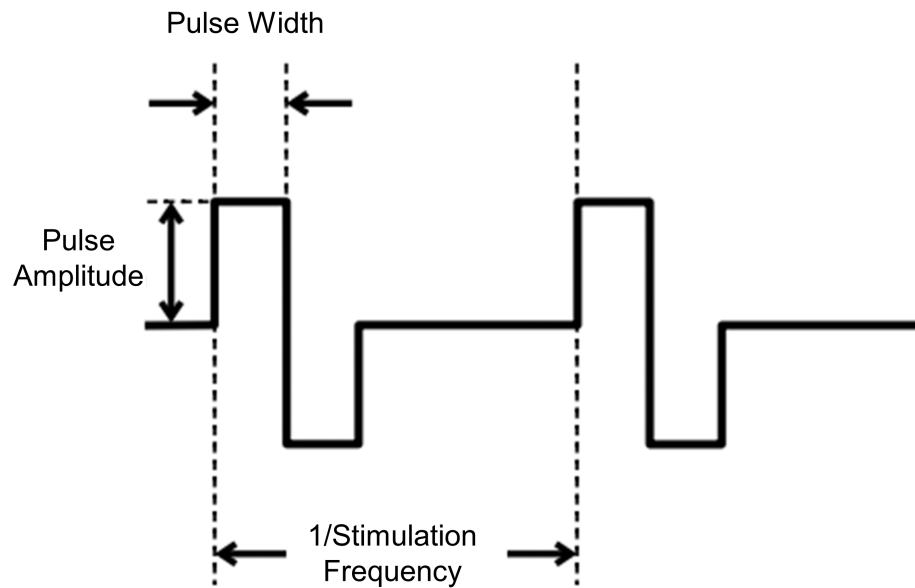


Figure 1.10: Parameters of biphasic electric pulse utilized in FES (Adapted from [35]).

1.5.4 Lower-limb FES Cycling

With nearly four decades of history behind it [47], lower-limb FES cycling stands out as one of the most common and secure FES applications for rehabilitating paralyzed muscles. FES cycling can be conducted on motorized/non-motorized stationary ergometers or tricycles designed for mobile cycling. In contrast to walking, cycling is performed in a seated position, ensuring that the patient is not at risk of sudden falls and bone fractures. Additionally, at the initial stages of rehabilitation, paralyzed muscles may not possess sufficient strength for walking training. Cycling offers a less demanding alternative, reducing the patient's dependency on family or clinic staff. Furthermore, non-stationary outdoor cycling can enhance the enjoyment of the rehabilitation process [48], [49]. FES cycling provides various health benefits, including motor relearning, improvements in muscle bulk and strength, local blood circulation, gas exchange kinetics, and aerobic metabolism [50]–[53].

Most cycling devices are equipped with encoders to measure the crank angle at each moment, thereby stimulating the proper muscle(s) to generate torque that ensures a smooth rotation of both legs. The stimulated muscle groups comprise the quadriceps group serving

as the knee extensor, the hamstrings group functioning as the knee flexor, and the gluteal muscles acting as the hip extensor. The quadriceps group encompasses four muscles: rectus femoris, vastus lateralis, vastus medialis, and vastus intermedius. The latter is situated deeply and cannot be effectively stimulated using surface electrodes. The hamstrings group is constituted of the biceps femoris, semitendinosus, and semimembranosus muscles. The gluteal group encompasses the gluteus maximus and gluteus medius muscles. Although ankles are typically secured to the pedals using orthosis to prevent injuries, the tibialis anterior and calf muscles can be stimulated to increase blood circulation. Among the mentioned muscle groups, the quadriceps is the primary torque generator [54], [55].

The timing or angle range during which each muscle is stimulated is termed the stimulation pattern. This pattern varies for each individual based on anthropometric characteristics, trunk angle, seating position in relation to the ground and crank center, crank arm length, and cycling velocity. The force generated by each muscle within the muscle groups is multiplied by the corresponding moment arm length, converted into joint torque, and then transferred to crank torque, which can be modeled through torque transfer functions. The summation of the transferred torques, combined with the torque generated by the motor, results in the cycling motion. The motor can be utilized in assistive and/or resistive modes during FES cycling. In the assistive mode, it aids in overcoming biomechanical deadpoints, facilitating a smoother cycling motion. Furthermore, the motor extends the duration of exercise, potentially yielding increased physiological and psychological benefits. In resistive mode, it enhances the level of difficulty, making cycling sessions more challenging [56].

1.5.5 Limitations of FES

For at least six decades, FES has been employed in clinical applications, providing diverse physiological and psychological benefits to individuals with neurological disorders [34], [57]. Despite its long-standing application and advantages, FES still faces significant challenges that must be addressed for it to maintain its position as a prominent rehabilitation technique. In this section, we will meticulously explain the most important bottlenecks.

When applied non-invasively using transcutaneous electrodes, FES generates an electric field beneath the electrodes, inducing an ionic charge flow from the anode to the cathode. Consequently, the axons of α -motoneurons near the cathode electrode become surrounded by positive ions. This accumulation of positive ions triggers the opening of sodium channels, leading to the propagation of action potentials and muscle contraction. As previously mentioned, larger α -motoneurons, with their larger diameter axons, are more easily activated compared to smaller ones due to the lower resistance of their membranes. However, these larger diameter axons primarily innervate less fatigue-resistant and fast-twitch muscle fibers. Thus, FES recruits motor units based on their proximity and in reverse order compared to physiological recruitment, as described by Henneman's size principle in previous sections. Moreover, FES typically recruits a limited number of motor units close to the skin synchronously at frequencies of about 20 to 50 Hz to produce fused contractions. In contrast, the CNS accesses all motor units and recruits them asynchronously with a firing rate of 4 to 12 Hz, allowing more rest for the motor units [46]. Furthermore, the CNS recruits synergistic muscles, regardless of their position and depth, with precise activation levels and timings to produce the required power output for complex activities, such as lower limb cycling. These distinctions between FES and CNS recruitment methods are the primary causes of the earlier onset of muscle fatigue and lower power output in FES compared to voluntary contraction. It is noteworthy that following SCI, the muscle fibers undergo a transformation into the less fatigue-resistant type IIb fibers [58], [59]. This transformation is another contributing factor to muscle fatigue in SCI patients. Another issue with FES-induced muscle contraction is the simultaneous activation of sensory, motor, and pain fibers, particularly at high intensities, a phenomenon not observed in voluntary muscle contraction. This simultaneous activation can be problematic regarding the perceived discomfort for patients with intact sensory function, such as those with incomplete SCI and stroke. It may even lead to patients refusing to participate in therapy sessions. The strength-duration curves for sensory, motor, and pain fibers, presented in Figure 1.11, provide valuable insights into the occurrence of painful contractions at high stimulation

intensities. Transcutaneous stimulation reveals distinct thresholds for sensory ($A\beta$), motor ($A\alpha$), and pain fibers ($A\delta$ for sharp pain and C for dull pain). At lower stimulation intensities, the sensory threshold is the most easily reached, representing the minimal level of stimulation required to activate sensory nerve fibers. Following this, the motor threshold is surpassed, indicating the minimum intensity needed to elicit a muscular response. Finally, at higher stimulation intensities, the pain fibers threshold is reached, signifying the point at which the nervous system perceives and transmits the sensation of pain [60].

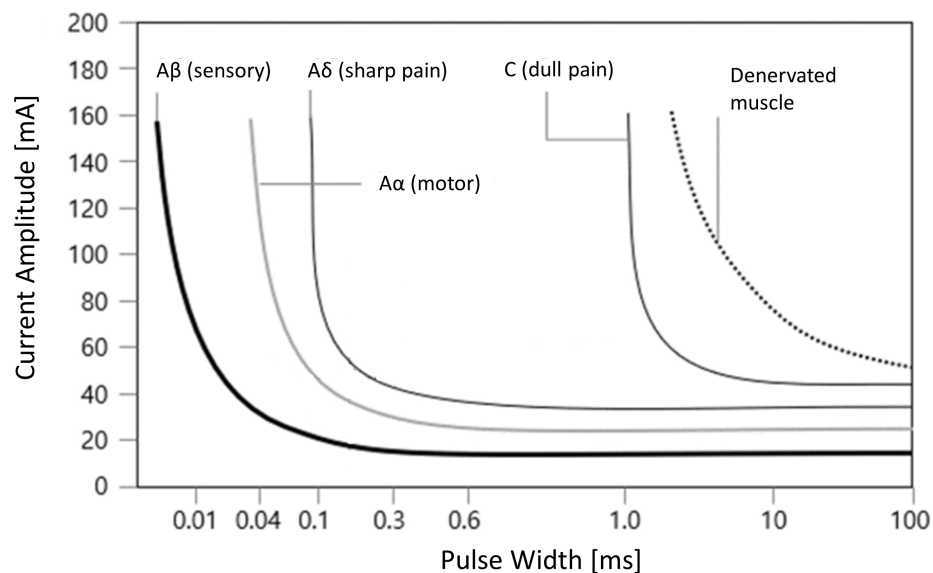


Figure 1.11: Strength-duration curve of sensory, motor, and pain fibers (Adapted from [60]).

Finally, disposable self-adhesive hydrogel electrodes are commonly used in clinical FES applications. Despite their initial good adhesiveness, they require careful storage and handling to maintain effectiveness. However, they are still prone to drying out and losing conductivity over time. This degradation can lead to reduced stimulation efficacy and comfort. Additionally, these electrodes present hygienic challenges, as they are neither washable nor easily sanitized. These issues underscore the need for alternative electrode solutions that can provide patients with electrical stimulation that is comfortable, consistent, and efficient.

1.6 Thesis Objectives

This thesis aims to overcome the limitations of FES through a multifaceted novel approach that concentrates on transcutaneous electrodes, stimulation strategies, and biomechanical perspectives. The first study focuses on the development and assessment of garments embedded with textile electrodes, aiming to enhance user comfort, temporal consistency, and the efficiency of electrical stimulation. The subsequent two studies explore the potential of asynchronous electrical stimulation strategies to improve performance in terms of fatigue resistance and output power, concentrating on both isometric exercises and cycling tasks. In the final study, biomechanical optimization is examined to maximize crank torque during FES cycling.

The objectives of this thesis can be separated into the following subcategories:

1. Development and assessment of garments embedded with textile electrodes for FES applications

In this research, the effectiveness of garments embedded with textile electrodes is compared with that of commercially available self-adhesive hydrogel electrodes. This comparison focuses on three critical aspects: perceived discomfort by the participants, temporal consistency of the electrode performance, and stimulation efficiency during isometric knee extension tasks. The primary goal of this study is to deepen our understanding of the potential clinical applications of textile electrodes in rehabilitation settings. Such insights are anticipated to inform future design and usage strategies for textile electrodes in therapeutic practices.

2. Assessment of asynchronous stimulation strategies during isometric and cycling exercises

This segment of the thesis delves into the asynchronous stimulation strategy, specifically its application in delaying muscle fatigue and enhancing muscle force. Despite its potential, this strategy has not yielded consistent results across various studies.

This inconsistency raises questions about the underlying mechanisms and optimal conditions for its effectiveness. This research aims to unravel these ambiguities, focusing on how asynchronous stimulation can be optimized for maximum efficacy in both isometric exercises and cycling. By identifying the factors that contribute to its varied outcomes, this study seeks to refine the strategy for more reliable and effective use in rehabilitation settings.

3. Biomechanical optimization of seating position and stimulation pattern in FES cycling

This simulation study aims to propose a novel method to find the optimal position of the seat concerning the crank center, trunk angle of the user, and crank arm length as well as stimulation pattern while pedaling at the proper cadence for SCI patients. To meet this aim, an easy-to-use and precise model of the skeletal muscle was combined with the torque transfer functions of the lower body joints. Furthermore, the impact of muscle force (joint torque)-velocity (joint angular velocity) factor in finding the optimal point was investigated. This method can be employed in clinics with different ergometer types to help the patients keep their exercise for a longer duration.

1.7 Thesis Outline

Following this introduction chapter, the thesis is structured into the following chapters:

- **Chapter 2** presents a novel garment embedded with textile electrodes and compared with self-adhesive hydrogel electrodes regarding the perceived discomfort, temporal consistency, and stimulation efficiency during isometric knee extension tasks.

E. Jafari, V. Bergeron, A. Metani, and L. Popović-Maneski, “Assessing Comfort and Consistency of Dry Electrodes for Functional Electrical Stimulation”. *Orally Presented at RehabWeek Conference 2023, Singapore. In preparation for journal submission*

- **Chapter 3** reports the findings of the study comparing the fatigue-reducing ability of high-intensity spatially distributed sequential stimulation (SDSS) versus moderate-intensity SDSS in subjects with SCI performing isometric contractions of the quadriceps muscle group.

E. Jafari^{*}¹, P. Kajganić^{*}, V. Bergeron, A. Metani, and L. Popović-Maneski, “Comparing the Efficiency of Moderate and High-Intensity Spatially Distributed Sequential Stimulation in Subjects with Spinal Cord Injury”. *Orally Presented at RehabWeek Conference 2023, Singapore. In preparation for journal submission*

- **Chapter 4** reports the results of the case series assessing the efficacy of SDSS versus SES applied to the paralyzed quadriceps muscles of four subjects while performing a functional cycling task.

P. Kajganić^{*}, **E. Jafari**^{*}, L. Popović-Maneski, V. Bergeron, and A. Metani, “SDSS Applied to the Paralyzed Quadriceps Muscles While Performing Motor-Assisted FES Cycling – A Case Study”. *Poster Presented at RehabWeek Conference 2023, Singapore. In preparation for journal submission*

- **Chapter 5** presents the results of a biomechanical optimization study aimed at determining the best seating position, trunk angle of the user, and crank arm length as well as stimulation pattern for FES cycling in SCI patients.

E. Jafari, E. A. Aksoez, P. Kajganić, A. Metani, L. Popović-Maneski, and V. Bergeron, ”Optimization of Seating Position and Stimulation Pattern in Functional Electrical Stimulation Cycling: Simulation Study,” *2022 44th Annual International Conference of the IEEE Engineering in Medicine & Biology Society (EMBC)*, Glasgow, Scotland, United Kingdom, 2022, pp. 725-731, doi:

¹An asterisk indicates co-first authors.

10.1109/EMBC48229.2022.9871339.

- **Conclusion and Future Prospects** summarizes the results and provides a discussion of the content presented in this thesis, how the aims were achieved along with potential avenues for further exploration to build upon the current research.

Chapter 2

Textile versus Hydrogel Electrodes: Comfort, Consistency, and Efficiency

Abstract

The efficacy and comfort of neuromuscular electrical stimulation (NMES) largely depend on the type of electrodes used. Traditional self-adhesive hydrogel electrodes, while effective, pose limitations in terms of wearability, skin compatibility, and reusability. This study investigates the performance of textile electrodes integrated into garments for NMES of lower extremities, with a focus on their potential rehabilitative applications for patients with neurological disorders such as stroke, multiple sclerosis (MS), and spinal cord injury (SCI). We compared textile electrodes with conventional self-adhesive hydrogel electrodes in terms of comfort, temporal consistency, stimulation efficiency, and electrical impedance under isometric conditions. Ten healthy subjects participated in tests evaluating these metrics during isometric knee extension exercises. Our findings revealed no significant difference between the two types of electrodes across all evaluated parameters. The textile electrodes, used after applying moisturizing lotion to enhance the electrode-skin interface, demonstrated comparable levels of comfort, consistency, and efficiency to hydrogel electrodes. This equivalence, coupled with the advantages of washability and reusability, positions textile electrodes as a promising alternative for NMES applications, particularly in rehabilitation settings.

2.1 Introduction

E-textiles, derived from “electronic textiles,” merge electrical and electronic functionalities with traditional textile products, such as garments, enhancing their utility and versatility. These innovative textiles incorporate a range of components, including conductive threads, sensors, microcontrollers, and batteries, broadening their applicability across diverse domains [61], [62]. Their integration into various sectors such as healthcare, sports, leisure, fashion, and the military highlights their versatility in meeting various user needs [63], [64]. In particular, the healthcare industry has seen significant advancements with the incorporation of e-textiles into practical applications [65], [66].

Wearable healthcare devices emerge as a prominent application in the e-textile domain, serving dual pivotal roles: diagnostic and therapeutic [67]. On the diagnostic front, these devices harness the human body’s inherent electrical signals—from cardiac rhythms to muscular and cerebral activities—which can be precisely captured using electrodes embedded in textile substrates. Consequently, they enable continuous monitoring of vital signs and facilitate key medical assessments such as electrocardiography (ECG) [68], [69], electromyography (EMG) [70], [71], and electroencephalography (EEG) [72]. This integration transforms everyday garments into powerful tools for gaining insights into an individual’s health status, not confined to clinical settings but also during routine activities of daily life [66]. Therapeutic e-textile applications encompass electrotherapy, a pivotal healthcare domain that applies regulated electrical currents to manage various medical conditions [66], [67]. This modality demonstrated efficacy in the realm of analgesia, notably through transcutaneous electrical nerve stimulation (TENS) [73], and is instrumental in the neuromuscular rehabilitation process [36].

Neuromuscular electrical stimulation (NMES) is a well-established electrotherapy technique that involves the controlled application of low-charge electrical pulse trains to superficial nerve trunks or muscle motor points using two surface electrodes to elicit artificial muscle contractions [74]. NMES can bring about physiological and psychological bene-

fits, such as increased muscle strength and improved cerebrovascular and cognitive functions [35], [42].

NMES can be integrated into functional regimens, targeting different muscle groups in a rhythmic pattern, allowing individuals to perform tasks such as cycling [75]–[77], walking [32], and grasping [78], [79]. This specialized application is known as functional electrical stimulation (FES) [40]. Previous studies have shown that FES can bring about significant advantages, including improvements in cardiovascular function [80], enhanced muscle tone [81], increased bone density [82], and faster healing of pressure ulcers [83]. These benefits are of particular significance to individuals affected by neurological disorders (e.g., stroke, spinal cord injury (SCI), multiple sclerosis) or intensive care unit (ICU) acquired weakness [84] (more details are provided in section 1.5).

NMES is typically applied on the skin surface using disposable self-adhesive hydrogel electrodes. These multi-layer electrodes consist of the skin interface layer, featuring a conductive hydrogel, that is easily removable. A second hydrogel layer connects to a low-resistive substrate (the outer layer), offering strong adhesion. The substrate may comprise carbon film, wire mesh, or other conductive materials, with a wiring cable linking to the electric stimulator. A scrim layer can be placed between the hydrogel layers to prevent slippage and reinforce the multi-layer substrate. This multi-layer structure leads to high conductivity, which allows the hydrogel electrodes to deliver a strong, consistent, and evenly distributed electrical current over the electrode and skin surface. Moreover, high adhesivity to the skin surface reduces the risk of electrode displacement or loss of contact during treatment [85].

However, the practicality and patient compliance with self-adhesive hydrogel electrodes are limited by several disadvantages. These electrodes, not being embeddable into garments, demand careful storage and handling to maintain their effectiveness, yet they are still prone to drying out and losing conductivity over several months of storing or weeks of use. This degradation leads to reduced stimulation efficacy and comfort [86]–[88]. Their rigid nature limits flexibility and conformity to body contours, often causing peeling and

wrinkling during movement [89], [90]. This necessitates individual, manual positioning by trained personnel, complicating their application. Moreover, their disposability contributes to environmental concerns and increases costs, as they require frequent replacement. Additionally, these electrodes pose hygienic challenges, as they are neither washable nor easily sanitized. The discomfort associated with their adhesive properties, especially upon removal, and the potential for skin irritation or allergic reactions [91], further detract from their user-friendliness. Their limited durability, coupled with the expense and potential skin displacement issues, compounds the challenges they present [74].

These drawbacks highlight the necessity for improved electrode designs, such as customizable and washable textile electrodes, which offer integration with garments, enhanced patient comfort, and mass-production viability at reduced costs. Prior research has concentrated on diverse aspects of textile electrode production and subsequent evaluation metrics. From the viewpoint of manufacturing, investigations have delved into methods of production and integration, choice of conductive materials, and the utilized electrolyte in instances involving wet skin-electrode interfaces. In terms of evaluation, newly developed electrodes have been compared based on one or multiple benchmarks, which include the level of discomfort experienced by the user, the electric charge required to attain motor threshold or stimulation efficiency, and the impedance behavior of the materials used [74].

Textile electrodes are fabricated using various textile production techniques such as embroidery [74], [92], printing [93]–[96], coating [90], [97], knitting [89], [98], [99], and weaving [100]. These methods range from adding conductive materials onto a textile substrate to integrating them into the textile structure at various levels of sophistication. Incorporating electrodes directly into wearable systems in a unified process presents the opportunity to fabricate both the garment and the electrodes simultaneously. Adding-on techniques such as embroidery usually require cutting and sewing the fabric to form electrodes, a process that can lead to material waste, particularly depending on the specific shape and size of the electrodes [74]. On the other hand, methods like knitting and weaving, while widely used, have their limitations. They can be expensive and may restrict design flexibility due

to their one-step fabrication process. Furthermore, these fabrication techniques might lead to non-uniform resistance, not only due to inconsistent spacing of conductive yarns but also because of the stretching experienced while the electrodes are being worn [95]. This stretching is a crucial factor to consider, as it can significantly alter the performance of the electrodes, affecting their ability to provide consistent electrical stimulation [95].

Regarding the conductive materials, textile electrodes are predominantly fabricated using silver due to good conductivity and antibacterial properties, typically in the form of metal-coated polyamide threads, occasionally combined with elastane to enhance flexibility [74]. When initially worn, textile electrodes that utilize polymer coatings infused with silver demonstrate favorable impedance levels and a comfortable stimulation experience. Nevertheless, these positive attributes tend to diminish significantly after the electrodes undergo washing and extended wear. Particularly for products with substantial silver content, the electrode surfaces often fail to withstand the rigors of washing due to oxidation. Similarly, fabrics and embroidery based on silver and steel are unsuitable for high-quality e-textiles, as they tend to lose their quality following washing and regular use [101].

Textile electrodes are available as dry and/or wet variants. Dry electrodes benefit from higher fabric densities to enhance skin hydration through sweat retention [74]. For wet applications, utilized electrolytes are water [87], [89], [99], saline [102], and hydrogel [74], [87]. The choice of electrolyte can modulate the impedance at the skin-electrode interface, subsequently influencing the level of discomfort experienced by the user and stimulation efficiency. However, only a limited number of studies have quantitatively measured the changes in impedance that result from electrode wetting. Zhou et al. [87] explored the comfort associated with electrical stimulation using textile electrodes in relation to conventional hydrogel electrodes. Spectral analysis of electrical impedance revealed suboptimal skin contact with the dry textile electrode, which improved when the textile electrode was moistened. Their experimental observations indicated that dry textile electrodes could induce pain at low electrical currents, in contrast to wet textile electrodes and hydrogel electrodes, during foot dorsiflexion movements. Theoretical models suggest that the pain-

sensing fibers are more easily activated by a dry textile electrode as compared to a wet textile electrode or hydrogel electrode.

Nevertheless, wetting the electrodes poses its own challenges. It does not offer any significant advantage in placement efficiency over hydrogel electrodes, as the wetting process can be as time-consuming as the placement of traditional electrodes [74]. In [89], the developed textile electrodes had to be moistened with water to have high conductivity, making the stimulation unpleasant when the electrodes were dried approximately within 9 to 18 minutes. These studies underscore the necessity for a skin-friendly moisturizing solution capable of sustaining its conductive properties throughout a training session, needless of recurrent application.

Stimulation comfort plays a crucial role in the effectiveness of stimulation electrodes since it is vital that the intensity remains within the patient's tolerance threshold. Previous studies demonstrated that electrolyte [87], [99], electrode dimension [85], [79], and pressure [99], [103] are the most effective parameters on perceived discomfort level [74]. Smaller electrodes may intensify pain at certain stimulation amplitudes, potentially compromising the efficacy of NMES by necessitating lower intensities [85]. In [99], it was shown that applying pressure enhances the performance of the textile electrodes. These studies highlight the necessity of consistent pressure application and the use of electrodes with identical dimensions in comparative studies, such as those evaluating textile (dry or wet condition) versus hydrogel electrodes.

In the current study, multi-layer textile electrodes with biocompatible silicon surface from Nanoleq AG were integrated into pants using a hot-pressing technique. These electrodes were compared to commercially available self-adhesive hydrogel electrodes of the same dimensions, focusing on perceived discomfort, temporal consistency, and stimulation efficiency during isometric knee extension tasks, in ten healthy subjects, with controlled pressure applied to the electrodes. With textile electrodes, moisturizing lotion was applied to ensure a more uniform current distribution over the skin surface. Impedance spectroscopy was utilized to assess the electrical properties of textile electrodes both with

and without lotion, alongside hydrogel electrodes, before and after a single session with one subject. The present work aims to enhance the understanding and future clinical application of textile electrodes in motor rehabilitation of patients with neurological disorders such as stroke, MS, and SCI, prioritizing comfort, reliability, and effectiveness.

2.2 Methods

2.2.1 Participants

Ten healthy subjects, consisting of seven males and three females, with a mean age of 28.9 years (standard deviation $\sigma = 5.80$), a mean height of 176.3 cm ($\sigma = 8.51$), and a mean weight of 71.3 kg ($\sigma = 14.65$), volunteered to participate in this study. Except for three of them, all participants had prior experience with FES (Table 2.1). Participants were excluded if they had any known neuromuscular or skeletal disorders, or if they presented with open wounds or rashes at the sites where electrodes were to be placed. Before participating in the experiments, participants were provided with a detailed description of the purpose and testing procedures. Each participant provided written informed consent. The project was approved by the local Institutional Review Board (NCT06421753) and conducted in accordance with the Declaration of Helsinki.

2.2.2 Instrumentation

In this study, we utilized the ElectroSkin STIM textile electrode (Nanoleq AG, Zurich, Switzerland). This electrode is composed of the following layers: a biocompatible silicone rubber surface that interfaces with the skin, a conductive core layer, and an insulating thermally adhesive layer on the back, featuring a designated contact spot for electrical connections. The textile electrode sized at $5 \times 9 \text{ cm}^2$ and the thermo-adhesive backing was hot-pressed onto stretchable pants (74% Polyamide, 26% Elastane), available in four sizes for males and females (S, M, L, XL), in a single step using a lamination temperature of

Table 2.1: Demographic characteristics of the participants.

Participants	Gender	Age (years)	Height (cm)	Weight (kg)	FES naive	Dominant Leg
P1	F	23	164	46	No	R
P2	M	27	184	85	No	R
P3	M	39	175	65	No	R
P4	M	37	192	102	Yes	R
P5	M	32	183	75	No	R
P6	M	33	175	75	No	R
P7	F	23	165	55	No	R
P8	F	27	168	65	No	L
P9	M	27	176	72	Yes	R
P10	M	21	181	73	Yes	R

130-150 °C and a lamination time of 20-30 seconds. The positions of these electrodes were carefully determined based on the pants sizes and anatomical landmarks to ensure comprehensive coverage of the quadriceps femoris (QF) motor points [104]. The electrical connection was established with snap buttons via the PhantomLink connection patch (Nanoleq AG, Zurich, Switzerland). A side zipper was added to the pants to make it easier to put on and take off. In addition to the QF, the developed pants have the capability to stimulate various lower limb muscles on both sides including the gluteus maximus, hamstrings group, tibialis anterior, fibularis longus, and gastrocnemius. However, it's important to note that our primary focus in this study was on the QF muscle groups (Figure 2.1). In sessions involving textile electrodes, moisturizing lotion (CeraVe Moisturizing Lotion for dry to very dry skin), enough for epidermal hydration beneath the position of the electrodes, was applied to the participant's skin before they donned the garments to improve electrode-skin adhesion.

To assess the performance of the textile electrodes, we utilized self-adhesive hydrogel electrodes (Compex Dura-Stick plus, 5 x 9 cm²) as a benchmark in this study.

Compensated asymmetric biphasic electrical pulses were applied to the QF of the par-



Figure 2.1: Stretchable pants embedded with textile electrodes to stimulate lower limb muscles.

ticipants using an 8-channel programmable current-controlled MotiMove stimulator (3Fit-Fit Fabricando Faber, Belgrade, Serbia) which was connected to a laptop via a USB-RS485 converter [105]. The stimulation pulse characteristics, including frequency, pulse width (PW), and pulse amplitude (PA), were controlled by a custom-made program developed in LabVIEW 2019 (National Instruments, Austin, TX, USA). A universal membrane force sensor (EMSYS, EMS30-500 N, Slovakia) was incorporated into a custom metal structure to measure the isometric force generated during electrical stimulation tests. For maximum voluntary isometric contraction (MVIC) tests, a Chronojump force sensor kit (Chronojump-Boscosystem, Barcelona, Spain) with a maximum capacity of 500 kg was employed. The force samples were recorded at a frequency of 80 Hz and recorded in a text file for subsequent data analysis (Figure 2.2). To conduct the impedance spectroscopy analysis of the electrodes, a Keysight (Agilent/HP) 4284A Precision LCR Meter, which has a frequency range of 20 Hz to 1 MHz, in conjunction with a Keysight (Agilent/HP) 16047C test fixture was used. A custom LabVIEW program was developed to allow the selection of measurement parameters and frequencies. This program was set to RX mode to measure the resistance (R) and reactance (X) of the load at specified frequencies. The data collected were automatically saved to a text file for subsequent impedance analysis.



Figure 2.2: Illustration of the experimental setup for the isometric knee extension task using pants embedded with textile electrodes. Details concerning the different components and procedures are provided in the text of the manuscript.

2.2.3 Experimental Protocol

2.2.3.1 Comfort, Consistency, and Efficiency Tests

Each participant underwent two separate sessions, spaced at a minimum interval of 48 hours. One session involved the use of textile electrodes with lotion, while the other used hydrogel electrodes. The order of electrode types was randomized. Participants were positioned on an adjustable-height bed, ensuring that their popliteal fossa (the area behind the knee) was in contact with the edge of the bed, their thigh was parallel to the ground, and their feet were suspended in the air, lacking contact with the ground. The knee joint angle

was fixed at 90°, and a cushioned backrest was used to achieve a posterior inclination of 115° (Figure 2.2).

At the beginning of each session, participants were introduced to the testing procedure. This included familiarizing them with the perceptions of burning sensation and maximum tolerable intensity induced by electrical stimulation. To avoid muscle fatigue in the dominant leg, this familiarization was conducted on the non-dominant leg using the corresponding type of electrode. In sessions involving textile electrodes, moisturizing lotion was applied to the participant's skin before they donned the garments. During the test, a train of pulses was initiated at a PA of 15 mA, with a frequency of 40 Hz and a PW of 400 µsec. The PA was manually increased by the experimenter until the participant reached a burning sensation intensity (BSI) and subsequently, maximum tolerable painful intensity (I_{MAX}). BSI (mA) was defined as the minimum intensity at which the participant felt a burning sensation on the skin beneath the electrode. The I_{MAX} (mA) was defined as the maximum tolerable stimulation intensity for the subject, indicating the point beyond which the pain becomes intolerable. This test was repeated at least twice to ensure the participant could confidently identify both burning sensation and maximum tolerable intensities.

After transitioning to the dominant leg for the main test, we began with the MVIC test. Participants performed three consecutive 5-second MVIC trials of knee extension using the dominant leg, with a 55-second rest interval between each trial. The average value of these three tests was calculated as the MVIC (N.m). Participants were not permitted to view the measurements, were instructed to keep their arms crossed over their chests, and received verbal encouragement during the test. Following a 5-minute rest, the corresponding electrodes were set up. In the case of textile electrodes, moisturizing lotion was applied. We then administered a sequence of electrical pulses consisting of 5-second stimulation and 5-second rest periods. The parameters were as follows: PW = 400 µsec, frequency = 40 Hz, and an initial PA of 15 mA. The pulse amplitude automatically increased by 3 mA after each 5-second rest period for the subsequent train of pulses until the participant reached the BSI (mA), at which point the stimulation stopped. This procedure was repeated at 10, 20,

30, and 40-minute intervals. However, for the final trial, the stimulation continued until the I_{MAX} (mA) was achieved. Thus, at the end of each session, we obtained five BSI (mA) values and one I_{MAX} (mA) value. Throughout the electrical stimulation tests, participants were instructed to remain relaxed and passive to minimize the impact of volitional torque.

Both types of electrodes were identical in size and were consistently positioned on the same skin area for each subject. To ensure accurate replication of their placement with the other set of electrodes, pictures, and measurements of the electrode positions relative to body landmarks were taken. To maintain matched electrode pressure across both sessions for each subject, we adopted the following methodology: For sessions involving hydrogel electrodes, the electrodes were first placed on the subject's skin. The garments were then worn to simulate the condition of the textile electrode. Straps equipped with Velcro tapes were subsequently wrapped around both proximal and distal electrodes (visible from the outer surface of the garment) to secure them. The tightness of the straps was adjusted to ensure comfort and to avoid excessive pressure on the muscles. This tightness was matched between the two sessions for each subject based on the starting and ending positions of the strap around the leg. These measurements and strap sizes were documented to replicate the electrode pressure from the first session to the second session.

2.2.3.2 Electrical Impedance Spectroscopy Test

Electrical impedance spectroscopy was used to evaluate the conductivity behavior of the developed textile electrode, both with and without lotion, and to compare these results with those from self-adhesive hydrogel electrodes. The subject for this analysis was a healthy 30-year-old male who had previous experience with FES. The measurements were carried out at frequencies of 20, 40, 60, 80, 100, and 1000 Hz, using sinusoidal alternating current (AC) input signals of 1 Volt (RMS). To ensure accuracy and consistency, the measurement was repeated five times at each frequency. The setup for electrode placement and the overall experimental procedure were identical to those used in the previous section tests, but with a key difference: all three tests (textile electrode without lotion, textile electrode with

lotion, and self-adhesive-hydrogel electrode) were performed on the same day. To eliminate potential interference in subsequent tests, the skin was cleansed with 75% isopropyl alcohol and dried with tissue before each test. Additionally, a two-hour break was scheduled between each test. Impedance spectroscopy was conducted twice for each electrode test: once before the test began and again approximately 40 minutes later, immediately after the test was completed. The ambient temperature was maintained at approximately 22°C during the tests to eliminate any potential bias related to sweating conditions.

2.2.4 Data Analysis and Statistics

The recorded data were analyzed using Microsoft Excel (Microsoft Corporation, USA) and MATLAB R2023a (MathWorks, Natick, USA) to assess the comfort, temporal consistency, stimulation efficiency, and impedance for textile and hydrogel electrodes.

To evaluate comfort, we compared the I_{MAXS} (mA) and average BSIs (mA) for each participant across the two types of electrodes. For assessing temporal consistency, we calculated the slope of a linear regression model using BSI values (mA) as the dependent variable and repetitions (minutes) as the independent variable during each participant's sessions, with 5 data points per session. Consequently, each participant had two slopes representing temporal consistency: one for the session using textile electrodes with lotion and another for the session using hydrogel electrodes.

To assess the stimulation efficiency of the electrodes, the minimum intensity required to evoke active torque (I_{min}) was measured. The I_{min} (mA) was defined as the minimum intensity needed to generate torque exceeding the average baseline torque by more than three standard deviations. For each session, five I_{min} values were detected (corresponding to 0, 10, 20, 30, 40 minutes intervals). Moreover, the average active torques produced over each 5 seconds periods of stimulation during the last trial (after 40 minutes) were calculated. To provide same number of data points between the tests with different electrode types for each participant, the average active torques were calculated for intensities from 21 (mA) up to the smaller I_{MAX} (mA). The average active torques for each participant were normalized

by the corresponding MVIC to be comparable between different participants.

For electrical impedance spectroscopy, at first the absolute impedance ($k\Omega$) was calculated from resistance and reactance at the specified frequencies using the following equation:

$$|Z| = \sqrt{R^2 + X^2} \quad (2.1)$$

For comparative analysis, the average and standard deviation of absolute impedances were calculated, using five recorded values for each frequency. Subsequently, these average values at different frequencies were compared across three electrode types: textile without lotion, textile with lotion, and hydrogel electrodes, both before and after the tests.

To confirm the assumption of normality, the Shapiro-Wilk test was applied to the distribution of the difference vectors for corresponding parameters in the tests performed with different electrode types. If the p-value was greater than 0.05 (normality was confirmed), the two-tailed paired t-test (parametric test) was employed to identify any differences. Otherwise, the Wilcoxon signed-ranked test (non-parametric test) was applied. The p-values and d-values (Cohen's d) were used to indicate the significance and effect size of parametric tests. The p-values and r-values (Z-score divided by the square root of sample size) were used for the same purpose in non-parametric tests. In this study, a p-value lower than 0.05 indicates statistical significance.

In the box-and-whisker plots, the lower and upper edges of the box represent the first quartile (Q1), and third quartile (Q3), respectively. The center line of the box indicates the median value (Q2). An outlier is characterized as a data point that deviates by more than 1.5 times the interquartile range ($IQR = Q3 - Q1$) from either the lower or upper edge of the box. The whiskers extend to the most extreme data points not considered outliers. The outliers are included in the statistical tests.

2.3 Results

2.3.1 Comfort, Consistency, and Efficiency Tests

Figures 2.3a and 2.3b showcase the generated torque as a percentage of MVIC for all repetitions (after 0, 10, 20, 30, and 40 minutes) with respect to time (seconds) and PA (mA) for P1 in hydrogel and textile electrode with lotion sessions, respectively.

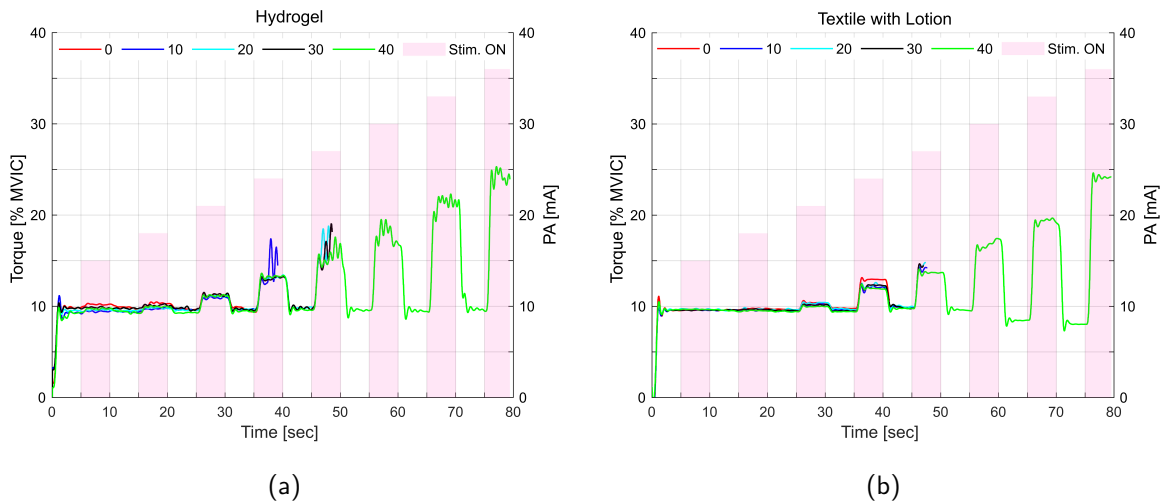


Figure 2.3: Torque as a percentage of maximum voluntary isometric contraction (%MVIC) across multiple repetitions at time intervals of 0, 10, 20, 30, and 40 minutes from the commencement of the test. Different colors distinguish these repetitions. The data is presented concerning time (seconds) on the x-axis, utilizing (a) hydrogel electrodes and (b) textile electrodes with lotion for one participant (P1). The right axis of each figure illustrates pulse amplitude (PA) during 5-second active stimulation intervals (Stim. ON) denoted by pink-shaded columns.

2.3.1.1 Comfort

In Figure 2.4a, two box-and-whisker plots illustrate the average BSIs (mA) for all participants and their variation between the two electrode types. During hydrogel electrode sessions, the average BSI had a mean value of 42.6 ± 15.6 mA, a median of 38.40 mA, Q1 of 31.8 mA, Q3 of 48 mA, and ranging from 23.4 mA to 73.2 mA. In textile electrode ses-

sions, the average BSI showed a median of 40.5 mA, Q1 of 28.8 mA, Q3 of 46.8 mA, and a range from 25.2 mA to 77.4 mA. Statistical analysis using a Wilcoxon signed-rank test indicated no statistically significant difference between the hydrogel and textile electrodes concerning average BSIs (p -value = 0.557, r = 0.186).

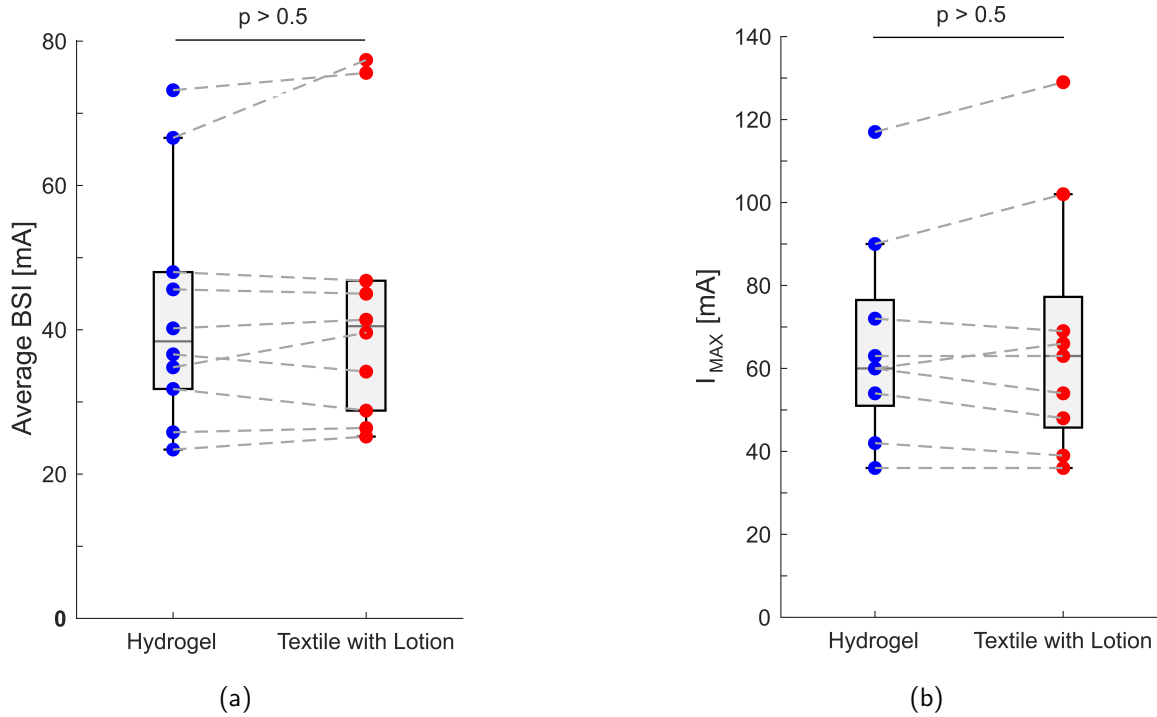


Figure 2.4: Box-and-whisker plots of (a) average burning sensation intensity (BSI) for each participant ($n = 10$) and (b) maximum tolerated intensity (I_{MAX}) ($n = 9$) using both hydrogel electrodes and textile electrodes with lotion. One participant was excluded from the second analysis on I_{MAX} due to muscular spasms.

Moving to 2.4b presents two box-and-whiskers plots illustrating the I_{MAXS} (mA) for nine participants and their variations between the two electrode types. I_{MAXS} were analyzed for nine participants as P10 requested to discontinue the final repetition with textile electrodes due to a painful muscular spasm before reaching the I_{MAX} threshold. During hydrogel electrode sessions, the I_{MAX} had a mean value of 66 ± 23.4 mA, a median of 60 mA, Q1 of 51 mA, Q3 of 76.5 mA, and ranged from 36 mA to 117 mA. In textile electrode sessions, it had a mean value of 67.3 ± 28.6 mA, with a median of 63 mA, Q1 of 45.8 mA,

Q3 of 77.3 mA, and ranged from 36 mA to 129 mA. A paired t-test found no significant difference between the hydrogel and textile electrodes with respect to I_{MAXS} (p-value = 0.586, $d = 0.189$).

2.3.1.2 Temporal Consistency

Figures 2.5a and 2.5b display the linear regression models between BSIs for each participant during hydrogel and textile electrode sessions, respectively. In these figures, each subject is represented by a color.

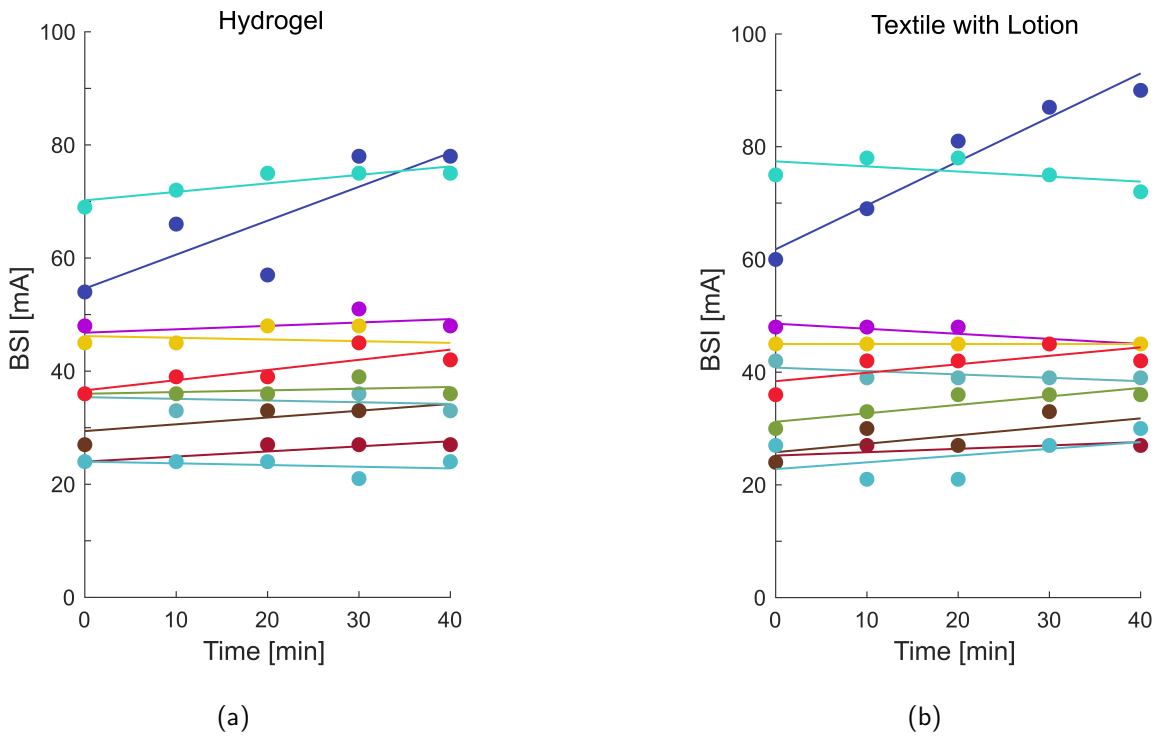


Figure 2.5: Linear regression models of burning sensation intensity (BSI) points ($n = 5$) for each participant ($n = 10$) across multiple repetitions at time intervals of 0, 10, 20, 30, and 40 minutes from the commencement of the test. Each participant is presented with a specific color. The data is presented concerning repetition time intervals (min) on the x-axis, utilizing (a) hydrogel electrodes and (b) textile electrodes with lotion.

In Figure 2.6, two box-and-whiskers plots illustrate the slope of BSIs (mA/min) for all participants and their variation between the two electrode types. The slope of the linear

regression model for the hydrogel electrode had a median of 0.075, Q1 of -0.03, Q3 of 0.6, and ranging from -0.03 to 0.6, while for the textile electrode, the slope of the regression line had a median of 0.09, Q1 of -0.06, Q3 of 0.15, with a range from -0.09 to 0.78. Conducting a Wilcoxon-signed rank test, we found no significant difference between the slopes of subjects across the two electrode types (p -value = 0.919, r = 0.032).

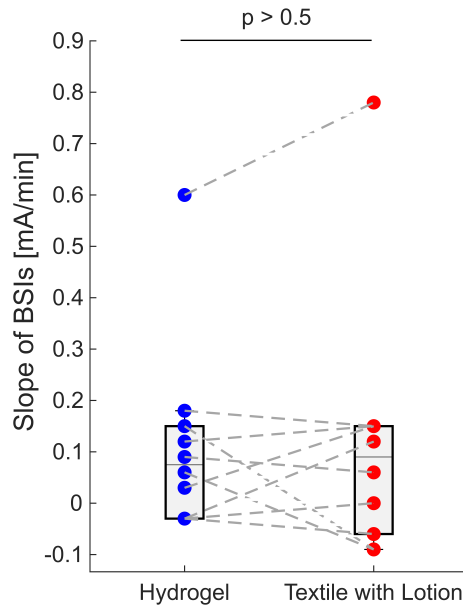


Figure 2.6: Box-and-whiskers plots of the slope of BSIs regarding electrode types.

2.3.1.3 Efficiency

In Figure 2.7a, two box-and-whisker plots illustrate the average I_{\min} s (mA) for all participants and their variation between the two electrode types. During hydrogel electrode sessions, the average I_{\min} had a median of 24 mA, Q1 of 19.2 mA, Q3 of 25.2 mA, and ranged from 17.4 mA to 26.4 mA. In textile electrode sessions, it had a mean value of 23.6 ± 3.6 mA, median of 23 mA, Q1 of 20.4 mA, Q3 of 26.4 mA, and ranged from 19.8 mA to 30 mA. A paired t-test found no significant difference between the hydrogel and textile electrodes with respect to average I_{\min} s (p -value = 0.500, d = 0.222).

To elucidate the relationship between the average active torque (%MVIC) and the stimulation intensity (mA) for each type of electrode, linear regression models were generated

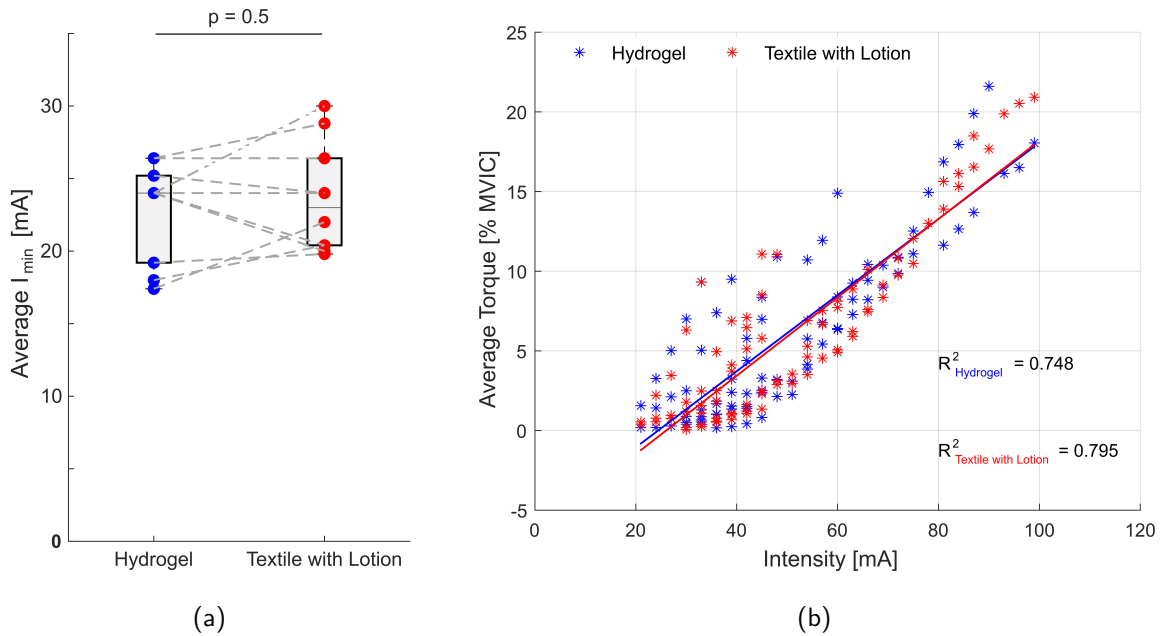


Figure 2.7: a. Box-and-whisker plots of average minimum intensity required to evoke torque (I_{\min}) for each participant ($n = 10$) using hydrogel electrodes (blue) and textile electrodes with lotion (red). b. Linear regression models of Average Torque [%MVIC] = $a + B \cdot \text{Intensity [mA]}$ for hydrogel electrodes (blue) and textile electrodes with lotion (red) extracted from the final trial (after 40 minutes). The number of data points for each electrode type is equal ($n = 84$).

(Figure 2.7b). The outcomes of these models are detailed in Table 2.2. The R^2 values for the hydrogel electrode and the textile electrode with lotion were 0.748 and 0.795, respectively. Both models demonstrated that stimulation intensity is a significant predictor of average active torque.

Additionally, a combined model incorporating all data points and including electrode type as a categorical variable was generated (Table 2.3). This combined model yielded an R^2 of 0.772. The F-statistic for stimulation intensity was notably high (540.97) with an extremely small p-value ($3.3753e-53$), confirming its role as a highly significant predictor of average active torque. Conversely, the F-statistic for electrode type was very low (0.25654) with a non-significant p-value (0.61321), indicating that electrode type alone does not have a significant impact on average active torque. The interaction term also had a low F-statistic (0.10978) and a non-significant p-value (0.74083), suggesting that the in-

teraction between stimulation intensity and electrode type does not significantly influence average active torque. In other words, the effect of intensity on the average active torque does not differ significantly between the two electrode types.

Table 2.2: Coefficients of linear regression model of Average Torque [%MVIC] = a + B*Intensity [mA] for each electrode.

Electrode Type	Coefficients	Estimate	SE	tStat	p-value
Hydrogel	a	-5.8322	0.8447	-6.9044	1.0824e-09
	B	0.23894	0.015494	15.422	1.1115e-25
Textile	a	-6.3916	0.76012	-8.4087	1.2763e-12
	B	0.24585	0.013942	17.633	2.735e-29

Table 2.3: Analysis of variance of linear regression models of Average Torque [%MVIC] = Intensity [mA] * Electrode Type.

Variables	SumSq	DF	MeanSq	F	p-value
Intensity	3757.3	1	3757.3	540.97	3.3753e-53
Electrode Type	1.7818	1	1.7818	0.25654	0.61321
Intensity : Electrode Type	0.7625	1	0.7625	0.10978	0.74083
Error	1111.3	160	6.9455	-	-

2.3.2 Electrical Impedance Spectroscopy Test

Figure 2.8 depicts the mean of absolute impedance values ($k\Omega$) for tests conducted using textile electrodes (both with and without lotion) and hydrogel electrodes at various frequencies (20, 40, 60, 80, 100, and 1000 Hz), measured both before and after the tests, with approximately 40 minutes in between. The standard deviation was negligible since the measurement was performed on one subject.

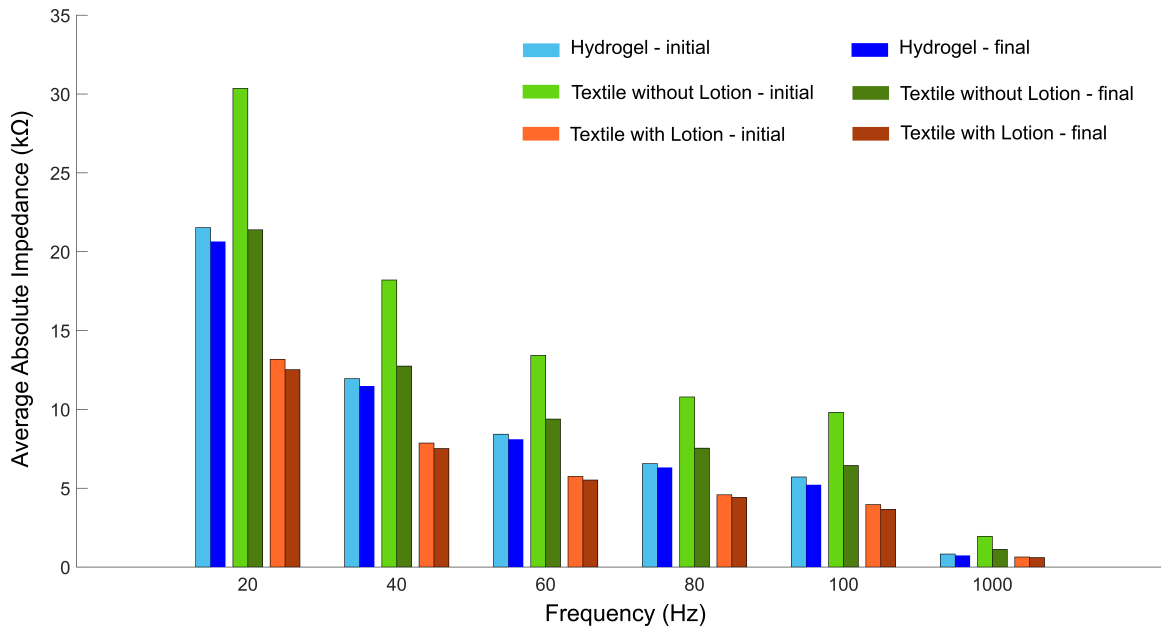


Figure 2.8: Average absolute impedance values ($k\Omega$) for tests conducted on one participant with hydrogel electrodes (blue), textile electrodes without lotion (green), and textile electrodes with lotion (orange) at various frequencies (20, 40, 60, 80, 100, and 1000 Hz). Measurements were taken both before (initial) and after (final) the tests, with approximately 40 minutes in between.

2.4 Discussion

This study explored the performance of a novel garment embedded with textile electrodes for neuromuscular electrical stimulation regarding comfort, temporal consistency, efficiency, and electrical impedance. For comparative analysis, a self-adhesive hydrogel electrode, commonly used in clinical settings served as a benchmark. Our garment, in combination with moisturizing lotion, enough for epidermal hydration, showed no statistically significant difference compared to self-adhesive hydrogel electrodes of similar shape and size under identical pressure regarding the proposed metrics during isometric knee extension exercise. One of the primary limitations associated with hydrogel electrodes is their disposability, non-washability, and hygienic challenges. In this study, we employed new hydrogel electrodes, whereas the garments embedded with textile electrodes had been used at least five times and washed once prior to the tests. This distinction underscores the

significant importance of the developed garments with textile electrodes, as they not only retain the benefits of hydrogel electrodes but also overcome their limitations.

In this study, we utilized electrical impedance spectroscopy to analyze the electrode-skin interface, with a specific focus on the impact of time (before and after a 40-minute session) and electrode type (textile without lotion, textile with lotion, and hydrogel) on conductivity changes. Across all types of electrodes, a general trend of decreasing absolute impedance values was observed with increasing frequency, from 20 to 1000 Hz. The textile electrode with lotion and hydrogel electrode exhibited lower absolute impedance values compared to the textile electrode without lotion. This analysis is pivotal particularly for stroke patients, as the impedance of electrode-skin interface is a key determinant of stimulation comfort [87]. Excessive impedance levels can lead to discomfort, such as a burning sensation beneath the electrodes at lower intensities, potentially limiting the electrode's effectiveness in achieving the desired level of muscle contraction.

The average absolute impedance values were lower after the tests compared to those recorded before the tests. Specifically, at 40 Hz, a commonly used stimulation frequency in literature, the average absolute impedance for the hydrogel electrode decreased from 11.95 (k Ω) before the test to 11.48 (k Ω) after the test (a decrease of 3.93%). For the textile electrode with lotion, the average absolute impedance reduced from 7.87 (k Ω) before the test to 7.52 (k Ω) after the test (a decrease of 4.41%). The textile electrode without lotion showed a significant decrease in impedance, from 18.21 (k Ω) before the test to 12.75 (k Ω) after the test (a decrease of 29.99%). These findings suggest superior impedance consistency in hydrogel electrodes and textile electrodes with lotion, compared to those without lotion. This is particularly noteworthy considering that in previous research [89], where water was used to moisten textile electrodes, impedance increased over time, leading to discomfort after 16 minutes of stimulation. While all electrode types exhibited a reduction in impedance, the textile electrodes without lotion showed an approximately tenfold greater decrease compared to the others, highlighting their inconsistent temporal behavior. We believe that the tenfold decrease in impedance can be attributed to the effect of perspiration, which, after

40 minutes, enhances the interface, thereby approaching the immediate efficacy observed with lotion application. The results suggest that the application of moisturizing lotion can significantly enhance the conductivity of the textile electrode-skin interface. Unlike water, lotion does not require frequent reapplication; a single application per session suffices. Given the amount needed for each application, it avoids creating a sensation of wetness both during and after the test.

This study was initially planned to compare all three types of electrodes. However, due to painful contractions experienced when using textile electrodes without lotion, and based on the results of spectroscopy analysis, our primary protocol was adjusted. We focused on a cohort of ten subjects to assess comfort, consistency, and efficiency, limiting the comparison to textile electrodes with lotion and hydrogel electrodes. The comparative results indicated no significant difference between the textile electrode with lotion and the hydrogel electrode in terms of motor threshold intensity, the intensity at which subjects experienced a burning sensation and maximum tolerable intensity. These results hold significant importance, as an effective electrode should facilitate strong contractions while minimizing discomfort. The burning sensation experienced during electrode use primarily stems from uneven contacts at the electrode-skin interface. This unevenness leads to an inhomogeneous flux of current across small areas of the skin, resulting in the early activation of pain-sensing $A\delta$ fibers [87], [45].

While previous studies [87] have employed various subjective sensations such as tingling, aching, and stinging as evaluative metrics at the same time, the precise definition and identification of these sensations present a challenge and can be confusing for subjects. Although this issue also pertains to the measurement of burning sensation intensity in our protocol, we believe that determining and detecting the maximum tolerable painful intensity appears to be more straightforward. In this study, we aimed to streamline the evaluation process by minimizing the reliance on subjective sensations, thereby simplifying and clarifying the testing procedure. This approach is particularly pertinent considering the intended application of the final product for patients with neurological disorders, who

may experience verbal and cognitive difficulties. The use of simpler and more straightforward protocols is especially advantageous in such contexts, ensuring more accessible and reliable assessment methods.

In this study, we meticulously ensured uniform testing conditions across different electrode types to obtain comparable results. These standardized conditions included the size, shape, and placement of the electrodes, as well as the ambient temperature and the pressure applied to each electrode's surface for every subject. Simulating pressure and sweating conditions comparable to those of textile electrodes was achieved by using hydrogel electrodes with garments as well as Velcro straps of identical lengths around the electrodes during both sessions. Additionally, to minimize external influences on the data, subjects were instructed to remain silent and focused during testing. It was observed during initial tests that engaging in concurrent activities, such as using mobile phones or talking, could impact the results. Another critical aspect of our methodology was the protocol familiarization on the non-dominant side, which was intended to ensure that the measurements were taken on non-fatigued muscles, thereby enhancing the accuracy of our findings.

The principal limitation of this study is its exclusive reliance on healthy subjects, rather than including individuals with neurological conditions. This selection has significant implications, particularly in the measurement of force output. Healthy subjects are capable of providing volitional torques, especially at higher stimulation intensities (due to pain), which may not be representative of responses in individuals with neurological impairments. Consequently, our analysis primarily focused on the motor threshold intensity, occurring at low intensities, as a measure of stimulation efficiency. This reliance limited our ability to investigate the effects of higher intensities on force production. Future research should address this gap by incorporating a diverse participant group, including those with neurological conditions such as SCI and stroke, to fully understand the range of responses to neuromuscular electrical stimulation and to enhance the generalizability of our findings.

A notable limitation of the study protocol was the inability to blind participants to the types of electrodes used. This aspect could introduce a form of bias, particularly if subjects

had pre-existing preferences or perceptions about the different electrode types. Such biases might influence their subjective experience and feedback during the study, potentially affecting the reliability of the results in terms of perceived comfort. Future studies could benefit from incorporating a double-blind design, where neither the participants nor the researchers know which electrode type is being used, to minimize this potential source of bias and enhance the validity of the findings.

This study specifically targeted the quadriceps femoris muscle group, which, due to its large size, necessitates the use of relatively large electrodes. However, it is important to note that prior research has indicated that smaller electrodes induce greater discomfort due to higher current density. This is a critical consideration as smaller electrodes are essential for achieving selective muscle stimulation and reducing muscle fatigue. Consequently, these findings underscore the need for further experiments involving smaller electrodes. Such studies would not only address the aspect of comfort with different electrode sizes but also evaluate the effectiveness of stimulation in smaller muscle groups, thereby contributing to a more comprehensive understanding of neuromuscular electrical stimulation using textile electrodes.

It is important to acknowledge that the scope of this study was confined to isometric conditions. As such, it does not offer insights into the comparative performance of textile electrodes versus hydrogel electrodes during dynamic activities, like cycling and walking. Recognizing this gap, our future research will specifically focus on evaluating the performance of textile electrodes in dynamic scenarios.

2.5 Conclusion

This comprehensive study presents a detailed analysis of the performance and application of textile electrodes embedded in garments for neuromuscular electrical stimulation, particularly focusing on their use in stroke, MS, and SCI rehabilitation. By juxtaposing these textile electrodes against conventional self-adhesive hydrogel electrodes, the study

delves into key aspects such as stimulation comfort, temporal consistency, efficiency, and electrical impedance behavior under isometric conditions. The research demonstrates that textile electrodes, when used with a moisturizing lotion, exhibit similar levels of comfort, consistency, and efficiency to hydrogel electrodes, evident in parameters like motor threshold intensity, burning sensation intensity, and maximum tolerable intensity. The research methodology ensured standardized testing conditions, bolstering the reliability of the findings. The study's findings are promising for the application of textile electrodes in motor rehabilitation, enhancing patient compliance and therapy outcomes. Future studies should include individuals with neurological conditions to understand the full spectrum of responses to neuromuscular electrical stimulation and enhance the generalizability of findings.

Chapter 3

Efficacy of High versus Moderate-Intensity SDSS in Subjects with Spinal Cord Injury – an Isometric Study

Abstract

For producing isometric contractions, spatially distributed sequential stimulation (SDSS) was proven to be better than the traditional functional electrical stimulation (FES) that uses a single electrode stimulation (SES) in terms of fatigue-reducing ability and the power output produced by the muscle. However, the influence of the stimulation parameters (mainly stimulation intensity) on the effectiveness of SDSS is not well understood. The aim of this work is to scientifically compare the fatigue-reducing capabilities of SDSS at high and moderate electrical stimulation intensities in individuals with spinal cord injuries (SCI). Two experiments were conducted, involving isometric contractions of the quadriceps muscle group (Experiment 1) and the vastus lateralis muscle (Experiment 2). The effectiveness of high-intensity SDSS was compared to moderate-intensity SDSS, with SES serving as a reference. Seven SCI subjects with lower-limb motor-complete participated in the study. Fatigue measurements, including time to fatigue (TTF) and force-time integral (FTI), were analyzed for both intensity levels. Statistical analysis revealed that moderate-intensity SDSS applied to the quadriceps muscle group significantly increased TTF and force output compared to high-intensity SDSS. These findings offer valuable scientific insights into the practical applications of SDSS, such as FES cycling, and contribute to a better understanding of its mechanisms in reducing muscle fatigue.

3.1 Introduction

Functional electrical stimulation (FES) is a method used to activate paralyzed skeletal muscles to perform functional tasks. FES and the benefits of FES exercise are explained in greater detail in Section 1.5. In the following chapter, conventional functional electrical stimulation that employs one cathode electrode placed over the motor point of the stimulated muscle will be referred to as FES using a single electrode stimulation (SES).

Maintaining high output force levels for a prolonged period of time is necessary for performing functional tasks such as walking, cycling and rowing. However, a major limitation of SES is the rapid onset of muscle fatigue resulting in the decline in force produced by the stimulated muscles. Voluntary muscle contractions are achieved by recruiting motor units based on their size, from smaller axons that innervate slow fatigue-resistant muscle fibers, to larger axons innervating fast easily fatigable muscle fibers [18]. As the size of an axon defines the axon's activation threshold, low-level electrical stimulation is more likely to activate larger axons resulting in an earlier onset of muscle fatigue. Additionally, conventional electrical stimulation (SES) uses rather large transcutaneous electrodes (5x5 cm² or larger) located over the same motor units activating them with every stimulation pulse whereas, during voluntary contractions, motor units are randomly activated at lower frequencies, resulting in longer periods of rest for each motor unit. A more detailed explanation of the limitations of the technology is provided in Section 1.5.

By mimicking voluntary contractions, SES-induced muscle fatigue can be reduced by distributing the stimulation across multiple smaller electrodes that cover different motor points. Each electrode activates different motor units at a lower frequency than standard SES activation while maintaining a strong fused contraction of the muscle. This method was shown to be effective at reducing muscle fatigue when the electrodes are placed over different synergistic muscle bellies (sum of muscle fibers) [106]–[109] or over the same muscle belly [78], [110]–[119]. The latter approach, termed spatially distributed sequential stimulation (SDSS), delivers the pulses through four small closely spaced electrodes

placed identically over the same location of the SES electrode setup. Individual electrodes stimulate at one-fourth of the typical SES frequency (10-15Hz) with an implemented 90° phase shift between the electrodes.

Higher fatigue resistance of SDSS compared to SES was shown when performing isometric contractions of the quadriceps muscle group in subjects with SCI [111], [113], [120]. A similar electrode setup was chosen in all three studies, a 2x2 matrix of 4.5 x 2.5 cm² electrodes placed over the belly of the entire quadriceps muscle groups. Similar results were reached in the studies using SDSS to perform a dynamic knee extension task in able-bodied [115] and SCI subjects [118]. In both cases, the 2x2 matrixes of 4.5 x 2.5 cm² electrodes were placed as close as possible to the motor points of m. vastus medialis and m. vastus lateralis. However, in two recent studies [121], [122], a significant difference in fatigue resistance of the SDSS was not observed. One of the possible reasons for this is the higher intensity used during the experiment. Although the fatigue-reducing ability of SDSS compared to SES was shown in paralyzed muscles with different electrode configurations, none of the studies have purposefully investigated the effect of the stimulation parameters, such as the higher stimulation intensity alluded to above. One hypothesis is that since the electrodes are closely spaced with SDSS, it is reasonable to assume that with the increase of the stimulation intensity, electric fields created by each electrode overlap over a larger area activating a greater number of muscle fibers more frequently, and thus diminishing the intended effect of SDSS. This effect was also noticed in a theoretical computational analysis of the electric fields generated by SDSS in a Tibialis Anterior muscle [123]. An overlap of the activated muscle fibers parallel to the electrodes increased with the stimulation intensity. This case differed from the experimental studies in that the simulation was performed on a smaller muscle and the stimulation intensity was limited to 60 mA.

The present study compares the fatigue-reducing ability of SDSS at high and moderate electrical stimulation intensities in subjects with motor-complete SCI. The effects of the stimulation strategies were assessed during isometric contractions of the quadriceps muscle groups (Experiment 1) and isometric contractions of the vastus lateralis muscles

(Experiment 2). The primary purpose of the study was to compare the effectiveness of high-intensity SDSS to moderate-intensity SDSS using SES as a reference. Although deduction can be made, the experiments were not designed to produce a direct comparison of SDSS and SES. The outcome of these experiments provides further insight into practical applications of SDSS (particularly FES-cycling due to the effect quadriceps muscles have on cycling performance) and hopefully a better understanding of the mechanisms behind SDSS.

3.2 Methods

3.2.1 Participants

Seven adult male subjects with lower-limb motor-complete spinal cord injury participated in the study. Five subjects had previous experience with FES of the studied muscles, four of which were undergoing FES-cycling strength training at the time of the study. In an effort to mitigate the effects of residual fatigue, all subjects were asked to refrain from using FES for at least 48 hours before the experiments were conducted. One subject (P6) was excluded from the study due to experiencing intense spasms during the test, despite receiving antispasmodic medication (Baclofen). All subjects met the inclusion criteria, which required a spinal cord injury spanning from cervical 4 to thoracic 12 spinal segments, no voluntary movement or pain sensation in the legs (ASIA A or B), and at least 12 months having elapsed since the injury. The exclusion criteria stipulated that the subjects must not have sustained lower limb fractures within the past year or have open wounds or rashes on the skin surface where the electrodes would be placed. Before participating in the experiments, participants were provided with a detailed description of the purpose and testing procedures. Each participant provided written informed consent. The project was approved by the local Institutional Review Board (NCT06421753) and conducted in accordance with the Declaration of Helsinki. More information about the participants is provided in [Table 3.1](#).

Table 3.1: Demographic characteristics of the participants.

Participants	Age (years)	Injury level	ASIA	Time after spinal cord injury (years)	FES naive	Current FES training
P1	46	C7 - C8	B	11	No	Yes
P2	30	C5 - C6	B	14	No	Yes
P3	59	T9 - T10	B	6	No	Yes
P4	59	C6 - C7	A	6	No	Yes
P5	62	C6 - C7	B	10	No	No
P6	49	T5 - T6	B	30	Yes	No
P7	38	C5 - C6	A	20	Yes	No

3.2.2 Instrumentation

Subjects were seated on a height-adjustable mat table with the posterior of the knee (Popliteal Fossa) in contact with the edge of the table and their thigh parallel to the ground. The angle of the knee joint was set to 90° and a cushioned backrest was used to achieve the posterior inclination of 115°. In cases where trunk control was insufficient, straps were employed to stabilize the torso. The table height was adjusted such that the foot sole could not touch the ground.

An 8-channel MotiMove stimulator (3F-Fit Fabricando Faber, Belgrade, Serbia) [105], controlled with a custom-made LabVIEW program (National Instruments, Austin, TX, USA), was utilized to produce asymmetric biphasic electrical pulses at a frequency of 48 Hz and a pulse width of 400 μ s. To distribute pulses in SDSS mode, an anti-fatigue unit (AFU) device (3F-Fit Fabricando Faber, Belgrade, Serbia) was connected to the cathode of one of the stimulation channels. The force produced by the stimulated muscle was measured with a force meter (Chronojump-Boscosystem, Barcelona, Spain) secured to the shank of the stimulated leg. The height of the mat table and the position of the sensor on the shank were measured to ensure identical experimental conditions between sessions. Force measurements were acquired with a frequency of 80 Hz and recorded in a text file

for subsequent data analysis. An illustration of the experimental setup is shown in Figure 3.1.

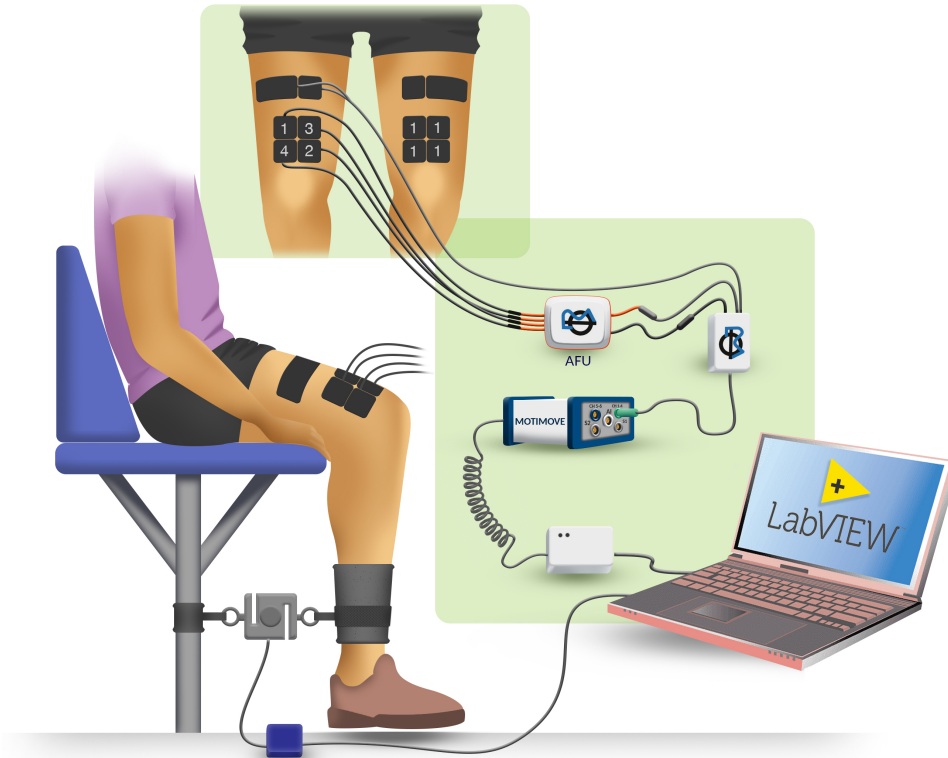


Figure 3.1: Illustration of the experimental setup for performing isometric muscle contractions to assess muscle fatigue using SDSS and SES electrode configurations. Details concerning the different components and procedures are provided in the text of the manuscript.

3.2.3 Electrode Configuration

Two types of experiments with different electrode configurations were conducted to compare the fatigue-reducing ability of SDSS at moderate and high electrical stimulation intensities. What we refer to as “Experiment 1” was conducted on the quadriceps muscle group while “Experiment 2” was performed on the vastus lateralis muscle. In all experiments, four self-adhesive surface electrodes (Compex Dura-Stick plus) were placed distally (cathodes) while the reference electrode (anode) was placed proximally. This electrode

configuration was chosen considering literature protocols [114] and the preliminary tests conducted during the study design phase. Before applying the electrodes, proximal and distal motor points of the rectus femoris (RF) and the vastus lateralis (VL) muscles were detected using the measured anatomic landmarks [104] and served as reference points for electrode placement. Motor points were marked with an indelible marker pen to ensure identical electrode placement across the sessions. Prior to electrode placement, the thigh skin was sanitized with an antiseptic spray to prevent skin irritation and ensure a clean surface.

In Experiment 1, the proximal electrode was made by connecting two electrodes to the anode of the same stimulation channel and thus creating an electrode with an effective surface area of $5 \times 14 \text{ cm}^2$. Electrodes used for the anode were a $5 \times 5 \text{ cm}^2$ electrode placed on the proximal motor point of the RF muscle and a $5 \times 9 \text{ cm}^2$ electrode placed laterally, between the proximal motor points of the RF and VL muscles, just to the side of the $5 \times 5 \text{ cm}^2$ electrode. Distal (cathode) electrodes, measuring $5 \times 5 \text{ cm}^2$, were placed distally (cathodes) in close proximity to each other, forming a 2×2 matrix just below the distal motor point of the RF muscle (see Figure 3.2a). Positions of the electrodes were confirmed or modified based on visual observations and gentle touch of the muscle contraction resulting from a short train of pulses sent to each electrode separately. In order to minimize fatigue, the pulses used were slightly above the motor threshold. The electrode configuration for Experiment 1 is shown in Figure 3.2a.

In Experiment 2, the proximal (anode) electrode ($5 \times 9 \text{ cm}^2$) was placed on the motor point of the VL muscle. Four independent distal (cathode) electrodes, with a surface area of $2.5 \times 4.5 \text{ cm}^2$ each, were placed around the distal motor point of the VL muscle. Similar to Experiment 1, the position of each electrode was tested separately and adjusted until the appropriate positioning was achieved. The electrode configuration for Experiment 2 is shown in Figure 3.2b.

In both Experiment 1 and 2, the described electrode configuration was used for both SDSS and SES. Unlike previous studies that have explored the topic of SDSS, in the SES

mode, all four distal electrodes were connected to the cathode of the same stimulation channel effectively forming a single large electrode (indicated in Figure 3.2 using electrode numeration 1,1,1,1). This was done to ensure that the electrode positioning and the area covered by the electrodes remained identical during SES and SDSS. Conversely, in the SDSS mode, each distal electrode was connected to a different output channel of the AFU device, thereby producing the SDSS effect (indicated in Figure 3.2 using electrode numeration 1,2,3,4).

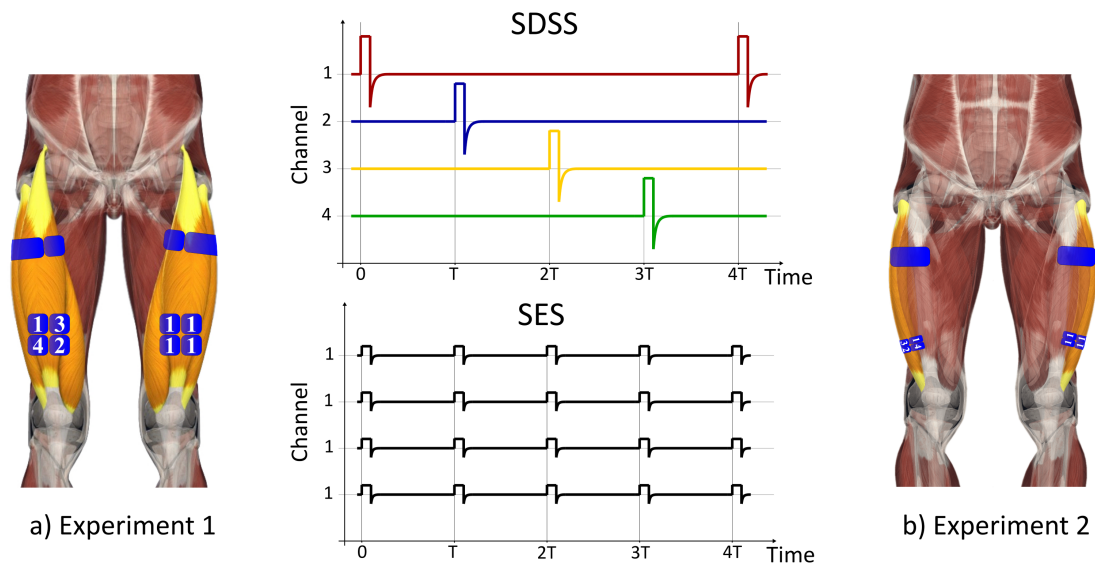


Figure 3.2: Schematics of electrode configurations for Experiment 1 and Experiment 2, together with typical electrical pulse trains for SDSS and SES protocols. In the graphs, electrode channels are labeled on the y-axis versus time (in arbitrary units) on the x-axis. The orange regions in the schematics correspond to the stimulated muscle groups. The proximal electrodes are colored blue while distal electrodes are colored blue and labeled with a number. Colors in the SDSS plots are to remind the reader that different electrodes (regions around the motor point) are activated at different times.

3.2.4 Experimental Protocol

All experiments were divided into two types of experimental sessions, one with high-intensity stimulation (order of 130 mA) and the other with moderate-intensity stimulation

(order of 70 mA) - the sequence of which was chosen at random for each subject tested. To eliminate the possibility of residual fatigue from previous experimental sessions, a minimum of 48 hours in between them was imposed. For each subject, before the first experimental session, SDSS was randomly assigned to one leg while SES was applied to the other leg. The chosen leg-stimulation arrangement was kept throughout all experimental sessions.

During the experiments, the pulse width was set to 400 μ s and the stimulation frequency was 48 Hz for SES and 12 Hz per channel for SDSS (composite frequency of 12 Hz x 4 = 48 Hz). Each experimental session began with determining the high and moderate stimulation intensities for the quadriceps muscle group (Experiment 1) or vastus lateralis muscle (Experiment 2) on a randomly selected leg. High and moderate stimulation intensities were calculated based on the muscle's motor threshold intensity (intensity at which the muscle produces a measurable force) and the force plateau intensity (intensity at which the muscle produces maximal force). Using the SDSS configuration, stimulation pulses were sent with increasing intensity while the output force was measured. Every second, the stimulation intensity was programmatically increased in increments of 5 mA from 0 mA to 130 mA (Experiment 1) or from 0 mA to 100 mA (Experiment 2). If the force plateau was observed, the corresponding intensity was chosen as the high intensity, otherwise, the maximum intensity of 130 mA (Experiment 1) or 100 mA (Experiment 2) was used. The moderate stimulation intensity was calculated as the mean value of the detected motor threshold intensity and the high stimulation intensity. After a 5-minute break, fatigue measurement was carried out by continuously applying the stimulation intensity (high or moderate) chosen for the experimental session using the configuration (SDSS or SES) assigned to the selected leg until the measured force fell under 70% of the maximum produced force (MPF) value.

Subsequently, using the SDSS configuration, high and moderate stimulation intensities were determined for the quadriceps muscle group (Experiment 1) or vastus lateralis muscle (Experiment 2) on the other leg. After a 5-minute break, fatigue measurement was carried out by applying the same stimulation intensity (high or moderate) using the other electrode

configuration (SES or SDSS). The entire process was repeated for the other experimental session by switching the stimulation intensity used during the fatigue measurements while maintaining the same leg-stimulation arrangement.

3.2.5 Data Analysis and Statistics

The forces recorded during each fatigue measurement were analyzed using MS Excel (Microsoft Corporation, Redmond, WA, USA) and MATLAB (MathWorks, Natick, MA, USA). Time to fatigue (TTF) was calculated as the time difference from the stimulation on-set to the moment the output force fell under 70% of the maximum produced force (MPF). The integral of the produced force over this period was termed force-time integral (FTI), and the ratio of FTI to TTF is given the term average produced force until fatigue (APF). The elicited outcome parameters are TTF, MPF, and APF. Any differences between using SDSS versus SES are calculated at the end of each experimental session using the following equations:

$$\%TTF_{\text{difference}} = 100 \times \left(\frac{TTF_{\text{SDSS}} - TTF_{\text{SES}}}{TTF_{\text{SES}}} \right) \quad (3.1)$$

$$\%MPF_{\text{difference}} = 100 \times \left(\frac{MPF_{\text{SDSS}} - MPF_{\text{SES}}}{MPF_{\text{SES}}} \right) \quad (3.2)$$

$$\%APF_{\text{difference}} = 100 \times \left(\frac{APF_{\text{SDSS}} - APF_{\text{SES}}}{APF_{\text{SES}}} \right) \quad (3.3)$$

As described in the previous section, the subjects participated in two types of experimental sessions, one with moderate intensity and the other with high intensity. The elicited outcome parameters were then classified into two groups based on the level of intensity for statistical analysis. To confirm the assumption of normality, the Shapiro-Wilk test was applied to the distribution of the difference vectors for corresponding parameters in the tests performed with different intensities. If the p-value was greater than 0.05 (normality was confirmed), the two-tailed paired t-test (parametric test) was employed to identify any

differences. Otherwise, the Wilcoxon signed-ranked test (non-parametric test) was applied. The p-values and d-values (Cohen's d) were used to indicate the significance and effect size of parametric tests. The p-values and r-values (Z-score divided by the square root of sample size) were used for the same purpose in non-parametric tests. In this study, a p-value lower than 0.05 indicates statistical significance.

In the box-and-whisker plots, the lower and upper edges of the box represent the first quartile (Q1), and third quartile (Q3), respectively. The center line of the box indicates the median value (Q2). An outlier is characterized as a data point that deviates by more than 1.5 times the interquartile range ($IQR = Q3 - Q1$) from either the lower or upper edge of the box. The whiskers extend to the most extreme data points not considered outliers. The outliers are included in the statistical tests. The whiskers extend from both upper and lower edges to include the extreme data points from the median but are not classified as outliers.

3.3 Results

3.3.1 Experiment 1

Figure 3.3a and Figure 3.3b depict the fatigue measurements of subject P3 for moderate electrical stimulation intensity (80 mA) and high electrical stimulation intensity (130 mA) conditions. These figures represent force (N) versus time (seconds) graphs. During the first experimental session, the subject underwent high-intensity testing where the left quadriceps muscle group was stimulated using the SES configuration and the right quadriceps muscle group was stimulated with the SDSS configuration. In the subsequent experimental session, the moderate electrical stimulation intensity was tested with the same electrode-leg-stimulation configurations (SES-Left quadriceps muscle group and SDSS-Right quadriceps muscle group). The horizontal black lines and shaded areas under the force-time curve represent TTF and FTI, respectively. Under moderate electrical stimulation intensity conditions, the TTF for SDSS and SES electrode configurations were 20.00 seconds and 11.47 seconds, respectively ($\%TTF_{\text{Difference}} = 74.37\%$), whereas, for high electrical stimulation

intensity, the TTF for SDSS and SES electrode configurations were 13.18 seconds and 10.34 seconds, respectively ($\%TTF_{\text{Difference}} = 27.47\%$). For moderate electrical stimulation intensity, the FTI for SDSS and SES electrode configurations were 636.26 N and 111.01 N, respectively ($\%APF_{\text{Difference}} = 228.70\%$). For high electrical stimulation intensity, the FTI for SDSS and SES were 836.03 N and 408.85 N, respectively ($\%APF_{\text{Difference}} = 60.42\%$).

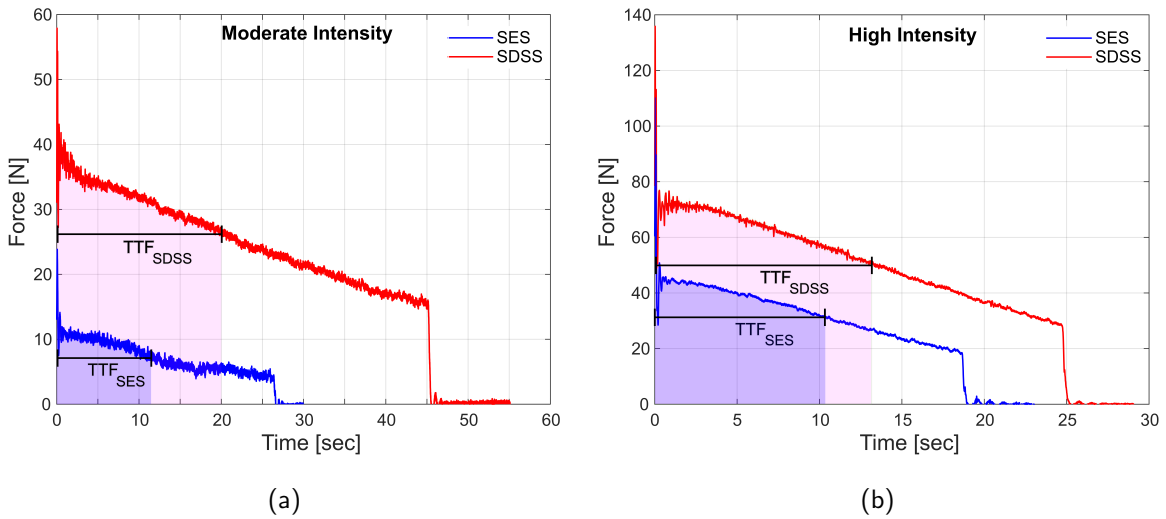


Figure 3.3: Measurements conducted on subject P3 of the force produced by the quadriceps muscle group (Experiment 1) stimulated with a) moderate electrical stimulation intensity (80 mA) and b) high electrical stimulation intensity (130 mA). Forces produced by the quadriceps muscle group stimulated with SDSS and SES electrode configurations are presented with red and blue lines, respectively. Horizontal black lines and shaded areas under the force-time curves represent TTF and FTI, respectively.

Figure 3.4a portrays the $\%TTF_{\text{Difference}}$ values for all subjects under moderate (indicated by blue circles) and high (indicated by red circles) electrical stimulation intensity conditions. The $\%TTF_{\text{Difference}}$ for moderate electrical stimulation intensity had a median of 118.83%, ranging from 51.90% to 262.44%, while the $\%TTF_{\text{Difference}}$ for high electrical stimulation intensity had a median of 40.28%, ranging from 9.84% to 110.28%. Statistical analysis reveals that the $\%TTF_{\text{Difference}}$ for moderate electrical stimulation intensity was significantly larger than that for the high electrical stimulation intensity tests (group mean \pm standard deviation, $135.01 \pm 71.10\%$ for moderate electrical stimulation intensity

and $48.17 \pm 32.37\%$ for high electrical stimulation intensity, Figure 3.4b, as determined by paired t-test ($p = 0.0065$, $d = 1.83$).

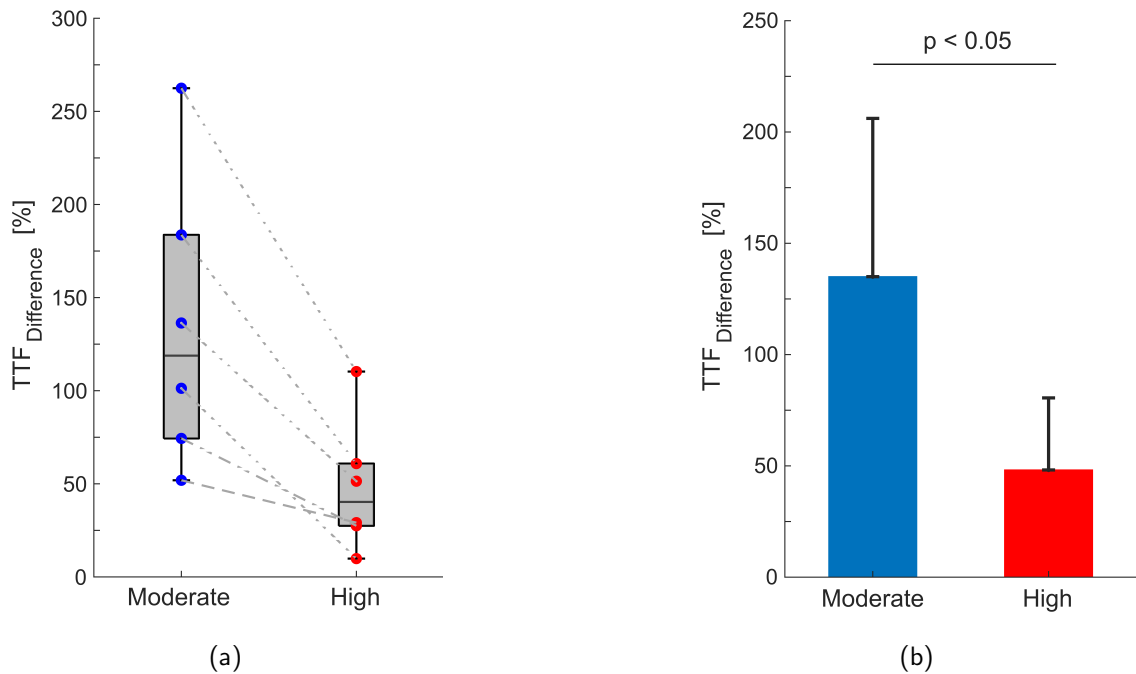


Figure 3.4: Summary of the results from Experiment 1 of %TTF_{Difference} values for the entire study group under moderate (colored blue) and high (colored red) electrical stimulation intensity conditions. In 3.4 a), the median %TTF_{Difference} values for the entire study group for moderate and high electrical stimulation tests are provided. The %TTF_{Difference} results for each subject are presented as a pair of blue (result from moderate electrical stimulation intensity test) and red (result from high electrical stimulation intensity test) circles connected with a dashed line. In 3.4 b) statistical analysis showing the group mean and the standard deviation for moderate and high electrical stimulation intensities is provided.

Figure 3.5a illustrates the %MPF_{Difference} values for all subjects under moderate (indicated by blue circles) and high (indicated by red circles) electrical stimulation intensity conditions. The %MPF_{Difference} for moderate electrical stimulation intensity had a median of 151.92%, ranging from 79.28% to 246.92%, whereas the %MPF_{Difference} for high electrical stimulation intensity had a median of 35.68%, ranging from 0.88% to 66.98%. The %MPF_{Difference} for moderate electrical stimulation intensity was found to be significantly

higher than that for high electrical stimulation intensity ($156.19 \pm 54.83\%$ for moderate electrical stimulation intensity and $34.95 \pm 28.60\%$ for high electrical stimulation intensity, Figure 3.5b, as determined by paired t-test ($p = 0.0023$, $d = 2.32$).

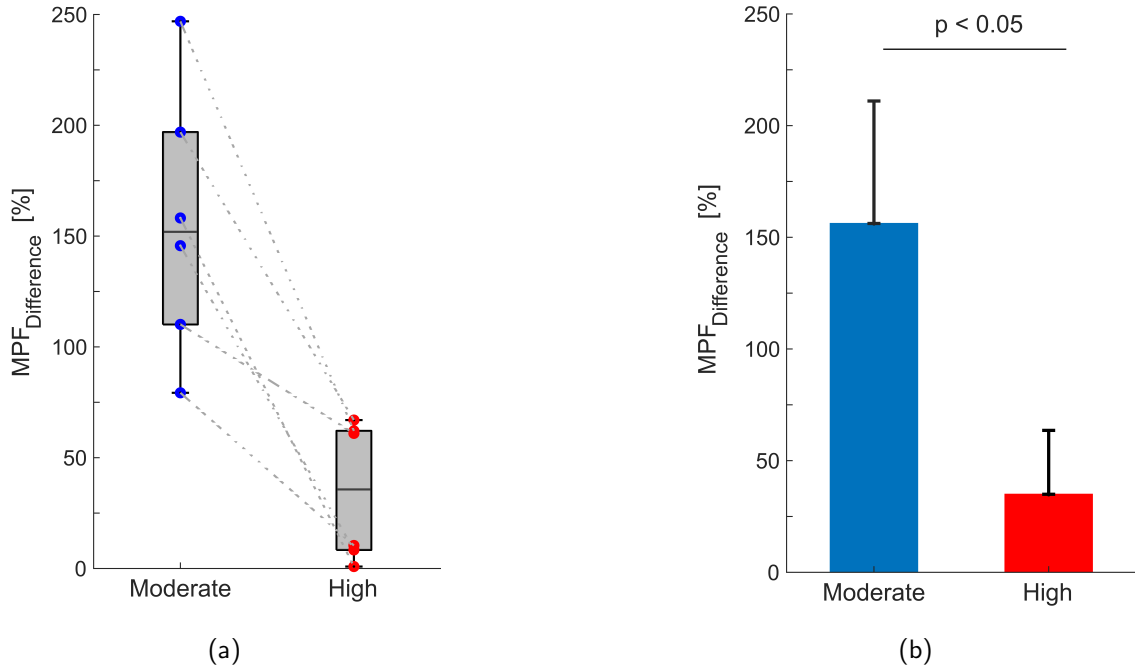


Figure 3.5: Summary of the results from Experiment 1 of $\%MPF_{\text{Difference}}$ values for the entire study group under moderate (colored blue) and high (colored red) electrical stimulation intensity conditions. In 3.5 a), the median $\%MPF_{\text{Difference}}$ values for the entire study group for moderate and high electrical stimulation tests are provided. The $\%MPF_{\text{Difference}}$ results for each subject are presented as a pair of blue (result from moderate electrical stimulation intensity test) and red (result from high electrical stimulation intensity test) circles connected with a dashed line. In 3.5 b) statistical analysis showing the group mean and the standard deviation for moderate and high electrical stimulation intensities is provided.

Figure 3.6a portrays the $\%APF_{\text{Difference}}$ values for all subjects under moderate (indicated by blue circles) and high (indicated by red circles) electrical stimulation intensity conditions. The $\%APF_{\text{Difference}}$ for moderate electrical stimulation intensity had a median of 149.73%, ranging from 80.08% to 228.70%, while the $\%APF_{\text{Difference}}$ for high electrical stimulation intensity had a median of 35.81%, ranging from 0.08% to 70.33%. The

$\%APF_{\text{Difference}}$ for moderate electrical stimulation intensity was significantly higher than that for high electrical stimulation intensity ($152.40 \pm 51.79\%$ for moderate electrical stimulation intensity and $35.48 \pm 28.53\%$ for high electrical stimulation intensity, Figure 3.6b, as determined by paired t-test ($p = 0.0022$, $d = 2.35$).

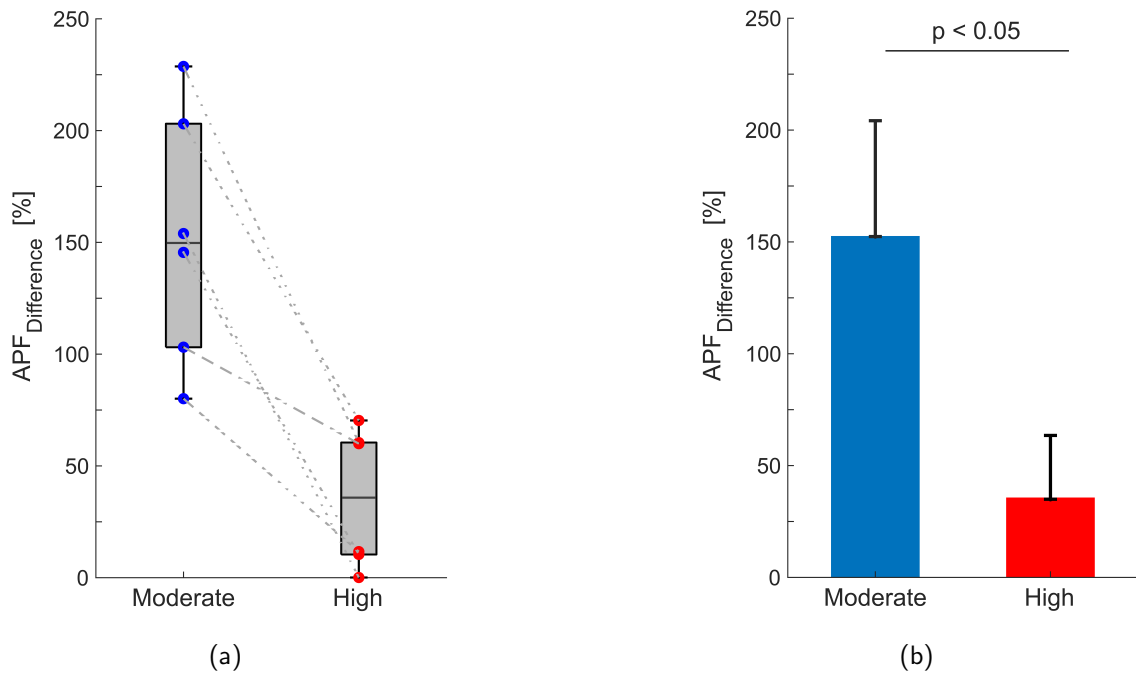


Figure 3.6: Summary of the results from Experiment 1 of $\%APF_{\text{Difference}}$ values for the entire study group under moderate (colored blue) and high (colored red) electrical stimulation intensity conditions. In 3.6 a), the median $\%APF_{\text{Difference}}$ values for the entire study group for moderate and high electrical stimulation tests are provided. The $\%APF_{\text{Difference}}$ results for each subject are presented as a pair of blue (result from moderate electrical stimulation intensity test) and red (result from high electrical stimulation intensity test) circles connected with a dashed line. In 3.6 b) statistical analysis showing the group mean and the standard deviation for moderate and high electrical stimulation intensities is provided.

The values of TTF, MPF, FTI, APF, $\%TTF_{\text{Difference}}$, $\%MPF_{\text{Difference}}$, and $\%APF_{\text{Difference}}$ for moderate and high electrical stimulation intensity with respect to the associated stimulation configuration (SES and SDSS) are shown in Table 3.2.

Table 3.2: The summary of the results from each subject from Experiment 1 conducted on the quadriceps muscle group.

Subj.	Intensity [mA]	SDSS				SES				Difference		
		TTF [sec]	MPF [N]	FTI [N.sec]	APF [N]	TTF [sec]	MPF [N]	FTI [N.sec]	APF [N]	TTF [%]	MPF [%]	APF [%]
P1	70	34.1	43.1	1261	36.9	14.4	20.5	262	18.2	136	110	103
	130	17.3	201.6	3083	178.0	11.4	125.2	1273	111.3	51.4	60.9	59.9
P2	130	17.3	220.9	3312	191.4	15.7	219.1	3012	191.3	9.8	0.88	0.08
	70	24.9	65.2	1410	56.4	12.4	25.3	276	22.2	101	158	154
P3	130	13.2	72.1	836	63.4	10.3	44.5	409	39.5	27.5	62.1	60.4
	80	20.0	37.8	636	31.8	11.5	10.9	111	9.7	74.4	247	229
P4	80	38.0	8.2	275	7.2	10.5	3.3	31	2.9	262	146	145
	130	19.6	23.8	411	20.9	9.3	21.9	177	18.9	110	8.4	10.4
P5	80	27.8	15.5	385	13.9	9.8	8.6	75	7.7	184	79.3	80
	130	14.6	42	543	37	9.1	38.1	302	33.1	61	10.4	11.7
P7	85	10.0	10.6	92	9.2	6.6	3.6	20	3.0	51.9	197	203
	130	7.9	12.5	88	11.1	6.1	7.5	40	6.6	29.1	67	70.3

3.3.2 Experiment 2

Figure 3.7a and Figure 3.7b depict the fatigue measurements of P5 under conditions of moderate electrical stimulation intensity (60 mA) and high electrical stimulation intensity (100 mA). These figures represent force (N) versus time (sec) graphs. In the initial experimental session, the subject underwent moderate-intensity testing where the left VL was stimulated with the SDSS configuration and the right VL was stimulated using the SES configuration. In the subsequent experimental session, a high-intensity test was conducted with the same electrode-leg-stimulation configuration (SES-Right VL and SDSS-Left VL). The horizontal black lines and shaded areas under the force-time curve represent TTF and FTI, respectively. The TTF values for SDSS and SES electrode configurations under mod-

erate electrical stimulation intensity were 17.90 seconds and 12.65 seconds, respectively, resulting in a $\%TTF_{\text{Difference}}$ of 41.50%. At high electrical stimulation intensity, the TTF values for SDSS and SES electrode configurations were 11.96 seconds and 11.22 seconds, respectively, resulting in $\%TTF_{\text{Difference}}$ of 6.60%. Regarding FTI, at moderate electrical stimulation intensity, the values for SDSS and SES electrode configurations were 147.03 N and 68.01 N, respectively ($\%APF_{\text{Difference}}$ of 52.78%). At high electrical stimulation intensity, the FTI values for SDSS and SES electrode configurations were 246.96 N and 300.87 N, respectively ($\%APF_{\text{Difference}}$ of -23.00%).

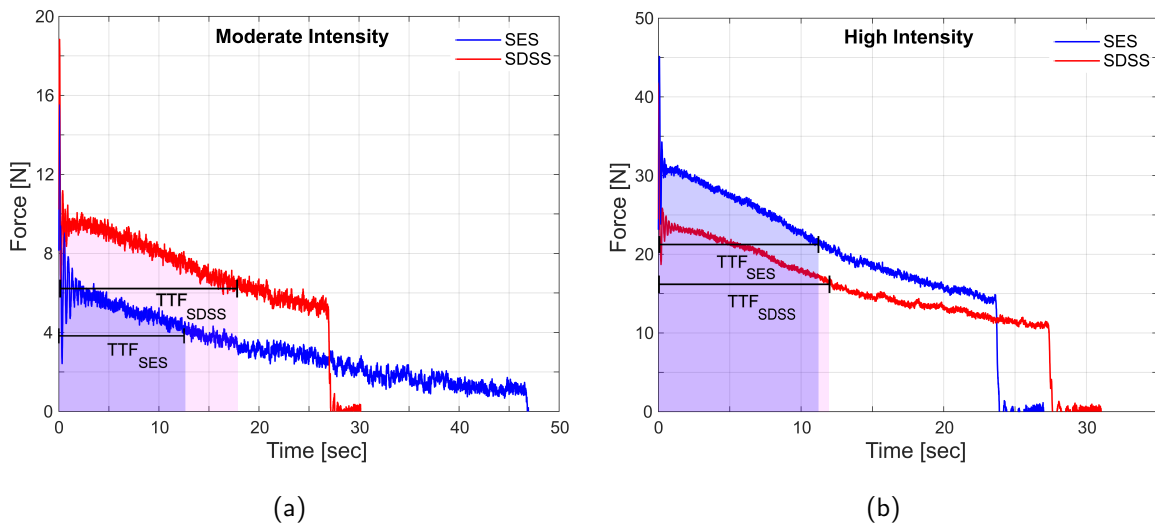


Figure 3.7: Measurements conducted on subject P5 of the force produced by the vastus lateralis muscle stimulated with a) moderate electrical stimulation intensity (60 mA) and b) high electrical stimulation intensity (100 mA). Forces produced by the quadriceps muscle group stimulated with SDSS and SES electrode configurations are presented with red and blue lines, respectively. Horizontal black lines and shaded areas under the force-time curves represent TTF and FTI, respectively.

In Figure 3.8, the $\%TTF_{\text{Difference}}$ values for all subjects are presented under conditions of moderate (represented by blue circles) and high (represented by red circles) electrical stimulation intensity. The median $\%TTF_{\text{Difference}}$ for moderate electrical stimulation intensity was 39.58%, ranging from -62.17% to 45.59%. For high electrical stimulation intensity, the median $\%TTF_{\text{Difference}}$ was -0.80%, ranging from -37.90% to 16.59%. Statis-

tical analysis utilizing the Wilcoxon signed-ranked test revealed no significant difference between $\%TTF_{\text{Difference}}$ for moderate and high electrical stimulation intensity ($p = 0.313$, $r = 0.452$).

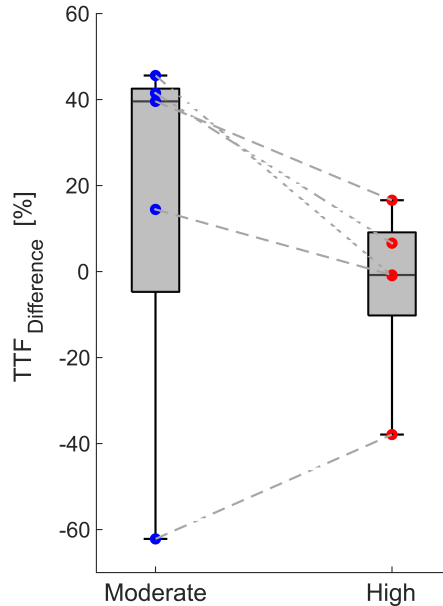


Figure 3.8: Median $\%TTF_{\text{Difference}}$ values for the entire study group for moderate and high electrical stimulation tests conducted on the vastus lateralis muscles (Experiment 2) are provided. The $\%TTF_{\text{Difference}}$ results for each subject are presented as a pair of blue (result from moderate electrical stimulation intensity test) and red (result from high electrical stimulation intensity test) circles connected with a dashed line.

Figure 3.9a depicts the $\%MPF_{\text{Difference}}$ values for all subjects under conditions of moderate (represented by blue circles) and high (represented by red circles) electrical stimulation intensity. The median $\%MPF_{\text{Difference}}$ for moderate electrical stimulation intensity was 2.03%, ranging from -51.83% to 98.98%. For high electrical stimulation intensity, the median $\%MPF_{\text{Difference}}$ was 8.95%, ranging from -26.72% to 69.64%. The statistical analysis indicated no significant difference between $\%MPF_{\text{Difference}}$ for moderate and high electrical stimulation intensity ($16.35 \pm 54.15\%$ for moderate electrical stimulation intensity and $15.97 \pm 39.03\%$ for high electrical stimulation intensity, as shown in Figure 3.9b), as determined by paired t-test ($p = 0.989$, $d = 0.007$).

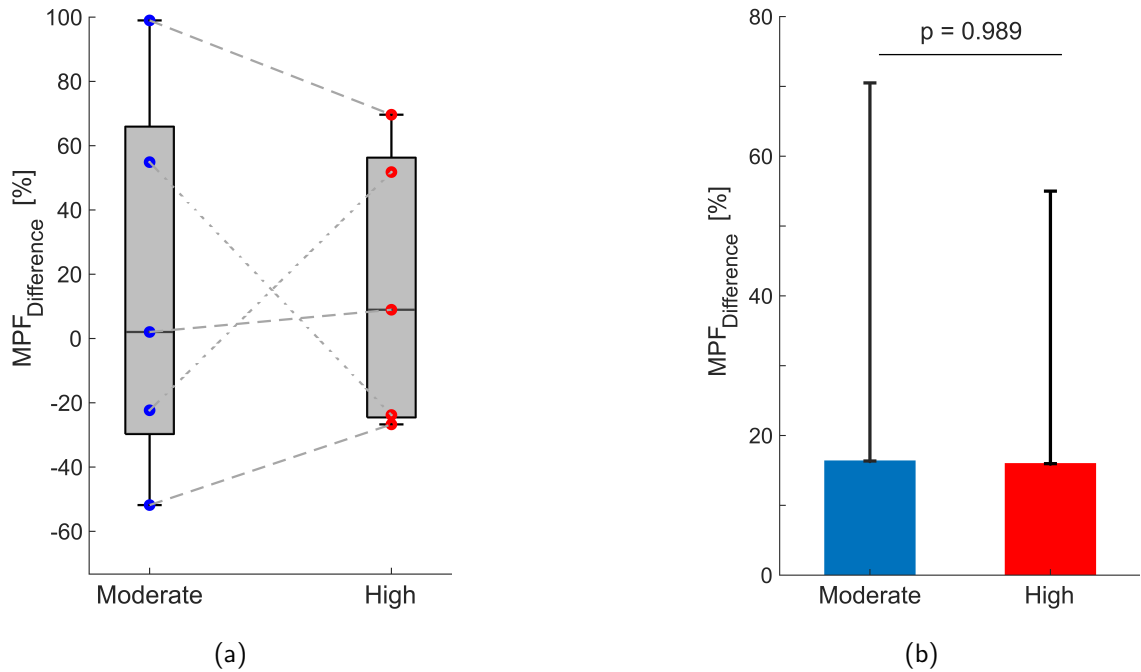


Figure 3.9: Summary of the results from Experiment 2 of $\%MPF_{Difference}$ values for the entire study group under moderate (colored blue) and high (colored red) electrical stimulation intensity conditions. In 3.9 a), the median $\%MPF_{Difference}$ values for the entire study group for moderate and high electrical stimulation tests are provided. The $\%MPF_{Difference}$ results for each subject are presented as a pair of blue (result from moderate electrical stimulation intensity test) and red (result from high electrical stimulation intensity test) circles connected with a dashed line. In 3.9 b) statistical analysis showing the group mean and the standard deviation for moderate and high electrical stimulation intensities is provided.

Figure 3.10a presents the $\%APF_{Difference}$ values for all subjects under moderate (indicated by blue circles) and high (indicated by red circles) electrical stimulation intensity conditions. The $\%APF_{Difference}$ for moderate electrical stimulation intensity had a median of 0.79%, ranging from -51.20% to 72.03%, while $\%APF_{Difference}$ for high electrical stimulation intensity had a median of 6.00%, ranging from -26.21% to 60.65%. Statistical analysis using a paired t-test showed no significant difference between $\%APF_{Difference}$ for moderate and high electrical stimulation intensity ($10.85 \pm 45.63\%$ for moderate electrical stimulation intensity and $13.61 \pm 36.23\%$ for high electrical stimulation intensity, Figure

3.9b) ($p = 0.914$, $d = 0.051$).

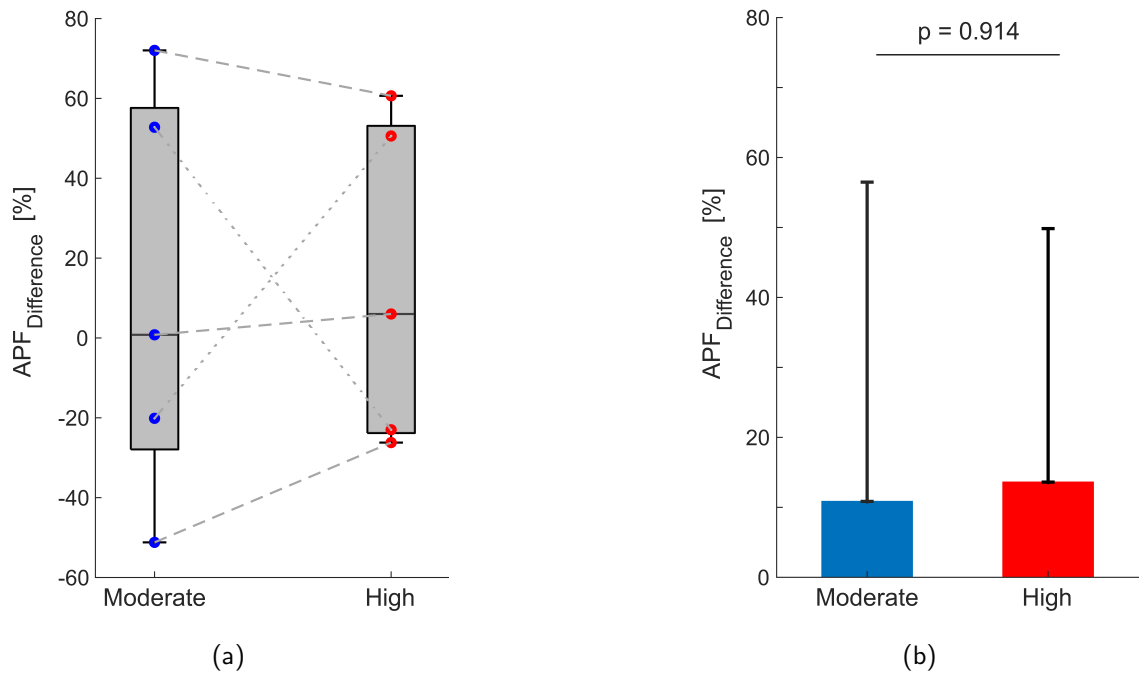


Figure 3.10: Summary of the results from Experiment 2 of %APF_{Difference} values for the entire study group under moderate (colored blue) and high (colored red) electrical stimulation intensity conditions. In 3.10 a), the median %APF_{Difference} values for the entire study group for moderate and high electrical stimulation tests are provided. The %APF_{Difference} results for each subject are presented as a pair of blue (result from moderate electrical stimulation intensity test) and red (result from high electrical stimulation intensity test) circles connected with a dashed line. In 3.10 b) statistical analysis showing the group mean and the standard deviation for moderate and high electrical stimulation intensities is provided.

Table 3.3 provides the values of TTF, MPF, FTI, APF, %TTF_{Difference}, %MPF_{Difference}, and %APF_{Difference} for moderate and high electrical stimulation intensity, corresponding to the associated stimulation configurations (SES and SDSS).

Table 3.3: The summary of the results from each subject from Experiment 1 conducted on the quadriceps muscle group.

Subj.	Intensity [mA]	SDSS				SES				Difference		
		TTF [sec]	MPF [N]	FTI [N.sec]	APF [N]	TTF [sec]	MPF [N]	FTI [N.sec]	APF [N]	TTF [%]	MPF [%]	APF [%]
P1	100	9.36	113.2	937	100.0	9.45	74.6	628	66.4	-0.9	51.8	50.6
	60	12.87	29.7	352	27.4	8.84	38.2	303	34.3	45.6	-22	-20
P2	100	13.7	85.6	1063	77.6	13.8	78.6	1011	73.2	-0.8	8.9	6.0
	60	15.3	37.7	495	32.4	13.4	37.0	429	32.1	14.4	2.0	0.8
P3	100	5.2	50.3	219	42.0	8.4	29.7	219	26.1	-38	69.6	60.6
	65	2.8	23.4	49	17.3	7.5	11.8	75	10.0	-62	99.0	72.0
P4	70	13.9	1.8	23.3	1.67	10.0	3.8	34.1	3.4	39.6	-52	-51
	100	10.5	21.7	205	19.5	9.0	29.6	238.7	26.4	16.6	-27	-26
P5	60	17.9	9.4	147	8.2	12.6	6.0	68	5.4	41.5	54.9	52.8
	100	12.0	23.3	247	20.6	11.2	30.6	301	26.9	6.6	-24	-23

3.4 Discussion

In the present study, we assessed the efficacy of spatially distributed sequential stimulation (SDSS) in comparison to the traditional FES using a single electrode stimulation (SES) with respect to the time to fatigue (TTF), maximum produced force (MPF), and average produced force until fatigue (APF) at moderate and high electrical stimulation intensities. The objective of each experimental session was to evaluate the efficacy of SDSS at the chosen stimulation intensity by comparing it to SES applied to the contralateral leg. It is important to note that the described protocol was not designed to directly measure the fatigue-reducing capabilities of SDSS compared to SES. Instead, the purpose was to utilize SES as a reference to ensure a fair comparison of the effectiveness of SDSS across multiple experimental sessions. A common challenge encountered when conducting measurements

over multiple days is the variation in the subject's strength, influenced by various physiological factors. By utilizing SES applied to the other leg as a reference, the discrepancies in the subject's strength are largely compensated for, as it can be reasonably assumed that both legs would be similarly affected.

Our research focused on the quadriceps muscle group and the Vastus Lateralis (VL) muscle of subjects with spinal cord injury (SCI). Our findings elucidated that the superior performance of SDSS over SES is considerably compromised for quadriceps muscle group under high-intensity modality. On average, the percentage increase in TTF observed during moderate-intensity stimulation was 2.80-fold greater than the corresponding value observed during high-intensity stimulation. Furthermore, in terms of the percentage increase in MPF and APF, the moderate-intensity modality exhibited a 4.47-fold and 4.3-fold greater increase, respectively, compared to the high-intensity modality. The superior performance of SDSS over SES is generally attributed to the higher current density and the asynchronous recruitment of motor units. Applying the same amount of current to a smaller area creates a higher current density allowing for the resulting electrical fields to reach deeper regions. Asynchronous activation of adjacent motor units at a lower stimulation frequency (12 Hz instead of 48 Hz in this study) allows for longer rest periods for the individual motor units resulting in greater fatigue resistance of SDSS compared to SES. However, higher stimulation intensities generate stronger electrical fields beneath the electrodes, resulting in excessive recruitment of overlapping motor units. Consequently, this situation resembles the configuration of SES, leading to heightened fatigue of the overlapping motor units. To the best of our knowledge, while this phenomenon has been previously observed [121], it has never been investigated directly. Schmoll et al. conducted a study involving SCI individuals performing knee extension tasks and found no significant difference in terms of fatigue resistance between four different distributed stimulation configurations and single electrode stimulation configuration. They postulated that a certain amount of spillover could potentially account for these findings [121]. In a study conducted by Sayenko et al., a similar SDSS configuration to the current work was employed and compared to SES in 2-minute

fatiguing isometric tests. They discovered that the mean peak torque during the initial 5 stimulations was not significantly different between SDSS and SES in both able-bodied and SCI individuals [124]. This observation could be attributed to the relatively high stimulation intensities utilized in both protocols, which diminishes the alternating stimulation effect of SDSS.

The primary objective of Experiment 2 was to examine the impact of the high intensity on the efficacy of SDSS compared to SES in individual muscles where the number of accessible motor points is limited, thereby potentially compromising the efficacy of the alternating recruitment strategy. In contrast to the findings from Experiment 1, our results obtained from the Vastus Lateralis muscle did not exhibit a significant difference between moderate and high-intensity modalities in terms of $\%TTF_{\text{Difference}}$, $\%MPF_{\text{Difference}}$, and $\%APF_{\text{Difference}}$. One possible explanation for this outcome could be attributed to the relatively large intensity chosen for the moderate tests. Given the relatively low output force of the Vastus Lateralis muscle and the presence of muscle weakness in individuals with spinal cord injuries (SCI), such intensity selections were inevitable to ensure meaningful stimulation responses. Furthermore, in certain subjects, instances of co-contraction of the Rectus Femoris muscle were observed. This phenomenon may be attributed to the relatively high stimulation intensities used and to the large size of the cathode electrode. The selection of electrode size for the Vastus Lateralis tests requires careful consideration due to the potential for inadvertently stimulating the motor fibers responsible for knee flexion, consequently inducing antagonistic stimulation of the thigh muscles. This delicate and sensitive nature of electrode sizing necessitates precise electrode placement and control to specifically target the intended muscle group and minimize any unintended activation of opposing muscle actions. Conducting further investigations with a larger sample size and repeating the tests using smaller electrodes on a muscle where co-activation of antagonistic muscles is less likely (e.g., Tibialis Anterior) could potentially elucidate the underlying cause for this observed outcome.

In contrast to previous studies [106]–[114], the electrodes employed in both SDSS and

SES tests were kept identical in size and shape (4 cathodic electrodes) to prevent inadvertent errors in electrode placement and adherence. To provide further clarification, previous investigations utilized a single large electrode for SES, while employing four smaller electrodes to cover the same area as SES in SDSS. However, the curved edges of the small electrodes used in SDSS result in an unequal overall coverage area compared to the size of the large single electrode used in SES. Additionally, when utilizing a large single electrode, the heterogeneous nature of skin resistance can facilitate the preferential passage of electrical currents through more conductive regions, potentially influencing the outcomes in terms of recruited motor points and subsequently affecting fatigue and force generation. The utilization of four smaller electrodes ensures a uniform distribution of electrical charge among the electrode set. Further investigation is warranted to explore the potential disparities in fatigue and force outcomes between the utilization of four smaller electrodes and a single large electrode during SES. Our future research aims to address this knowledge gap and provide a comprehensive understanding of the implications associated with electrode configuration on fatigue and force generation.

3.5 Conclusion

The study showed that the stimulation intensity has a significant impact on the efficacy of SDSS compared to SES. The superior performance of SDSS over SES is significantly compromised when applying high electrical stimulation intensity to the paralyzed quadriceps muscle groups. The output power increase and the fatigue-reducing ability of SDSS are more pronounced in moderate-intensity conditions than in high-intensity conditions. These findings contribute to the understanding of the mechanisms behind SDSS and form the basis for the assessment of applications of SDSS for performing functional tasks.

Chapter 4

SDSS Applied to the Paralyzed Quadriceps Muscles while Performing Motor-assisted FES Cycling – a Case Series

Abstract

In isometric and isokinetic studies, spatially distributed sequential stimulation (SDSS) was proven to be better than the traditional functional electrical stimulation (FES) that uses a single electrode stimulation (SES) in terms of fatigue-reducing ability and the power output produced by the muscles. The present case series aims to systematically assess the power output and fatigue-reducing properties of SDSS versus SES applied to the paralyzed quadriceps muscles of subjects performing motor-assisted FES cycling task. Four subjects without lower-limb motor function participated in two multiday experimental sessions. Each experimental session involved two stimulation phases, one with SDSS and one with SES stimulation. The stimulation parameters and the electrode configuration for SDSS and SES were chosen based on the results from the previous chapter. Muscles stimulated with the SDSS setup produced considerably higher overall mean power values in all subjects in all experimental sessions while inducing a similar amount of muscle fatigue. One subject experienced slightly more fatigue while three subjects showed slightly better fatigue resistance with the SDSS setup. The results of the present study strongly suggest that SDSS is superior to SES when applied to paralyzed muscles of subjects performing FES cycling task. Further research should be conducted with more participants in order to achieve statistical significance.

4.1 Introduction

As discussed in Section 1.5.5 and Chapter 3 of this thesis, two primary limitations of FES technology are the rapid onset of muscle fatigue and low power output produced by the stimulated muscles. Subsequently in Section 3.1, we have verified that under isometric electrical stimulation of quadriceps muscles, the use of multiple small electrodes over the motor points instead of one large electrode, combined with sequencing of the electrical stimulation pulses to each of the smaller electrodes surrounding the motor points with equivalent overall stimulation of one individual electrode, so-called single electrical setup (SES), the fatigue and power limitations of FES can be improved. This methodology is referred to as spatially distributed sequential stimulation (SDSS) and presumably prevents the entire muscle from being stimulated with every electrical pulse.

Our previous work also revealed that electrical stimulation intensity can have an effect on the level of improvement demonstrated by the SDSS protocol. Improvements were seen to be less dramatic at higher stimulation intensities, which we interpret as a greater overlap of the electrical fields created by each smaller electrode, thereby repeatedly activating a greater number of muscle fibers, negating the local muscle stimulation distribution created by having multiple smaller electrodes.

Despite the fact that some isometric and isokinetic studies have reported either substantial or slight gains in favor of SDSS versus SES, the benefits of performing a functional task such as FES cycling with SDSS are not clear. During these types of activities, the muscles and motor points are constantly moving relative to the electrodes which are attached to the skin surface and this in turn may negate any benefits observed during isometric and less active highly repetitive movements. To the best of our knowledge, only three studies have investigated the effects of SDSS when performing active FES exercise. Ye et al. [125] have reported that SDSS applied to the quadriceps muscles of able-bodied subjects reduced the muscle fatigue while performing FES rowing. The other two studies [120], [122] were conducted on the quadriceps muscle groups of a single SCI subject in preparation for the

Cyathlon (i.e., international sporting event for handicapped individuals) FES cycling race. However, the studies report conflicting results. Baptisia et al. [120] demonstrated better performance of SDSS while Ceroni et al. [122] found SES to be superior. That said, both studies involved multiple varying and uncontrolled parameters and Ceroni et al. were investigating four different stimulation strategies, both of which complicate drawing definitive conclusions.

The aim of the present case series was to systematically assess the power output and fatigue-reducing properties of SDSS versus SES applied to the paralyzed quadriceps muscles of subjects without lower-limb motor function, performing a controlled motor-assisted FES cycling task. Our previous isometric study (Chapter 3) allows us to have an in-depth understanding of the influence of the electrode placement and the stimulation parameters on the performance of SDSS. With this knowledge, we have designed a systematic study protocol to determine if SDSS provides similar benefits seen in isometric studies when applied to performing FES cycling exercises. As nearly all FES stationary cycling exercise devices are equipped with motor assistance to help prolong the exercise experience for individuals who do not have enough strength to cycle only with FES, we have conducted our experiments under motor-assisted conditions. This also helps us to conduct the experiments in a systematic way under constant speed conditions.

4.2 Methods

4.2.1 Participants

Three adult male subjects with lower-limb motor-complete spinal cord injury and one adult male with multiple sclerosis (MS) participated in the study. The subject with multiple sclerosis (P4) cannot produce voluntary muscle contractions in the lower limbs. All subjects had previous experience with FES of the studied muscles, three of whom had participated in our previous study involving SDSS (Chapter 3). In an effort to mitigate the effects of residual fatigue, all subjects were asked to refrain from using FES for at least 48 hours

before each experiment was conducted. The exclusion criteria stipulated that the subjects must not have sustained lower limb fractures within the past year or have open wounds or rashes on the skin surface where the electrodes would be placed. The project was approved by the local Institutional Review Board (NCT06421753) and conducted in accordance with the Declaration of Helsinki. More information about the participants is provided in Table 4.1 and Table 4.2.

Table 4.1: The demographic and clinical characteristics of participants with the spinal cord injury.

Participants	Age (years)	Injury level	ASIA	Time after spinal cord injury (years)	FES naive	Current FES training
P1	46	C7-C8	B	11	No	No
P2	30	C5-C6	B	6	No	Yes
P3	59	C6-C7	A	6	No	Yes

Table 4.2: The demographic and clinical characteristics of the subject with multiple sclerosis.

Participants	Age (years)	EDSS	MS Type	Disease duration (years)	FES naive	Current FES training
P4	38	8	Progressive	11	No	No

4.2.2 Instrumentation

The experiments were performed on the instrumented cycling ergometer platform (ICEP) [75]. The wall-mounted platform consists of a modified bicycle frame carrying force-torque measuring pedals, a magnetic ring encoder and a motorized actuator system. The actuator system was designed to assist the subjects with maintaining a constant cycling cadence which can be set using a custom-made LabVIEW program. Each pedal measures all three components (x-y-z axis) of the force and torque applied to their surface, as well

as the inclination angle of the pedal in reference to the crank arm. Measured forces, paired with the crank angle data acquired with the ring encoder are saved in a text file for later processing.

Subjects were seated on a modified recumbent tricycle (Carbontrikes, Bandhagen, Sweden) with their legs firmly attached to the force-measuring pedals using modified leg orthoses (Hase Bikes, Waltrop, Germany). The trike was secured to the cycling platform with a retractor system. The distance between the trike and the platform was measured to ensure an identical sitting position for each subject between the experimental sessions. An illustration of the experimental setup is provided in Figure 4.1.

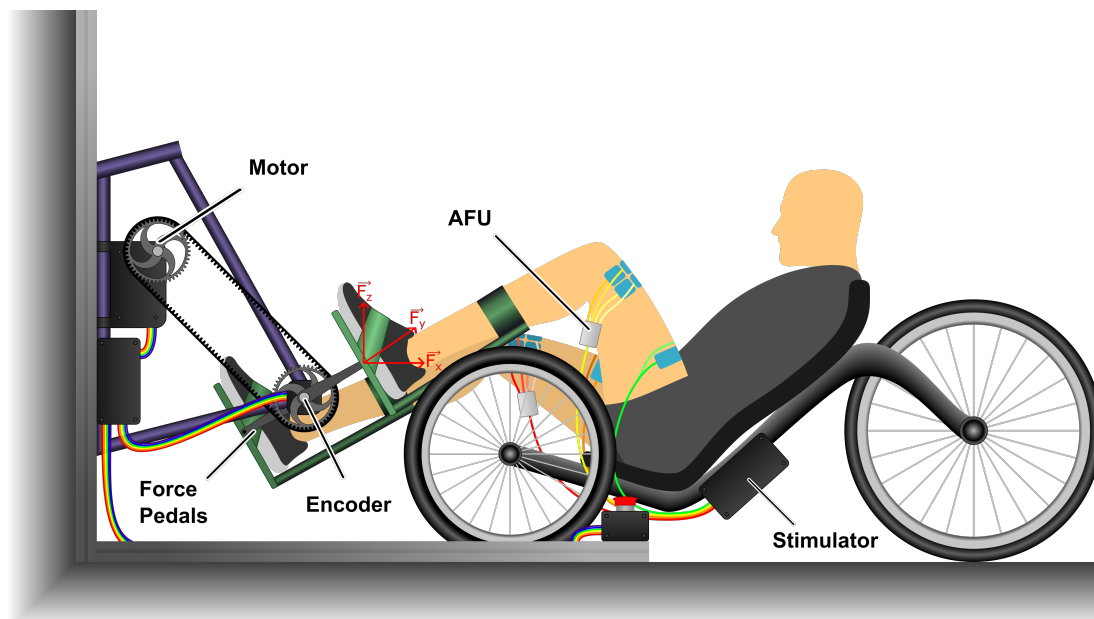


Figure 4.1: Illustration of the experimental setup for the assessment of the power output and fatigue-reducing properties of SDSS versus SES applied to the paralyzed quadriceps muscles of subjects performing motor-assisted FES cycling. The electrode placement and the colors of the wires correspond to the ones used in Figure 4.2. Details concerning the different components and procedures are provided in the text of the manuscript.

A PC-controlled 8-channel MotiMove stimulator [105] (3F-Fit Fabricando Faber, Belgrade, Serbia) was used to deliver asymmetric biphasic pulses to the paralyzed quadriceps muscles. The stimulator was synchronized with a crank encoder using a data acquisition

card (PCI-6009, National Instruments, Austin, TX, USA). A graphical user interface was implemented to set the stimulation parameters, cycling cadence and the crank angle ranges during which the stimulation was applied. SDSS was created by connecting so-called anti-fatigue unit (AFU) devices (3F-Fit Fabricando Faber, Belgrade, Serbia) to the cathodes of two stimulation channels (one per leg). These AFUs distribute the electrical stimulation to the different electrodes.

4.2.3 Electrode Configuration

Four self-adhesive surface electrodes (Compex Dura-Stick plus) were placed distally (cathodes) while the reference electrode (anode) was placed proximally over the quadriceps muscle groups. The chosen electrode configuration was identical to the configuration used in the prior isometric study conducted on the quadriceps muscle groups (Section 3.2.3). Before applying the electrodes, the skin was cleaned and proximal and distal motor points of rectus femoris (RF) muscles were found using the measured anatomic landmarks [104]. Motor points were marked with an indelible marker pen to ensure identical electrode placement across the experimental sessions.

The proximal electrode was made by connecting two electrodes to the anode of the same stimulation channel and thus creating an electrode with an effective surface area of 5 x 14 cm². Electrodes used for the anode were a 5 x 5 cm² electrode placed on the proximal motor point of RF muscle and a 5 x 9 cm² electrode placed laterally, to the side of the 5 x 5 cm² electrode (see Figure 4.2). Distal (cathode) electrodes, with a surface area of 5 x 5 cm² each, were placed as close as possible to each other, to form a 2x2 matrix just under the distal motor point of the RF muscle. Positions of the electrodes were confirmed or modified based on visual observations and gentle touch of the muscle contraction resulting from a short train of pulses sent to each electrode separately. In order to minimize fatigue, the pulses used were slightly above the motor threshold. The electrode configuration is illustrated in Figure 4.2.

The described electrode configuration was used for both SDSS and SES. Unlike previ-

ous studies that have explored the topic of SDSS, in the SES mode, all four distal electrodes were connected to the cathode of the same stimulation channel effectively making them into one large electrode. This was done to ensure the electrode positioning and the area covered by the electrodes remain absolutely the same during SES and SDSS. In the SDSS mode, each distal electrode was connected to a different output channel of the AFU device.

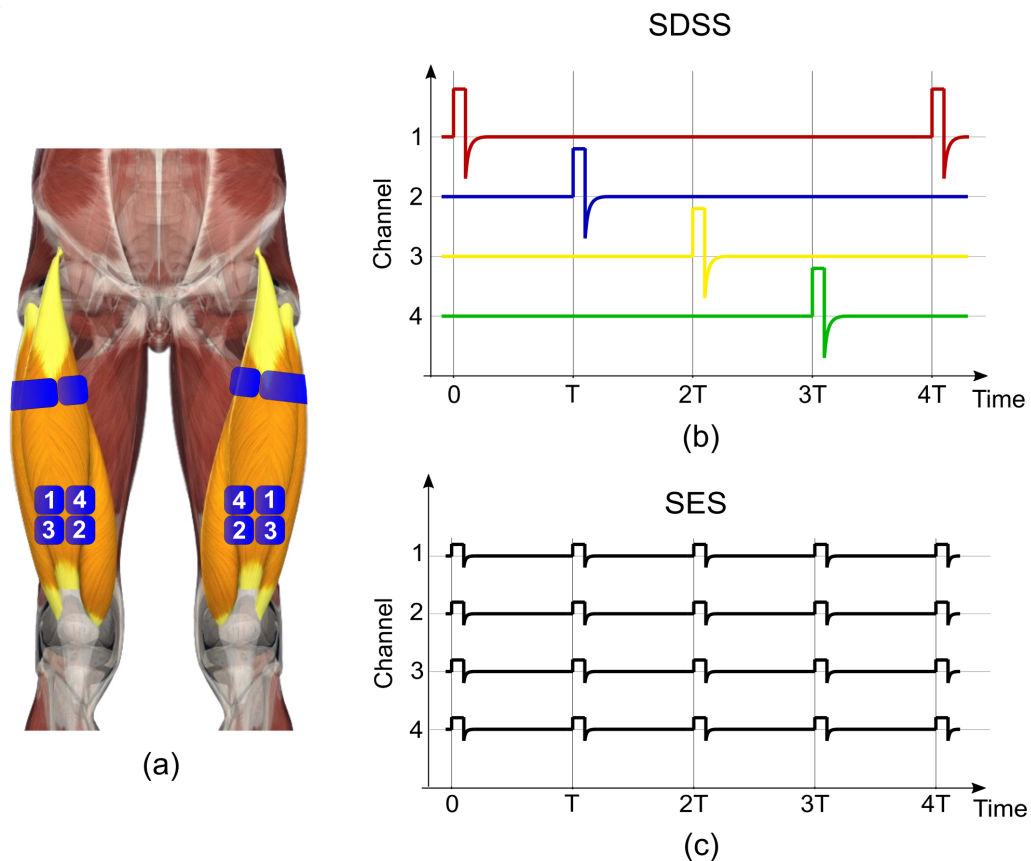


Figure 4.2: (a) An illustration of the electrode configuration used for both SDSS and SES. Stimulated muscle groups are highlighted in orange while the electrodes are colored blue. Distal (cathode) electrodes are labeled in correspondence with the y-axis of the schematics (b) and (c). Schematics represent electrical pulse trains delivered to each electrode (labeled on the y-axis) during four stimulation periods (b) creating the SDSS effect (colors emphasize the fact that different regions of the muscle were stimulated, this study did not investigate the order of which pulses were delivered to the different electrodes), or (c) creating the SES effect.

4.2.4 Stimulation Parameters

In our isometric SDSS study (Chapter 3), we found that moderate-intensity SDSS has a more pronounced improvement than high-intensity SDSS in terms of fatigue resistance and power produced. Thus, the electrical stimulation parameters used for SES and SDSS were set identically to the moderate stimulation parameters found in the previous study and were kept constant throughout the experiments. The stimulation pulse width was set to 400 μ s and the frequency was 48 Hz for SES and 12 Hz per channel ($12 \times 4 = 48$) for SDSS thus providing a composite frequency of 48 Hz, maintaining coherence in both experimental cases. The moderate stimulation intensity was calculated for each subject as the mean value of their motor threshold and the maximum stimulation intensity restricted to 130 mA. In no case did a subject experience pain during stimulation.

In order to maintain a constant electrical stimulation period for each subject, a crank angle range of 130° for the stimulation period of each set of quadriceps muscles was chosen (note: the motor assistance used is kept at a constant cycling cadence thus ensuring a fixed time-period for the stimulation when the stimulation angle range is fixed). Once the subject is properly positioned, to determine the optimal stimulation patterns (i.e., crank angles for which stimulation is initiated and terminated during the rotation of the crank) that produce the maximum force on the pedals, a comparison between the forces produced during passive cycling (motor-assisted cycling with the cadence of 50 rpm without muscle stimulation) and active cycling (motor-assisted FES cycling at 50 rpm) was made. For active cycling, stimulation pulses of moderate intensity are constantly sent to the muscles over a complete revolution of the crank. We refer to the difference in the force measured between the active and passive cycling over a full revolution as the subject's muscle force profile (MFP) and it represents the forces produced by the stimulated muscle groups on the pedals over the entire crank revolution. By analyzing the MFP and adhering to the chosen angular range of 130°, the optimal initiation and termination stimulation angles for producing the maximum force from the quadricep muscles is determined (i.e., the 130°

angle range was simply overlaid with the MFP for each subject and the intersection of the two were used).

However, to ensure that the muscles are activated at the correct position, the initiation stimulation angle needs to be shifted to compensate for the delay introduced by the system, the electrical stimulator delay and the muscle activation delay. The required angular shift depends on the cycling cadence and it can be calculated using equation 4.1, or it can be directly measured by comparing passive forces and active forces produced by the muscle stimulated between the determined initiation and termination stimulation angles. The required angular shift is the angular difference between the initiation angle and the angle where the muscle produces a noticeable force. The termination angle needs to be compensated only for the delay introduced by the system and the stimulator which can be calculated using equation 4.2.

$$\Delta\theta_i = \left(\frac{(D + D_s + \text{EMD}) \times 360}{60} \right) \omega \quad (4.1)$$

$$\Delta\theta_t = \left(\frac{(D + D_s) \times 360}{60} \right) \omega \quad (4.2)$$

where $\Delta\theta$ represents the angular shift [°], EMD is the muscle activation delay [s], D is the delay of the system [s], DS is the delay of the electrical stimulator [s] and ω is the cycling cadence [rpm]. The required angular shifts were applied to the determined initiation and termination angles to obtain the delay-compensated stimulation pattern. A more detailed description of the method used to determine the optimal stimulation pattern and the delay-compensated pattern is provided in [48].

4.2.5 Experimental Protocol

Each subject participated in two experimental sessions separated by at least 48h. Within each experimental session, quadriceps muscle groups of both legs were stimulated with SDSS and SES separated by a 15-minute break. To ensure that there was no systematic

influence of possible residual fatigue using a certain type of stimulation, the order of stimulation type was chosen at random for the first experimental session and inverted for the second experimental session (i.e., SDSS then SES versus SES then SDSS or SES then SDSS versus SDSS then SES). The cycling cadence was set to 50 rpm.

Preliminary experiments were conducted to ensure equivalent experimental conditions are achieved each day. The stimulation patterns were determined for each subject as described above. To conduct preliminary measurements, we began by determining the moderate stimulation intensity calculated based on the measured motor threshold. Following this step, a 1-minute warm-up (passive cycling) period was carried out. The MFP was then recorded using the calculated moderate intensity, and the optimal stimulation pattern was determined by overlaying the chosen 130° angle range providing the subject's initiation and termination angles for the experiments. After a 10-minute rest period, another 1-minute warm-up was performed followed by the procedure described earlier for measuring the angular shift at a cycling cadence of 50 rpm. The required angular shift was applied and the resulting delay-compensated initiation and termination angles were used throughout the experimental sessions. For each subject, the moderate intensity and the delay-compensated initiation and termination angles were measured before each experimental session to ensure that the sitting and electrode positions were identical between the experimental sessions. A notable difference between the calculated values would indicate that the sitting or electrode position needs to be adjusted.

After a 10-minute break period following the preliminary measurements, the actual experimental session commenced with a 3-minute warm-up phase followed by a 3-minute stimulation phase. During warm-up, the motor passively turned the legs and the electrical stimulation to the muscles was off. The set cycling cadence of 50 rpm was gradually (1 rpm increase per second) achieved in the first minute of warm-up and maintained throughout the rest of the warm-up and stimulation phases (represented by a blue line in Figure 4.3). During the stimulation phase, SES or SDSS was applied to the quadriceps muscle groups while the actuator system, with the motor, assisted with keeping the cadence constant. After

a 15-minute break, during which both the motor and the stimulation were off, another 3-minute warm-up and stimulation phases were performed using the stimulation type that was not applied during the first stimulation phase (SDSS or SES). After at least 48h, the preliminary measurements and the second experimental session were repeated using the inverse order of the stimulation phases. The protocol is illustrated in Figure 4.3.

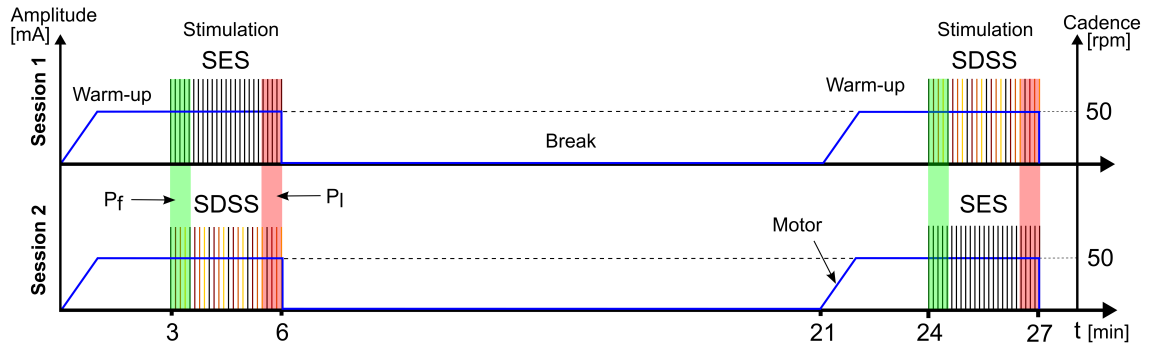


Figure 4.3: An illustration of the experimental protocol. Each subject participated in two experimental sessions involving 3 min warm-up phases, 3 min stimulation phases and a 15-minute break between experimental trials. The x-axis corresponds to the time in minutes. The blue line overlaid on the graph indicates the cadence of the motor assistance, while subsequent vertical lines correspond to electrical stimulation pulses. Vertical colored lines represent SDSS stimulation pulses while the black lines represent SES stimulation pulses. The areas of power produced (P_F) during the first 30 sec are shaded green and red-shaded areas are power produced (P_L) during the last 30 seconds of stimulation.

4.2.6 Data Collection and Analysis

Power was calculated as the product of the angular velocity, crank arm length and the tangential component of the force acquired by each pedal [48]. Mean power during each warm-up phase (after the set cadence was reached) was subtracted from the power produced during the subsequent stimulation phase to calculate the power produced only by the electrical stimulated muscles (P). The total mean power (P_m) for each stimulation phase was assessed. As a measure of induced muscle fatigue, a “fatigue index” (FI) was used.

Based on the mean power produced in the first (P_F) and last (P_L) 30s of each stimulation phase (Figure 4.3), the fatigue index was calculated according to the following equation:

$$FI = 100 \times \frac{P_F - P_L}{P_F} \quad [\%] \quad (4.3)$$

This fatigue index corresponds to the percent muscle fatigue over the 3 min stimulation period, (i.e., $FI = 0$ means no muscle fatigue while $FI = 1$ describes completely fatigued muscles.) All data analysis was carried out using Matlab (Mathworks Inc, Natick, MA, USA).

4.3 Results

4.3.1 Overall Outcomes

Muscles stimulated with the SDSS setup produced higher overall mean power values for all subjects (an increase of 240% for P1, 88% for P2, 198% for P3 and 116% for P4). The fatigue index indicated slightly better fatigue resistance with SDSS for subjects P1, P3 and P4 but worse for subject P2. The results for each experimental session with all subjects were summarized in Table 4.3. Individual results of the power developed in each experimental session are presented in Figure 4.4, Figure 4.5, Figure 4.6 and Figure 4.7.

4.3.2 Individual Cases

4.3.2.1 Case 1

Subject P1 had a lesion level C7-C8, AIS B and the injury occurred 11 years prior to the study. The subject had ample experience with FES of the quadriceps muscles as he had participated in the 2016 and 2020 editions of Cybathlon's FES cycling races. Even though not involved in FES strength training at the time of the study, the muscle strength remained high. No co-contractions or muscle spasms were observed or reported by the subject during

Table 4.3: Summary of the results for power produced and the fatigue index of each experimental session along with the overall mean power produced by each subject during both experimental sessions with SDSS and SES stimulations.

Participants	Sess.	Stim.	P _m [W]	P _F [W]	P _L [W]	FI [%]	Overall Power [W]		
							SDSS	SES	%
P1	S1	SES	4.06	10.75	1.8	83.2	10.98	3.23	240
		SDSS	11.8	21.54	6.81	68.4			
	S2	SDSS	10.16	20.14	4.67	76.8			
		SES	2.39	5.92	1.04	82.4			
P2	S1	SDSS	9.65	18.46	5.12	72.2	10.34	5.51	87.8
		SES	4.95	8.24	3.86	53.1			
	S2	SES	6.06	18.49	7.5	59.4			
		SDSS	11.03	17.02	6.82	59.9			
P3	S1	SES	3.61	11.16	0.64	94.3	9.42	3.17	197.6
		SDSS	8.73	16.21	4.65	71.3			
	S2	SDSS	10.11	18.82	4.8	74.5			
		SES	2.72	6.62	1.54	76.8			
P4	S1	SDSS	9.93	21.16	5.46	74.2	11.25	5.22	115.7
		SES	6.03	14.15	3.04	78.5			
	S2	SES	4.4	8.53	3.55	58.4			
		SDSS	12.57	17.63	8.16	53.7			

the measurements. The power produced by the left and right quadriceps muscle groups during the first and the second experimental sessions are shown in Figure 4.4. Stimulation parameters and the results for both experimental sessions are presented in Table 4.4.

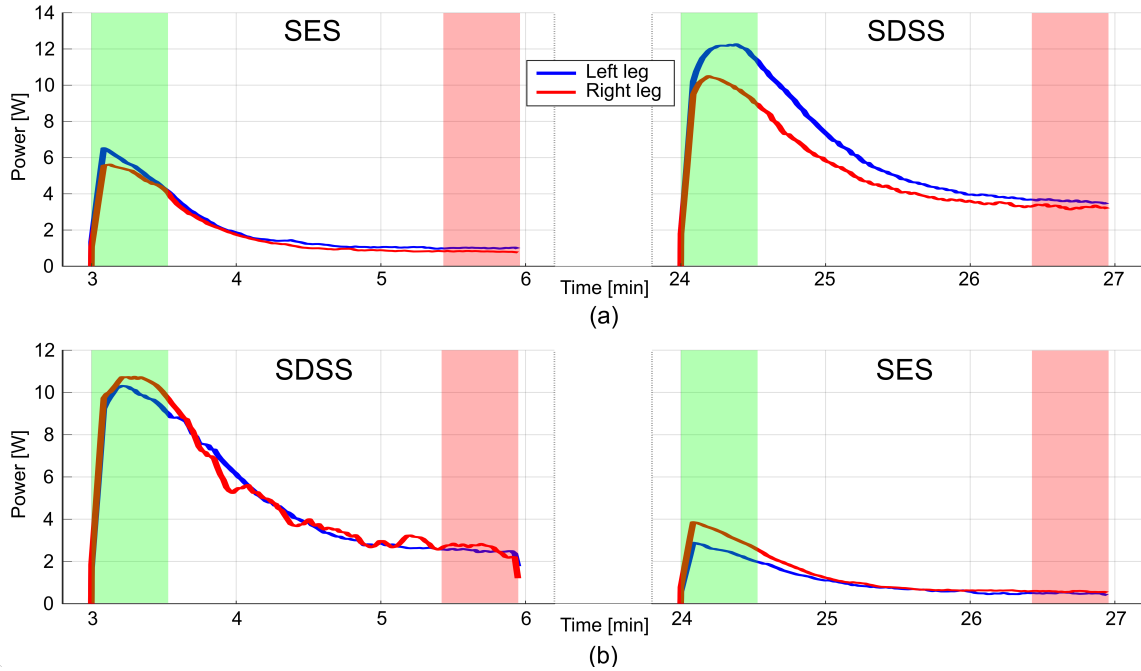


Figure 4.4: Power produced by the subject’s P1 left leg (blue) and right leg (red) during each stimulation phase of (a) the first experimental session and (b) the second experimental session. The areas where the power produced during the first (P_F) and the last (P_L) 30 seconds of each stimulation phase are highlighted in green and red, respectively.

Table 4.4: Stimulation intensity and stimulation patterns measured for subject P1 for each experimental session and the results of each stimulation phase presented in chronological order.

Sess.	Int. [mA]	Left Angles [°]		Right Angles [°]		Stim.	P_m [W]	P_F [W]	P_L [W]	FI [%]
		Init.	Term.	Init.	Term.					
S1	70	198	335	16	153	SES	4.06	10.75	1.8	83.2
						SDSS	11.8	21.54	6.81	68.4
S2	70	194	329	8	143	SDSS	10.16	20.14	4.67	76.8
						SES	2.39	5.92	1.04	82.4

4.3.2.2 Case 2

Subject P2 had a lesion level C5-C6, AIS B and the injury occurred 6 years prior to the study. The subject was undergoing FES-cycling strength training at the time of the study

(twice per week). The subject did not perform FES exercise for at least 48 hours before the experimental sessions. Due to the issues with the actuator system, the stimulation intensity used throughout the experimental sessions was lowered from the calculated 70 mA to 60 mA. In both experimental sessions, during the first warm-up phase, spastic leg activations were observed. During the stimulation phases, no muscle spasms were observed or reported by the subject. However, from the power recorded during the first experimental session provided in Figure 4.5a, it can be deduced that small spastic contractions occurred. The power produced by the left and right quadriceps muscle groups during the first and the second experimental sessions are shown in Figure 4.5. Stimulation parameters and the results for both experimental sessions are presented in Table 4.5.

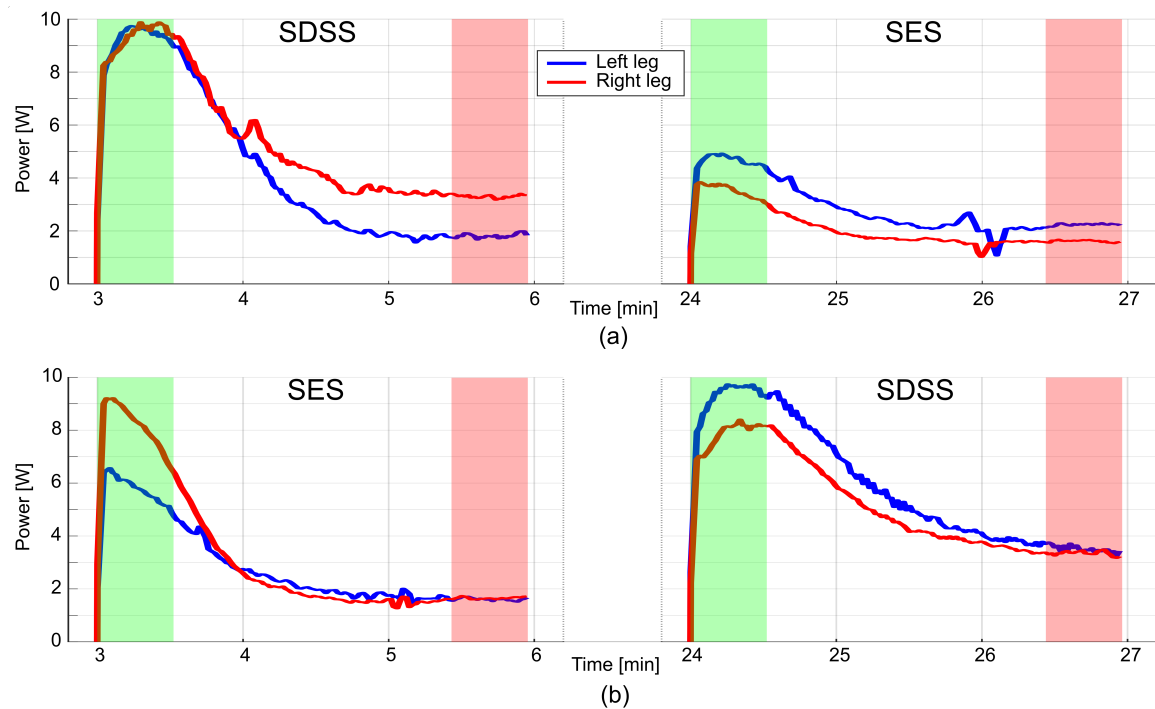


Figure 4.5: Power produced by the subject's P2 left leg (blue) and right leg (red) during each stimulation phase of (a) the first experimental session and (b) the second experimental session. The areas where the power produced during the first (P_F) and the last (P_L) 30 seconds of each stimulation phase are highlighted in green and red, respectively.

Table 4.5: Stimulation intensity and stimulation patterns measured for subject P2 for each experimental session and the results of each stimulation phase presented in chronological order.

Sess.	Int. [mA]	Left Angles [°]		Right Angles [°]		Stim.	P _m [W]	P _F [W]	P _L [W]	FI [%]
		Init.	Term.	Init.	Term.					
S1	60	190	327	10	147	SDSS	9.65	18.46	5.12	72.2
						SES	4.95	8.24	3.86	53.1
S2	60	193	324	13	144	SES	6.06	18.49	7.50	59.4
						SDSS	11.03	17.02	6.82	59.9

4.3.2.3 Case 3

Subject P3 had a lesion level C6-C7, AIS A and the injury occurred 6 years prior to the study. The subject was undergoing FES-cycling strength training at the time of the study (once per week). The subject did not perform any FES exercise for at least 48 hours before the experimental sessions. No co-contractions or muscle spasms were observed or reported by the subject during the measurements. The power produced by the left and right quadriceps muscle groups during the first and the second experimental sessions are shown in Figure 4.6. Stimulation parameters and the results for both experimental sessions are presented in Table 4.6.

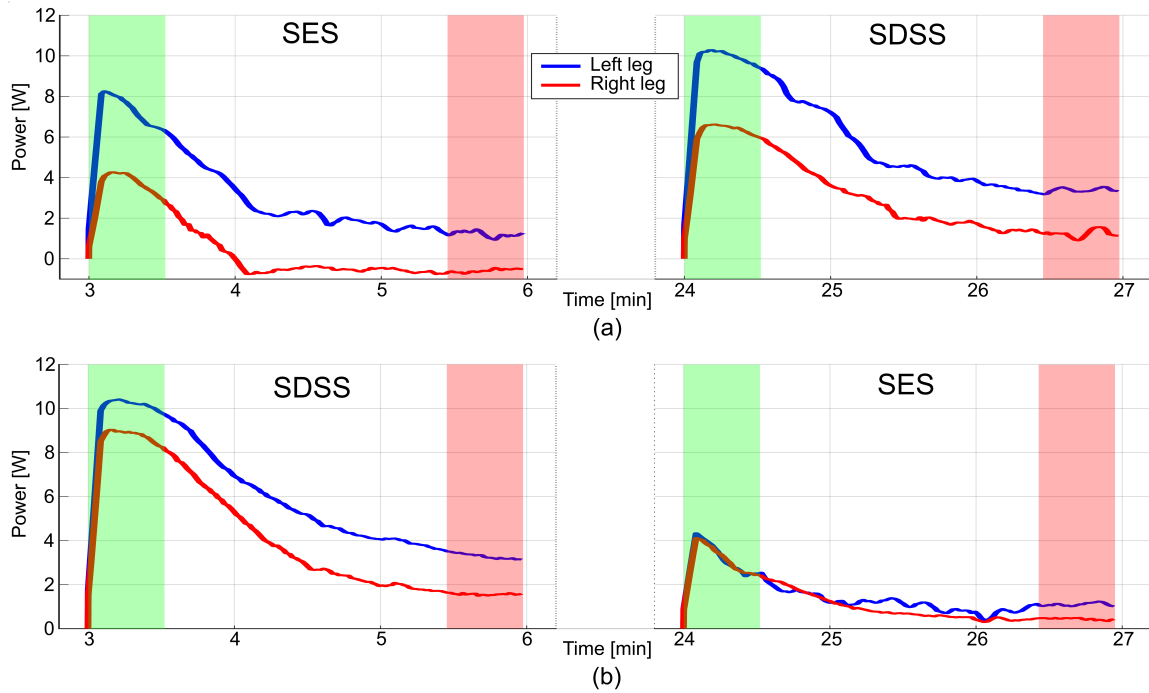


Figure 4.6: Power produced by the subject's P3 left leg (blue) and right leg (red) during each stimulation phase of (a) the first experimental session and (b) the second experimental session. The areas where the power produced during the first (P_F) and the last (P_L) 30 seconds of each stimulation phase are highlighted in green and red, respectively.

Table 4.6: Stimulation intensity and stimulation patterns measured for subject P3 for each experimental session and the results of each stimulation phase presented in chronological order.

Sess.	Int. [mA]	Left Angles [°]		Right Angles [°]		Stim.	P_m [W]	P_F [W]	P_L [W]	FI [%]
		Init.	Term.	Init.	Term.					
S1	85	145	279	349	123	SES	3.61	11.16	0.64	94.3
						SDSS	8.73	16.21	4.65	71.3
S2	85	143	277	346	120	SDSS	10.11	18.82	4.80	74.5
						SES	2.72	6.62	1.54	76.8

4.3.2.4 Case 4

Subject P4 had multiple sclerosis, an EDSS score of 8. The subject was unable to achieve voluntary muscle contractions in the lower limbs, but some sensory functions remained. The subject had prior experience with FES of the quadriceps muscles but was not involved in FES cycling training at the time of the study. The subject reported a brief spastic activation of the hamstring muscles during the beginning of the second SES stimulation phase. Later analysis showed that the 8-second-long spasm was triggered by the onset of the stimulation. Two data analyses were conducted, one considering and one disregarding the first 8 seconds of the second SES stimulation phase (results are provided in Table 4.7). In the latter case, the stimulation phase was considered to have begun after the spastic activation of the muscles had been finished, i.e., the stimulation phase was 172 seconds long. The power produced by the left and right quadriceps muscle groups during the first and the second experimental sessions (with discarded spastic muscle activation) are presented in Figure 4.7.

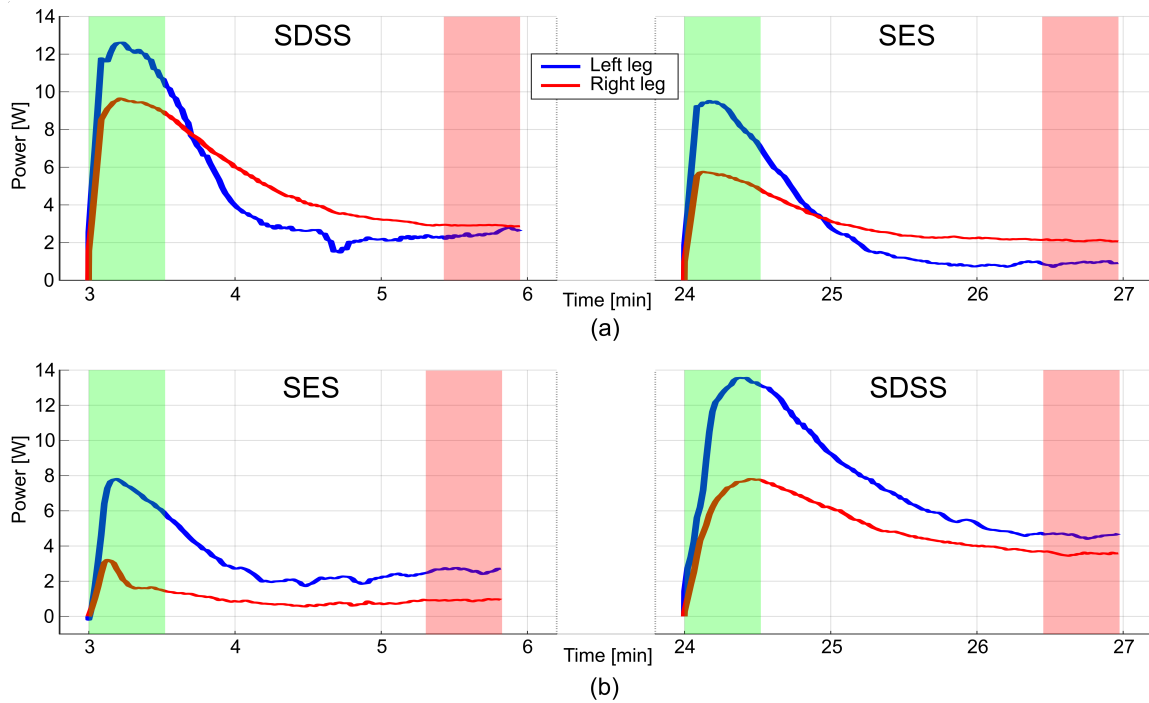


Figure 4.7: Power produced by the subject's P4 left leg (blue) and right leg (red) during each stimulation phase of (a) the first experimental session and (b) the second experimental session. The areas where the power produced during the first (P_F) and the last (P_L) 30 seconds of each stimulation phase are highlighted in green and red, respectively.

Table 4.7: Stimulation intensity and stimulation patterns measured for subject P4 for each experimental session and the results of each stimulation phase presented in chronological order.

Sess.	Int. [mA]	Left Angles [°]		Right Angles [°]		Stim.	P_m [W]	P_F [W]	P_L [W]	FI [%]
		Init.	Term.	Init.	Term.					
S1	75	165	295	345	115	SDSS	9.93	21.16	5.46	74.2
						SES	6.03	14.15	3.04	78.5
						SES _{SP}	4.54	8.37	3.55	57.5
S2	75	155	285	350	120	SES	4.40	8.53	3.55	58.4
						SDSS	12.57	17.63	8.16	53.7

4.4 Discussion

The goal of the present work was to compare the power output and the fatigue-reducing properties of spatially distributed sequential stimulation versus the traditional single electrode stimulation applied to the paralyzed quadriceps muscle groups of subjects performing motor-assisted FES cycling task. From prior isometric [78], [108], [110], [113], [124] and isokinetic studies [114], [115], [119], better performance of SDSS compared to SES can be expected. However, the only two studies that have compared SDSS to SES with SCI subjects performing FES cycling were reported with contrasting results [120], [122]. Both studies were conducted in preparation for the Cybathlon FES cycling race on the paralyzed quadriceps muscles of a single subject, and in either case was there motor assistance to maintain constant cycling cadence. Although these studies represent a more practical “real-life” test of SDSS application in FES cycling in a racing situation where motor assistance is not allowed, they involve a multitude of varying parameters such as stimulation intensity and cycling cadence which make drawing concrete conclusions more difficult. In that regard, we have designed a protocol to systematically evaluate the efficacy of SDSS versus SES where the number of variables is minimal. Furthermore, our study was designed for FES cycling under exercise and training conditions which have motor-assisted compensation for smooth constant speeds. For instance, stimulation parameters, stimulation time and cycling cadence are kept constant. We also note that an isometric study was conducted to examine the influence of the electrode placement and the stimulation parameters (specifically intensity) on the efficacy of SDSS (Chapter 3). Subsequently, we chose parameters that produced the best results for the present study in order to provide optimal conditions for SDSS. In contrast to the protocol in [120], each experimental session involved both stimulation phases (SES and SDSS) allowing for a direct comparison of the tested stimulation methods, circumventing the common challenge of variations in the subject’s strength and seating position over multiday tests.

Under moderate electrical stimulation conditions, quadriceps muscle groups produced

considerably more power when stimulated with SDSS compared to SES (from 88% to 240%). This was the outcome of each experimental session, regardless of the subject, the stimulated leg or the order of the stimulation phases (SES then SDSS versus SDSS then SES). When analyzing individual cases, it can be noticed that subject P3 produced negative power with the right leg during a part of the first SES stimulation phase. After closer inspection of the recorded forces, it was observed that the right quadriceps muscle group was completely fatigued, producing little to no force during the crank angle interval where the stimulation was operational. However, during the interval where the muscle was not stimulated, the recorded force did not perfectly match the reference force (force measured during the warm-up phase). We believe that this small discrepancy is most likely caused by a change of position of the leg in reference to the pedal, which appeared as a hindering force that resulted in a negative power value. Another point of discussion is the occurrence of a spastic muscle activation during the second SES stimulation phase of subject's P4 quadriceps muscle groups. After processing the data containing (SESSP) and excluding (SES) the power produced by the spastic activation of the muscles, it was evident that there was no noteworthy difference between P_m , P_F , P_L and FI values (Table 4.7). Thus, it was decided to exclude the first 8 seconds of data from the second SES stimulation phase. There is a possibility that the spastic activity altered the performance of the muscles. However, it is unlikely that the power produced during the second SES stimulation phase would be augmented to the degree that would impact the overall results of the experiment, especially when considering the results of the first experimental session.

Based on the fatigue index (Table 4.3), one subject experienced slightly more fatigue while three subjects showed slightly better fatigue resistance with SDSS. Coupled with the power produced during the last 30 seconds of each of the stimulation phases P_L , these results suggest that SDSS has better fatigue characteristics than SES. However, further investigation with more subjects is needed to draw statistically supported conclusions.

The overall outcome of the present work was that paralyzed quadriceps muscle groups stimulated with moderate electrical stimulation intensity SDSS produced substantially

more power with lower or equal levels of muscle fatigue than the equivalent SES stimulation while performing motor-assisted FES cycling. From the consensus of isometric studies comparing SDSS to SES, better performance of SDSS was expected under the conditions tested. Baptista et al. [120] reported modest benefits of SDSS whereas in the present study, the benefits of SDSS are much greater despite both studies stimulating the same muscle groups with a similar electrode configuration. This result may be due to the contrast in study protocols but the results from Chapter 3 suggest an alternative explanation. In Chapter 3, it was concluded that the efficacy of SDSS drops with the increase in electrical stimulation intensity. Indeed, we used moderate stimulation intensity in Chapter 4 to see if we could favor SDSS over SES during FES cycling conditions. We note, however, Baptista et al. used higher stimulation intensities that were increased as their study progressed. The same reasoning can explain the opposite result (worse performance of SDSS compared to SES) reported by Ceroni et al. [122].

The present study will be carried out with more subjects for statistical relevance. Moreover, using high stimulation intensities when performing FES cycling with SDSS should be investigated as well. Repeating the present study using high stimulation intensities would more rigorously test the performance of SDSS regardless of the stimulation parameters and it would provide new insight into the conclusion reached in Chapter 3.

Additionally, further investigation exploring a more practical use of SDSS applied to FES cycling should be conducted. By using a similar setup in a closed-loop configuration, the output power can be kept constant by altering the stimulation intensity. A protocol design around the aforementioned setup would be similar to most practical uses of FES cycling and it would provide a better assessment of the fatigue characteristics of SDSS. Another important factor for practical use is the electrode placement. Based on previous work (Chapter 3), we have concluded that placing a 2x2 matrix of cathode electrodes just under the distal motor point of the RF muscle is perhaps the optimal electrode configuration for the stimulation of the quadriceps muscle groups. This is supported by the results of the present study and work done by Baptista et al. [120]. However, the exact position for each

electrode was found through trial and error. Each electrode was activated separately in order to verify that the muscle achieved a fused contraction. This process requires experience with SDSS and it can take up to 15 minutes which is unreasonable for any clinical or personal use. Further examination of the electrode placement for SDSS applied to FES cycling should be conducted in order to determine more general and simple guidelines for electrode placement.

4.5 Conclusion

The present study demonstrated that, under the right conditions, SDSS can be superior to SES for performing motor-assisted FES cycling. Paralyzed quadriceps muscle groups stimulated with moderate electrical stimulation intensity SDSS produced substantially more power with lower or equal levels of muscle fatigue than the equivalent SES stimulation while performing motor-assisted FES cycling. Further studies should assess the efficacy of SDSS under suboptimal conditions and develop long-term training strategies suitable for clinical use.

Chapter 5

Optimization of Seating Position and Stimulation Pattern in Functional Electrical Stimulation Cycling: a Simulation Study

Abstract

Two significant challenges facing functional electrical stimulation (FES) cycling are the low power output and early onset of muscle fatigue, mainly due to the non-physiological and superficial recruitment of motor units and weakness of the antagonistic muscles. Thus optimization of the cycling biomechanical properties and stimulation pattern to achieve maximum output power with minimum applied charge is of great importance. The previous works ignored the muscle's force-velocity and force-length properties or employed complicated muscle models to find the optimal seating position and stimulation pattern which was a massive barrier to clinical experiments. In this work, an easy-to-use and precise muscle model in conjunction with Jacobian-based torque transfer functions were adopted to determine the optimal seating position, trunk angle, crank arm length, and stimulation intervals. Furthermore, the impact of muscle force-velocity factor in finding the optimal seating position and stimulation intervals was investigated. The simulation models showed the trivial effect of the force-velocity characteristics on the resulting optimal seating position of six healthy simulated subjects. This method can enhance the FES-cycling performance and shorten the time-consuming process of muscle model identification for optimization purposes.

5.1 Introduction

Even though the beneficial health outcomes of FES for motor-impaired individuals are extensively documented, two significant unresolved limitations confine the development of this method as global rehabilitation therapy. The significantly lower power generated by FES cycling than volitional cycling and the early onset of muscular fatigue limit the exercise duration (More details are provided in Section 1.5.5 and Chapter 3). These limitations enlighten the significance of optimizing the cycling biomechanical properties to achieve maximum output power with minimum applied electrical stimulus. Previous works focused on different aspects such as enhancing the mechanical structure of the ergometer [126]–[129], investigating the effects of changing the geometrical distances (e.g., seating position), and pedaling rate [129], [130], and finding optimum stimulation pattern of muscle groups [131], [132].

In [131], the muscle group torque transfer ratio was used to determine the ON and OFF times for stimulation of the gluteal, quadriceps, and hamstrings muscles. In this method, the length of leg segments of each patient and geometric properties of the stationary recumbent cycle were measured to determine each muscle group transfer ratio. The stimulation for each muscle group was ON only when the corresponding Jacobian element was greater than a threshold value determined by the trial-and-error method.

In [126], a complex dynamic model of the musculoskeletal structure of lower limbs of a paraplegic patient and a simulated leg cycling system was developed. The proposed model evaluated the effects of seating position, stimulation pattern, and cycling loads on improving cycling efficiency. This study showed that adjusting the geometrical properties has a significant impact on the performance of the virtual patient. Nevertheless, their proposed results have not yet been verified on real subjects.

In [132], a model of electrically stimulated muscle was combined with equations of motion of lower limbs on an ergometer to obtain a theoretical framework for investigating the contribution of each stimulated muscle group in the crank torque and finding the optimal

stimulation pattern. Their cost function considered the maximum power output generated by the lowest muscle force. Later in [133], they have investigated the influence of seating position and pedaling rate on the optimal stimulation pattern while pedaling on a non-circular path.

Rasmussen et al. [129], to eliminate the dead points of cycling, developed a four-bar linkage cycling mechanism by adding a lever arm and coupler. They determined the optimal stimulation pattern that could propel the muscles to produce constant torque around the crank cycle with minimum possible muscle force.

All of the mentioned works ignored the muscle's force-length and force-velocity properties or relied on complicated muscle models, which are complex and time-consuming to be identified in clinics for actual SCI patients. Moreover, most rehabilitation centers use commercial ergometers, e.g., Ergys, MOTomed, RT, which cannot provide a non-circular pedaling system or dead points-free cycling.

This study aims to propose a novel method to find the optimal position of the seat concerning the crank center, trunk angle of the user, and crank arm length while pedaling at the proper cadences for SCI patients. To meet this aim, an easy-to-use and precise model of the skeletal muscle was combined with the torque transfer functions of the lower body joints. Furthermore, the impact of muscle force (joint torque)-velocity (joint angular velocity) factor in finding the optimal point was investigated. As a beneficial corollary, an optimal stimulation interval for each active muscle group was determined based on the optimization functions. This method can be employed in most clinics with different ergometer types to help the patients to keep their exercise for a longer duration.

5.2 Methods

5.2.1 Model of Skeletal Muscle

The force produced by skeletal muscle in response to natural or artificial electrical stimulation has three major components: the activation dynamics factor (recruitment curve, contraction dynamics), force (joint torque)-length (joint angle) factor, and force (joint torque)-velocity (joint angular velocity) factor [134]–[136]. The first component imitates the relationship between stimulation strength, recruited fibers, and output force. According to the sliding filament theory, there is an optimal sarcomere length at which muscle force reaches its maximum capacity, while at shorter and longer lengths, the force decays to zero with nonlinear behavior [137], [138]. In this work, the following model was selected for isometric joint torque-angle factor from [139]

$$A_{TA}(\theta) = \cos\left(\frac{\pi}{\Delta\theta}(\theta - \theta_0)\right) \quad (5.1)$$

where θ is the joint angle, θ_0 is the joint angle where maximum force is generated, and $\Delta\theta$ is the range of joint angle in which active muscle force occurs.

To model the joint torque-angular velocity factor, the modified Hill equation was recruited from [139]

$$A_{TV}(\dot{\theta}) = \frac{2\omega_1\omega_2 + \dot{\theta}(\omega_1 - 3\omega_2)}{2\omega_1\omega_2 + \dot{\theta}(2\omega_1 - 4\omega_2)} \quad (5.2)$$

where ω_1 and ω_2 are the joint angular velocities at which muscle force reaches 50% and 75% of the isometric force. According to this equation, the force (torque) exerted by muscle decreases as the muscle shortening velocity increases.

This work assumes that stimulation intensity has its maximum possible value at each moment, so the activation dynamics factor is constant but still muscle-specific. Hence, combining equations 5.1 and 5.2 yields the final model for active muscle torque

$$T_{Active}(\theta, \dot{\theta}) = T_{MAX}A_{TA}(\theta)A_{TV}(\dot{\theta}) \quad (5.3)$$

where T_{MAX} is the maximum isometric joint torque. It should be mentioned that the moment arm which relates the muscle force to the corresponding joint torque is considered to be angle-independent for the sake of simplicity.

5.2.2 Model of Stationary Cycle

A planar model of a two-legged recumbent bike with lower limbs and trunk of a rider is presented in Figure 5.1a. This model consists of two closed kinematic chains for each leg connected at the hip joint and crank center. Each kinematic chain has four links (thigh, lower leg, crank arm, and frame of stationary cycle) and four revolute joints (hip, knee, pedal, and crank center). The cycle frame consists of a vertical segment and a horizontal segment that is fixed to the ground. The ankle joint is assumed to be fixed at 90° and rigidly connected to the pedal for side-to-side stability and safety of the rider. The proposed closed kinematic chains can be described entirely by the length of the links (l_{th} , l_l , l_{cr} , l_x , l_y) and crank angle of one side due to the following constraints: i) hip and crank center are fixed, ii) pedals have a constant 180° of phase difference.

To find q_h and q_k of one side concerning the crank angle of the corresponding side (q_{cr}), each link of the corresponding closed kinematic chain can be considered a vector in the x-y plane as depicted in Figure 5.1b. Projecting each vector on the x- and y-axis yields

$$l_{cr} \cos(q_{cr}) + l_l \cos(q_k) + l_{th} \cos(q_h) - l_x = 0 \quad (5.4)$$

$$-l_{cr} \sin(q_{cr}) - l_l \sin(q_k) + l_{th} \sin(q_h) + l_y = 0 \quad (5.5)$$

solving these two independent equations for q_h and q_k in terms of q_{cr} yields the following parametric solutions

$$q_h = \beta - \arccos \left(\frac{-\alpha_3}{\sqrt{\alpha_1^2 + \alpha_2^2}} \right) \quad (5.6)$$

$$q_k = -\arctan \left(\frac{-l_{cr} \sin(q_{cr}) + l_{th} \sin(q_h) + l_y}{l_{cr} \cos(q_{cr}) + l_{th} \cos(q_h) - l_x} \right) \quad (5.7)$$

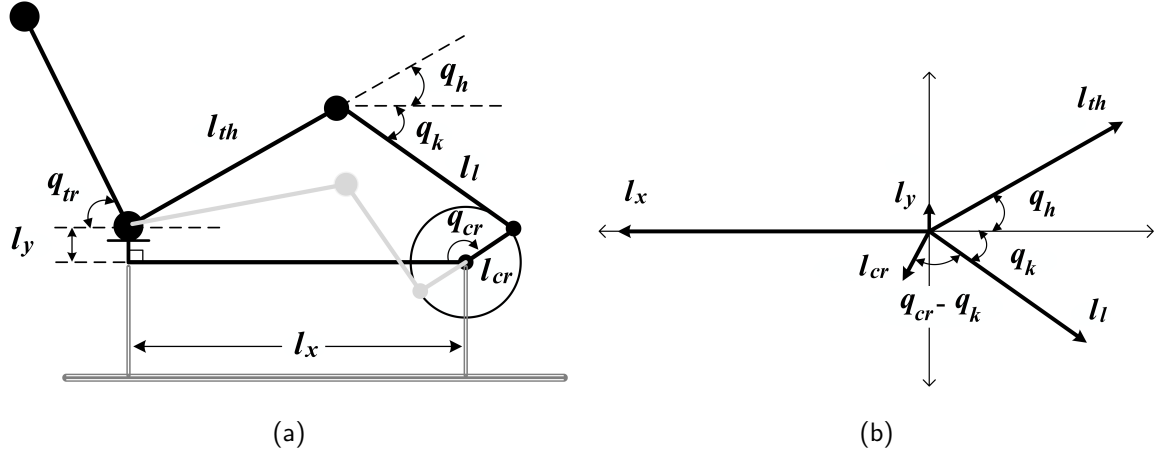


Figure 5.1: (a) Skeletal model of stationary cycling. q_{cr} , q_{tr} , q_h , and q_k are the crank angle, the trunk angle, the angle between thigh and ground, and the angle between shank and ground, respectively. l_{cr} , l_{th} , l_l , l_x , and l_y are the crank arm length, the thigh length, the lower leg length, the horizontal distance between the hip joint and the crank center, and the vertical distance between the hip joint and crank center, respectively. (b) Projected view of skeletal model segments on x-axis and y-axis.

where

$$\alpha_1 = -2l_{th}(l_{cr} \sin(q_{cr}) - l_y)$$

$$\alpha_2 = 2l_{th}(l_{cr} \cos(q_{cr}) - l_x)$$

$$\alpha_3 = l_x^2 + l_y^2 + l_{th}^2 - l_l^2 + l_{cr}^2 - 2l_{cr}(l_x \cos(q_{cr}) + l_y \sin(q_{cr}))$$

$$\beta = \pi + \arctan\left(\frac{\alpha_1}{\alpha_2}\right)$$

As mentioned in the previous section, the force exerted by muscle contraction in response to the stimulation produces torque around the corresponding joint. This torque is transferred from the leg joints to the crank axis via the torque transfer functions to rotate the pedals and legs. Quadriceps femoris (knee extensor), hamstrings (knee flexor), and gluteal (hip extensor) muscle groups are the main force actuators in cycling exercise which can be easily stimulated by surface electrodes. Torque transfer functions from hip and knee joints

to the crank center are defined as [140], [141]

$$J_h(q_{cr}) = \frac{\partial \theta_h}{\partial q_{cr}}, \quad J_k(q_{cr}) = \frac{\partial \theta_k}{\partial q_{cr}} \quad (5.8)$$

where $\theta_h = q_h + q_{tr}$, and $\theta_k = q_h + q_k$ are hip joint and knee joint angles, respectively. q_{tr} is the angle between the trunk of the subject and the ground, as depicted in Figure 5.1a. Since q_{tr} is constant during cycling motion, equation 5.8 can be rewritten as

$$J_h(q_{cr}) = \frac{\partial q_h}{\partial q_{cr}}, \quad J_k(q_{cr}) = \frac{\partial (q_h + q_k)}{\partial q_{cr}} \quad (5.9)$$

by taking time derivative from 5.4 and 5.5 and considering

$$\dot{q}_h = \frac{\partial q_h}{\partial q_{cr}} \dot{q}_{cr}, \quad \dot{q}_k = \frac{\partial q_k}{\partial q_{cr}} \dot{q}_{cr} \quad (5.10)$$

5.8 can be expressed in terms of q_{cr}

$$J_h(q_{cr}) = \frac{l_{cr}}{l_{th}} \left(\frac{\sin(q_k - q_{cr})}{\sin(q_k + q_h)} \right) \quad (5.11)$$

$$J_k(q_{cr}) = \frac{l_{cr}}{l_{th}} \left(\frac{\sin(q_k - q_{cr})}{\sin(q_k + q_h)} \right) - \frac{l_{cr}}{l_l} \left(\frac{\sin(q_h + q_{cr})}{\sin(q_k + q_h)} \right) \quad (5.12)$$

To elicit the torque transfer functions for the involved muscle groups, it should be noticed that clockwise torque about the crank axis is considered as positive torque. Hence (with respect to Figure 5.1a), the muscle torque transfer function for each muscle group is determined as

$$J_{\text{hams}}(q_{cr}) = \begin{cases} J_k(q_{cr}) & \text{if } J_k(q_{cr}) > 0 \\ 0 & \text{if } J_k(q_{cr}) \leq 0 \end{cases} \quad (5.13)$$

$$J_{\text{quad}}(q_{cr}) = \begin{cases} 0 & \text{if } J_k(q_{cr}) \geq 0 \\ -J_k(q_{cr}) & \text{if } J_k(q_{cr}) < 0 \end{cases} \quad (5.14)$$

$$J_{\text{glut}}(q_{cr}) = \begin{cases} 0 & \text{if } J_h(q_{cr}) \geq 0 \\ -J_h(q_{cr}) & \text{if } J_h(q_{cr}) < 0 \end{cases} \quad (5.15)$$

5.2.3 Optimization

Method 1: According to the previous sections, the muscle force (joint torque)-length (joint angle) factor, the muscle force (joint torque)-velocity (joint angular velocity) factor, and the torque transfer functions of the stimulated muscle groups have a pivotal role in obtaining the maximum forward torque about the crank from the provided electrical stimulation. Multiplication of these factors for each muscle group is defined as the muscle optimization function

$$\delta_m^1 = T_{MAX}^m \cdot A_{TA}^m(\theta_j(q_{cr})) \cdot A_{TV}^m(\dot{\theta}_j(q_{cr}, \dot{q}_{cr})) \cdot J_m(q_{cr}) \quad (5.16)$$

where $m \in \mathcal{M} \triangleq \{\text{hams}, \text{quad}, \text{glut}\}$ indicates muscle group, and $j \in \mathcal{J} \triangleq \{\text{hip}, \text{knee}\}$ indicates the joint. The final optimization function which should be maximized is constructed by taking integral of the muscle optimization functions 5.16 over a whole crank cycle for each muscle group and adding them together

$$\psi_1 = \sum_{m \in \mathcal{M}} \int_0^{2\pi} \delta_m^1 dq_{cr} \quad (5.17)$$

Method 2: Finding the parameters of 5.2 for three muscle groups of each subject is time-consuming and tedious. Moreover, the required tests to determine muscle shortening velocities at which muscle force reaches 50% and 75% of the isometric force may lead to early onset of muscle fatigue in paralyzed muscles. In this mode, we omitted the torque-angular velocity factor from 5.16 and the muscle optimization function is defined as

$$\delta_m^2 = T_{MAX}^m \cdot A_{TA}^m(\theta_j(q_{cr})) \cdot J_m(q_{cr}) \quad (5.18)$$

thus the final optimization function is

$$\psi_2 = \sum_{m \in M} \int_0^{2\pi} \delta_m^2 dq_{cr} \quad (5.19)$$

5.2.4 Constraints

As depicted in Figure 5.1a, the thigh segment, the lower leg segment, and the imaginary line which connects the hip joint to the pedal (l_b) are sides of an imaginary triangle. According to the triangle inequality, the following conditions must be satisfied over a crank cycle

$$l_l + l_{th} > \max(l_b), \quad l_l - l_{th} < \min(l_b) \quad (5.20)$$

the extremum values of l_b calculated with respect to l_x , l_y , and l_{cr} as

$$\max(l_b) = \sqrt{l_{cr}^2 + l_x^2 + l_y^2 + 2l_{cr}\sqrt{l_x^2 + l_y^2}}, \quad \min(l_b) = \sqrt{l_{cr}^2 + l_x^2 + l_y^2 - 2l_{cr}\sqrt{l_x^2 + l_y^2}} \quad (5.21)$$

The optimization ranges for l_x and l_y are $l_x \in [lb_x, ub_x]$, and $l_y \in [lb_y, ub_y]$, where

$$lb_x = l_{cr}, \quad ub_x = l_{th} + l_l - l_{cr},$$

$$lb_y = 0, \quad ub_y = l_{th} + l_l - l_{cr}$$

the upper bounds correspond to full knee extension when $l_y = 0$, and $l_x = 0$, respectively.

The optimization ranges for l_{cr} (cm) and q_{tr} (deg) are $l_{cr} \in [10, 30]$, and $q_{tr} \in [0, 90]$ selected from the literature [126].

Given that extensive joint angle ranges can induce spasms or pose risks to patients, the following constraints were applied [129]:

$$15^\circ \leq \theta_k \leq 135^\circ, \quad 0^\circ \leq \theta_h \leq 130^\circ, \quad \max(\theta_h) - \min(\theta_h) \leq 47^\circ$$

The cycling cadences of 35 rpm and 50 rpm were considered to represent low and high cycling rates for SCI patients, respectively.

Table 5.1: Summary of the characteristics of the subjects.

Subject	S1	S2	S3	S4	S5	S6
Gender	M	F	M	F	M	F
Age (years)	19.6	19.6	61.3	58.1	71.7	68.3
Height (cm)	174.8	160.6	174.7	162.6	174.3	161.7
Mass (kg)	72.8	62.1	87.7	66.0	86.2	64.5
l_{th} (cm)	42.82	39.34	42.80	39.83	42.70	39.61
l_l (cm)	49.81	45.77	49.78	46.34	49.67	46.08

5.3 Results

The specifications of six averaged subjects (three males and three females), including age, gender, height, and mass, averaged over 34 healthy subjects classified by age and gender, were taken from [139]. The humanoid dimensions (length of thigh and lower leg with respect to height) utilized here are extracted from the standard anthropometric human measurements introduced in [138] (Table 5.1).

The muscle model parameters corresponding to three muscle groups (gluteal as hip extensor, quadriceps as knee extensor, and hamstrings as knee flexor) of six averaged subjects were extracted from [139] and summarized in Table 5.2. The parameters for which the optimization was performed included the vertical distance between the hip joint and crank center (l_y), the horizontal distance between the hip joint and crank center (l_x), crank arm length (l_{cr}), and the angle between the trunk of the subject and the ground (q_{tr}). The optimization range and step size of parameters are presented in Table 5.3.

The muscle model and the optimization process were implemented in MATLAB R2020a (MathWorks, Natick, USA). The optimization process was conducted for both

proposed methods at cadences of 35 rpm and 50 rpm, with the optimal values presented in Table 5.3. For Method 2, the optimization is independent of cycling cadence, resulting in similar optimal values for both cadences.

Table 5.2: The Muscle model parameters of averaged subjects [139].

Muscle Groups	Muscle Parameters	S1	S2	S3	S4	S5	S6
Hip Extensor	T_{MAX}^*	0.161	0.181	0.171	0.140	0.144	0.138
	$\theta_0(rad)$	0.932	1.242	1.176	1.241	1.125	1.542
	$\pi/\Delta\theta$	0.958	0.697	0.922	0.830	0.896	0.707
	$\omega_1(rad/s)$	1.578	1.567	1.601	1.444	1.561	1.613
	$\omega_2(rad/s)$	3.190	3.164	3.236	2.919	3.152	3.256
Knee Extensor	T_{MAX}^*	0.163	0.159	0.156	0.128	0.137	0.124
	$\theta_0(rad)$	1.133	1.274	1.173	1.141	1.067	1.140
	$\pi/\Delta\theta$	1.258	1.187	1.225	1.286	1.310	1.347
	$\omega_1(rad/s)$	1.517	1.393	1.518	1.332	1.141	1.066
	$\omega_2(rad/s)$	3.952	3.623	3.954	3.469	3.152	2.855
Knee Flexor	T_{MAX}^*	0.087	0.080	0.081	0.060	0.069	0.060
	$\theta_0(rad)$	0.522	0.635	0.523	0.402	0.437	0.445
	$\pi/\Delta\theta$	0.869	0.873	0.986	0.967	0.838	0.897
	$\omega_1(rad/s)$	2.008	1.698	1.830	1.693	1.718	1.121
	$\omega_2(rad/s)$	5.233	4.412	4.777	4.410	4.476	2.922

* Normalized by body weight \times height.

The optimal values from both methods at 35 rpm and 50 rpm for all subjects were used to calculate the total generated torques over a crank cycle using equation 5.17. The generated torque using the optimal variables from Method 2 was then compared to that from Method 1. The differences ($\Delta\psi_1[\%]$) are shown in Table 5.4, indicating a slight difference between the torques generated by optimal variables from Method 2 and those generated by Method 1.

Table 5.3: Summary of optimized variables using Method 1 and Method 2 at 35 rpm and 50 rpm for all subjects.

Variables	Range (Step size)	Methods	S1		S2		S3		S4		S5		S6	
			35 rpm	50 rpm										
l_x (cm)	$lb_x - ub_x$	1	64	64	71	68	67	67	70	70	75	75	71	65
	(1 cm)	2	64		71		77		70		75		71	
l_y (cm)	$lb_y - ub_y$	1	44	44	4	17	39	39	18	18	19	19	10	28
	(1cm)	2	44		4		9		18		19		10	
l_{cr} (cm)	10 – 30	1	14	14	13	13.5	14	14	13	13	14	14	13	13.5
	(0.5 cm)	2	14		13		14		13		14		13	
q_{tr} (deg)	0 – 90	1	56	56	42	51	65	65	53	53	46	46	64	77
	(1°)	2	56		42		42		54		47		64	

Table 5.4: Summary of the difference in total generated torque over a crank cycle (%) between optimized variables from Method 1 and Method 2 at 35 rpm and 50 rpm for all subjects.

Subjects	$\Delta\psi_1$ [%]	
	35 rpm	50 rpm
S1	0	0
S2	0	0.1052
S3	<0.001	0.0018
S4	<0.001	0.0027
S5	<0.001	0.0028
S6	0	0.0108

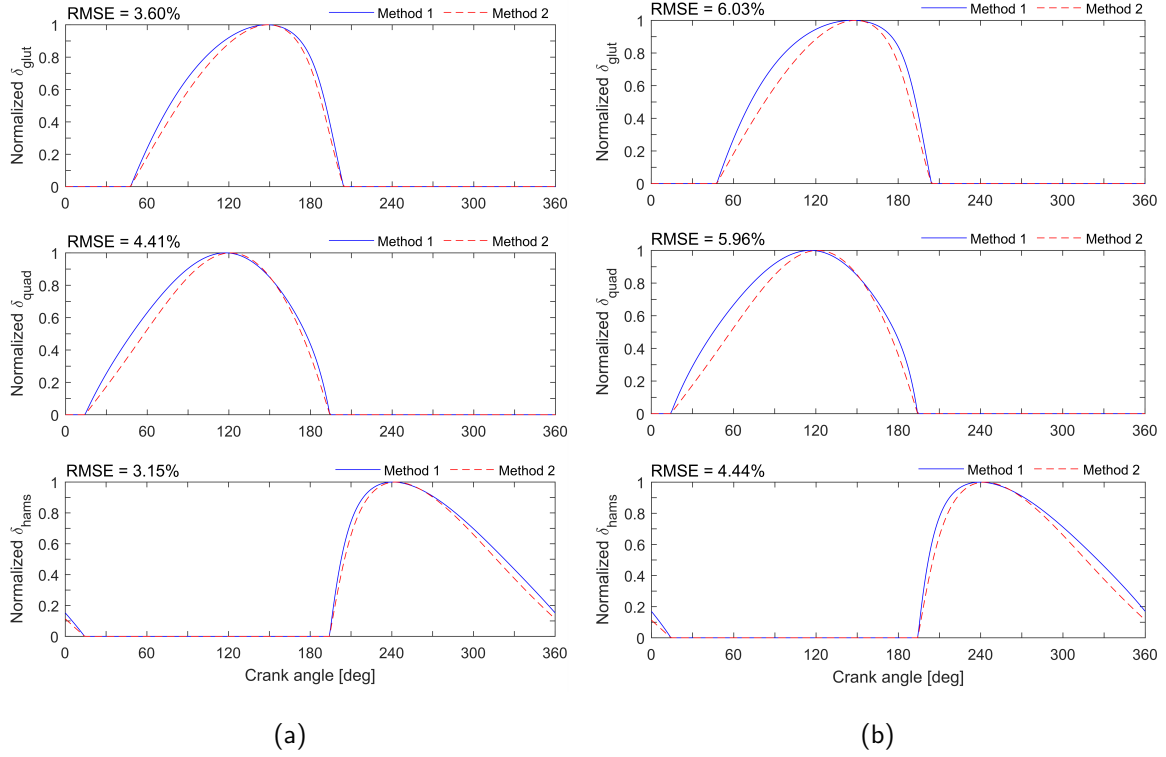


Figure 5.2: Normalized muscle optimization functions (δ_m^1 and δ_m^2) of gluteal, quadriceps, and hamstrings over a whole crank cycle using optimal seating position resulted from Method 2 for S5 at (a) 35 rpm and (b) 50 rpm.

After confirming that the total generated torques over a crank cycle at the optimal variables derived from Method 1 and Method 2 are nearly identical (below 1% difference), root mean square error (RMSE) was utilized to evaluate the difference between the normalized muscle optimization functions (δ_m^1 and δ_m^2) at the optimal variables from Method 2. The muscle optimization functions were normalized for ease of comparison.

The results of both methods for S5 at 35 rpm and 50 rpm are illustrated in Figure 5.2a and Figure 5.2b, respectively. Table 5.5 provides the RMSEs (%) across three muscle groups and all subjects. It is observed that the averaged RMSEs (%) are $3.63 \pm 0.19\%$, $4.17 \pm 0.38\%$, and $3.25 \pm 0.62\%$ at 35 rpm for gluteal, quadriceps, and hamstrings, respectively. At 50 rpm, the averaged RMSE (%) between both models are $6.07 \pm 0.38\%$, $5.80 \pm 0.48\%$, and $4.59 \pm 0.88\%$ for gluteal, quadriceps, and hamstrings, respectively.

The muscle optimization function can also provide efficient stimulation intervals for each muscle group. Indeed, each muscle group should be stimulated at the angles with large muscle optimization function values. This can be performed by considering a minimum threshold (e.g., 0.5) for each normalized muscle optimization function and turning the stimulation on for angles with greater than threshold values as presented in Table 5.6.

Table 5.5: The difference between the normalized muscle optimization functions of both methods (δ_m^1 and δ_m^2) for the optimal variables derived from Method 2 at 35 rpm and 50 rpm, evaluated across three muscle groups and all subjects.

Subjects	glut		quad		hams	
	RMSE (%)		RMSE (%)		RMSE (%)	
	35 rpm	50 rpm	35 rpm	50 rpm	35 rpm	50 rpm
S1	3.53	5.88	3.72	5.23	2.79	3.93
S2	3.65	6.11	4.14	5.81	3.42	4.83
S3	3.45	5.73	3.76	5.28	2.79	3.93
S4	4.03	6.87	4.17	5.86	2.83	3.98
S5	3.6	6.03	4.41	5.96	3.15	4.44
S6	3.49	5.81	4.83	6.67	4.54	6.42
Mean \pm SD	3.63 \pm 0.19	6.07 \pm 0.38	4.17 \pm 0.38	5.80 \pm 0.48	3.25 \pm 0.62	4.59 \pm 0.88

5.4 Discussion and Conclusion

In this work, two optimization schemes were developed to determine the optimal seating position and stimulation pattern for which the maximum crank torque is achieved during indoor recumbent FES-cycling. The proposed schemes relied on the torque transfer ratios and muscle model to find the optimal seating position from the muscle to the crank. Torque transfer ratios can be calculated using the patients' anthropometric characteristics. Despite the first method, which required a complete identification of isometric and isokinetic terms of a muscle model, the second method only relied on the isometric part. According to

the results, the second method can determine the optimal seating position and stimulation intervals with good accuracy at low and high pedaling rates in SCI patients.

Using the proposed method (Method 2) can shortcut the time-consuming process of muscle identification to find the proper seating position and stimulation pattern that can enable the patients to use the maximum strength of their muscles, ultimately extending the duration and efficiency of their exercise.

Table 5.6: Stimulation intervals measured from normalized muscle optimization functions (δ_m^1 and δ_m^2) greater than threshold value of 0.5 for the optimal variables derived from Method 2 at 35 rpm, and 50 rpm.

Subjects	Methods	glut		quad		hams	
		Stimulation Interval (deg)		Stimulation Interval (deg)		Stimulation Interval (deg)	
		35 rpm	50 rpm	35 rpm	50 rpm	35 rpm	50 rpm
S1	1	[97-211]	[93-213]	[67-195]	[64-196]	[224-344]	[223-346]
	2	[103-209]		[75-193]		[226-339]	
S2	1	[64-181]	[61-182]	[31-160]	[28-160]	[193-318]	[192-321]
	2	[71-178]		[39-158]		[195-311]	
S3	1	[69-184]	[65-185]	[38-166]	[35-167]	[196-311]	[195-313]
	2	[75-181]		[45-164]		[198-306]	
S4	1	[76-192]	[71-194]	[46-174]	[43-175]	[203-313]	[202-315]
	2	[83-189]		[55-172]		[205-309]	
S5	1	[76-191]	[72-193]	[49-177]	[45-178]	[203-323]	[202-325]
	2	[83-189]		[58-173]		[205-317]	
S6	1	[69-185]	[66-187]	[39-166]	[35-167]	[196-316]	[194-320]
	2	[76-183]		[49-163]		[199-308]	

Although the proposed method showed promising results, there are still some limitations that should be considered. First of all, the specifications of the simulated muscle model were extracted from healthy subjects. The bi-articular behavior of muscles, such as the biceps femoris, means that torque around one joint depends on another joint's position. Bi-articular muscles were not considered in the current model due to complexity.

Moreover, it should be noted that the proposed methods did not account for the electromechanical delay (EMD), which represents the time interval between the application of an electrical stimulus and the onset of force production by the muscle. This delay should be incorporated to appropriately shift the stimulation pattern backward relative to the crank rotation, ensuring that force is produced at the desired angles [48].

We will investigate the effect of these limitations and the efficiency of the proposed optimization method with actual SCI patients in our future work.

Conclusion and Future Prospects

This study adopted a comprehensive approach to overcome the limitations associated with functional electrical stimulation (FES)—namely, discomfort, premature muscle fatigue, and insufficient power output—faced by individuals with motor-deficit neurological disorders, such as spinal cord injury (SCI) and stroke.

The first study explored the performance of a novel garment embedded with textile electrodes for neuromuscular electrical stimulation regarding comfort, temporal consistency, efficiency, and electrical impedance. For comparative analysis, a self-adhesive hydrogel electrode, commonly used in clinical settings served as a benchmark. The developed garment, in combination with a minimal amount of moisturizing lotion, enough for epidermal hydration, showed no statistical difference compared to self-adhesive hydrogel electrodes of similar shape and size under identical pressure regarding motor threshold intensity, burning sensation intensity, and maximum tolerable intensity, during isometric knee extension exercise. The study's findings are promising for the application of textile electrodes in motor rehabilitation, enhancing patient compliance and therapy outcomes.

The principal limitation of this study is its exclusive reliance on healthy subjects, rather than including individuals with neurological conditions. This selection has significant implications, particularly in the measurement of force output. Healthy subjects are capable of providing volitional inputs, especially at higher stimulation intensities (due to pain), which may not be representative of responses in individuals with neurological impairments. Consequently, our analysis primarily focused on the motor threshold intensity, occurring at low intensities, as a measure of stimulation efficiency. This reliance limited our ability

to investigate the effects of higher intensities on force production. Future research should address this gap by incorporating a diverse participant group, including those with neurological conditions such as SCI and stroke, to fully understand the range of responses to neuromuscular electrical stimulation and to enhance the generalizability of our findings.

A notable limitation of the study protocol was the inability to blind participants to the types of electrodes used. This aspect could introduce a form of bias, particularly if subjects had pre-existing preferences or perceptions about the different electrode types. Such biases might influence their subjective experience and feedback during the study, potentially affecting the reliability of the results in terms of perceived comfort. Future studies could benefit from incorporating a double-blind design, where neither the participants nor the researchers know which electrode type is being used, to minimize this potential source of bias and enhance the validity of the findings.

This study specifically targeted the quadriceps femoris muscle group, which, due to its large size, necessitates the use of relatively large electrodes. However, it is important to note that prior research has indicated that smaller electrodes induce greater discomfort due to higher current density. This is a critical consideration as smaller electrodes are essential for achieving selective muscle stimulation and reducing muscle fatigue. Consequently, these findings underscore the need for further experiments involving smaller electrodes. Such studies would not only address the aspect of comfort with different electrode sizes but also evaluate the effectiveness of stimulation in smaller muscle groups, thereby contributing to a more comprehensive understanding of neuromuscular electrical stimulation using textile electrodes.

It is important to acknowledge that the scope of this study was confined to isometric conditions. As such, it does not offer insights into the comparative performance of textile electrodes versus hydrogel electrodes during dynamic activities, like cycling and walking. Recognizing this gap, our future research will specifically focus on evaluating the performance of textile electrodes in dynamic scenarios. Moreover, we are working on adding electromyography (EMG) signal acquisition capability to the developed garment to ana-

lyze muscular function, particularly muscle fatigue induced by electrical stimulation, and residual volitional contribution. The latter facilitates the regulation of both the duration and strength of stimulation. This enhancement significantly boosts the force output of weakened muscles, allowing individuals to manage the movement's execution directly. FES offers additional support, amplifying the therapeutic outcomes. This is particularly effective when the stimulation is applied simultaneously with the patient's voluntary effort [3], [142].

In the next study, we assessed the efficacy of spatially distributed sequential stimulation (SDSS) in comparison to the traditional FES using a single electrode stimulation (SES) with respect to the time to fatigue (TTF), maximum produced force (MPF), and average produced force until fatigue (APF) at moderate and high electrical stimulation intensities. Our research focused on the quadriceps muscle group and the Vastus Lateralis (VL) muscle of subjects with SCI. Our findings elucidated that the superior performance of SDSS over SES is considerably compromised for the quadriceps muscle group under high-intensity modality. The higher stimulation intensities generate stronger electrical fields beneath the electrodes, resulting in excessive recruitment of overlapping motor units. Consequently, this situation resembles the configuration of SES, leading to heightened fatigue of the overlapping motor units.

In a comparable study conducted on the Vastus Lateralis (VL), where the number of motor points available for stimulation is more restricted, no significant differences were observed when comparing the outcomes of high versus moderate electrical stimulation intensities. This lack of distinction could be attributed to the relatively high levels selected for what was considered moderate intensity, coupled with the simultaneous activation of antagonistic muscle groups. To gain deeper insights into the nuances of SDSS and to clarify the observed inconsistencies, it is suggested that future research should involve a greater number of participants. Additionally, conducting these experiments with smaller electrodes and reduced intensities of stimulation on muscles less prone to antagonistic muscle co-activation, such as the tibialis anterior, might provide more definitive results.

Although SDSS enhances fatigue resistance and power output, it induces more painful contractions compared to SES owing to a higher current density. Consequently, SDSS presents a viable stimulation method primarily for patients lacking sensory function. However, this approach is less advantageous for patients with incomplete SCI and stroke who retain some sensory perception, as they can experience discomfort from the stimuli. Recognizing this gap, our future research will be focused on activating the inactive electrodes in the SDSS method using a sensory threshold stimulation to improve the sensation while ensuring minimal involvement of motor fibers, allowing them to remain in a state of rest. Consequently, we aim to preserve the fatigue-resistant advantages of SDSS while reducing the discomfort sensation induced by stimulating smaller electrodes at lower frequencies during the SDSS configuration. By consistently administering a low-intensity stimulus, pain can be reduced. This interaction occurs through the mediation of inhibitory interneurons. Specifically, sensory fibers ($A\beta$) have the ability to inhibit pain fibers ($A\delta$ and C fibers), thereby preventing the transmission of pain signals to the brain (pain gate theory).

Drawing from the insights of the previous study into the impact of stimulation intensity on the efficacy of SDSS under isometric conditions, this research compared SDSS with SES while conducting motor-assisted cycling at a constant cadence in SCI patients. Our methodical evaluation focused on moderate-intensity stimulation scenarios. Throughout each testing phase, it was observed that the quadriceps muscles, when activated via SDSS, generated significantly more power while experiencing the same or reduced levels of fatigue than those stimulated by SES. The findings indicate that SDSS may outperform SES in motor-assisted FES cycling, although confirming statistical significance requires a broader participant base. To solidify these findings, it is essential to undertake additional research that examines a more extensive array of variables, such as the size and placement of electrodes and the intensity of stimulation within the context of FES cycling. Moreover, the development of a study incorporating a closed-loop system—whereby the power output from the stimulated muscles is maintained at a predetermined level, adjusting the stimulation intensity as muscles fatigues—would offer a more accurate evaluation of SDSS's

capability to minimize fatigue during high-intensity cycling conditions.

The final study involved a biomechanical simulation of FES cycling. This aimed to identify the optimal seat position relative to the crank center, the trunk angle of the user, and the crank arm length, in addition to the optimal stimulation pattern while maintaining an appropriate cadence for SCI patients. Moreover, it examined the role of the muscle force (joint torque)-velocity (joint angular velocity) relationship in determining the optimal configuration. According to the results, the second method can determine the optimal seating position and stimulation intervals accurately. This work considered a cycling cadence of 35 rpm, which corresponds to a comfortable pedaling rate that SCI patients should be able to achieve without problems.

Although the proposed method showed promising results, there are still some limitations that should be considered. First of all, the specifications of the simulated muscle model were extracted from healthy subjects. The bi-articular behavior of muscles, such as the biceps femoris, means that torque around one joint depends on another joint's position. Bi-articular muscles were not considered in the current model due to complexity. We will investigate the effect of these limitations and the efficiency of the proposed optimization method with actual SCI patients in our future work.

Bibliography

- [1] G. J. Tortora and B. H. Derrickson, *Principles of anatomy and physiology*, 16th ed. Nashville, TN: John Wiley & Sons, 2023, ISBN: 978-1-394-21021-3.
- [2] “Nervous system”. (Aug. 13, 2018), [Online]. Available: <https://www.encyclopedia.com/medicine/and-physiology/anatomy-and-physiology/nervous-system> (visited on 02/01/2024).
- [3] E. Kandel, J. D. Koester, S. H. Mack, and S. Siegelbaum, *Principles of neural science, sixth edition*, 6th ed. Columbus, OH: McGraw-Hill Education, 2021, ISBN: 978-1-259-64223-4.
- [4] “Neuronal structure and function”, in *Basic Physiology for Anaesthetists*, Cambridge University Press, 2019, pp. 189–191, ISBN: 978-1-108-56501-1. DOI: 10.1017/9781108565011.047.
- [5] A. L. Hodgkin and A. F. Huxley, “A quantitative description of membrane current and its application to conduction and excitation in nerve”, *J. Physiol.*, vol. 117, no. 4, pp. 500–544, 1952, ISSN: 0022-3751. DOI: 10.1113/jphysiol.1952.sp004764.
- [6] Wikipedia contributors, *Action potential*, in Nov. 13, 2023. [Online]. Available: [https://en.wikipedia.org/w/index.php?title=Action`potential&oldid=1184911660](https://en.wikipedia.org/w/index.php?title=Action%20potential&oldid=1184911660).
- [7] B. Kolb and I. Q. Whishaw, *Fundamentals of Human Neuropsychology*, 5th ed. New York, NY: W.H. Freeman, 2003, ISBN: 978-0-7167-5300-1.
- [8] Wikipedia contributors, *Neurotransmission*, in Jan. 21, 2024. [Online]. Available: <https://en.wikipedia.org/w/index.php?title=Neurotransmission&oldid=1197580187>.

- [9] “Skeletal muscle”. (Jan. 9, 2021), [Online]. Available: <https://my.clevelandclinic.org/health/body/2-skeletal-muscle> (visited on 02/01/2024).
- [10] Moore, *Clinically oriented anatomy*, 8th ed. Philadelphia, PA: Lippincott Williams and Wilkins, 2017, ISBN: 978-1-4963-4721-3.
- [11] E. N. Marieb and K. N. Hoehn, *Human Anatomy & Physiology: International Edition*, 9th ed. Upper Saddle River, NJ: Pearson, 2012, ISBN: 978-0-321-79917-3.
- [12] *Skeletal muscle contraction — concise medical knowledge*, Dec. 3, 2021. [Online]. Available: <https://www.lecturio.com/concepts/skeletal-muscle-contraction/> (visited on 02/01/2024).
- [13] *Muscle - actin-myosin, regulation, contraction*, in *Encyclopedia Britannica*. [Online]. Available: <https://www.britannica.com/science/muscle>.
- [14] L. Haggie, L. Schmid, O. Röhrle, T. Besier, A. McMorland, and H. Saini, “Linking cortex and contraction—integrating models along the corticomuscular pathway”, *Front. Physiol.*, vol. 14, 2023, ISSN: 1664-042X. DOI: 10.3389/fphys.2023.1095260.
- [15] R. Bhimani, F. Medina, and L. Carney-Anderson, “CE: Managing movement disorders: A clinical review”, *Am. J. Nurs.*, vol. 118, no. 12, pp. 34–40, 2018, ISSN: 0002-936X. DOI: 10.1097/01.naj.0000549666.20957.a3.
- [16] W. Scott, J. Stevens, and S. A. Binder-Macleod, “Human skeletal muscle fiber type classifications”, *Phys. Ther.*, vol. 81, no. 11, pp. 1810–1816, 2001, ISSN: 0031-9023. DOI: 10.1093/ptj/81.11.1810.
- [17] C. J. Heckman and R. M. Enoka, “Motor unit”, pp. 2629–2682, Oct. 2012, Publisher: Wiley. DOI: 10.1002/cphy.c100087.
- [18] E. Henneman, G. Somjen, and D. O. Carpenter, “Functional significance of cell size in spinal motoneurons”, *J. Neurophysiol.*, vol. 28, no. 3, pp. 560–580, 1965, ISSN: 0022-3077. DOI: 10.1152/jn.1965.28.3.560.

- [19] C. J. De Luca and E. C. Hostage, “Relationship between firing rate and recruitment threshold of motoneurons in voluntary isometric contractions”, *J. Neurophysiol.*, vol. 104, no. 2, pp. 1034–1046, 2010, ISSN: 0022-3077. DOI: 10.1152/jn.01018.2009.
- [20] U. Proske and S. C. Gandevia, “The proprioceptive senses: Their roles in signaling body shape, body position and movement, and muscle force”, *Physiol. Rev.*, vol. 92, no. 4, pp. 1651–1697, 2012, ISSN: 0031-9333. DOI: 10.1152/physrev.00048.2011.
- [21] P. H. Peckham and J. S. Knutson, “Functional electrical stimulation for neuromuscular applications”, *Annu. Rev. Biomed. Eng.*, vol. 7, no. 1, pp. 327–360, 2005, ISSN: 1523-9829. DOI: 10.1146/annurev.bioeng.6.040803.140103.
- [22] J. T. Mortimer, “Motor prostheses”, pp. 155–187, Dec. 1981, Publisher: Wiley. DOI: 10.1002/cphy.cp010205.
- [23] N. Garg, S. B. Park, S. Vucic, *et al.*, “Differentiating lower motor neuron syndromes”, *J. Neurol. Neurosurg. Psychiatry*, vol. 88, no. 6, pp. 474–483, 2017, ISSN: 0022-3050. DOI: 10.1136/jnnp-2016-313526.
- [24] I. Bersch and J. Fridén, “Upper and lower motor neuron lesions in tetraplegia: Implications for surgical nerve transfer to restore hand function”, *J. Appl. Physiol.*, vol. 129, no. 5, pp. 1214–1219, 2020, ISSN: 8750-7587. DOI: 10.1152/jappphysiol.00529.2020.
- [25] J. Mendoza and A. L. Foundas, *Clinical Neuroanatomy: A Neurobehavioral Approach*. New York, NY: Springer, 2007, ISBN: 978-0-387-36600-5. DOI: 10.1007/978-0-387-36601-2.
- [26] “Spinal cord injury levels & classification”. (Jun. 14, 2019), [Online]. Available: <https://www.sci-info-pages.com/levels-and-classification/> (visited on 02/01/2024).
- [27] C. S. Ahuja, J. R. Wilson, S. Nori, *et al.*, “Traumatic spinal cord injury”, *Nat. Rev. Dis. Primers*, vol. 3, no. 1, 2017, ISSN: 2056-676X. DOI: 10.1038/nrdp.2017.18.

- [28] S. A. Quadri, M. Farooqui, A. Ikram, *et al.*, “Recent update on basic mechanisms of spinal cord injury”, *Neurosurg. Rev.*, vol. 43, no. 2, pp. 425–441, 2020, ISSN: 0344-5607. DOI: 10.1007/s10143-018-1008-3.
- [29] C. H. Ho, L.-A. Wuermsler, M. M. Priebe, A. E. Chiodo, W. M. Scelza, and S. C. Kirshblum, “Spinal cord injury medicine. 1. epidemiology and classification”, *Arch. Phys. Med. Rehabil.*, vol. 88, no. 3, S49–S54, 2007, ISSN: 0003-9993. DOI: 10.1016/j.apmr.2006.12.001.
- [30] A. M. Bryden, H. A. Hoyen, M. W. Keith, M. Mejia, K. L. Kilgore, and G. A. Nemunaitis, “Upper extremity assessment in tetraplegia: The importance of differentiating between upper and lower motor neuron paralysis”, *Arch. Phys. Med. Rehabil.*, vol. 97, no. 6, S97–S104, 2016, ISSN: 0003-9993. DOI: 10.1016/j.apmr.2015.11.021.
- [31] S. Lalwani, P. Mathur, N. J. Jain, B. Behera, and M. Misra, “Spinal cord injury”, *Journal of neurosurgery. Spine*, vol. 15, no. 5, 576–7, authorreply577, 2011. DOI: 10.3171/2011.3.SPINE11153. [Online]. Available: <https://www.who.int/news-room/fact-sheets/detail/spinal-cord-injury> (visited on 02/02/2024).
- [32] D. B. Popović, “Advances in functional electrical stimulation (FES)”, *J. Electromyogr. Kinesiol.*, vol. 24, no. 6, pp. 795–802, 2014, ISSN: 1050-6411. DOI: 10.1016/j.jelekin.2014.09.008.
- [33] I. Bersch, “Upper and lower motoneuron lesions in tetraplegia : Diagnostic and therapeutic implications of electrical stimulation”, Ph.D. dissertation, University of Gothenburg, 2019. [Online]. Available: <http://hdl.handle.net/2077/60783>.
- [34] M. Milosevic, C. Marquez-Chin, K. Masani, *et al.*, “Why brain-controlled neuroprosthetics matter: Mechanisms underlying electrical stimulation of muscles and nerves in rehabilitation”, *Biomed. Eng. Online*, vol. 19, no. 1, 2020, ISSN: 1475-925X. DOI: 10.1186/s12938-020-00824-w.

- [35] C. Marquez-Chin and M. R. Popovic, “Functional electrical stimulation therapy for restoration of motor function after spinal cord injury and stroke: A review”, *Biomed. Eng. Online*, vol. 19, no. 1, 2020, ISSN: 1475-925X. DOI: 10.1186/s12938-020-00773-4.
- [36] L. L. Baker, *Neuromuscular Electrical Stimulation: A Practical Guide*. 2000, ISBN: 978-0-9676335-0-3.
- [37] M. R. Popovic, K. Masani, and S. Micera, “Functional electrical stimulation therapy: Recovery of function following spinal cord injury and stroke”, in *Neurorehabilitation Technology*, London: Springer London, 2012, pp. 105–121, ISBN: 978-1-4471-2276-0. DOI: 10.1007/978-1-4471-2277-7_7.
- [38] K. T. Ragnarsson, “Functional electrical stimulation after spinal cord injury: Current use, therapeutic effects and future directions”, *Spinal Cord*, vol. 46, no. 4, pp. 255–274, 2008, ISSN: 1362-4393. DOI: 10.1038/sj.sc.3102091.
- [39] M. C. Kutlu, “A home-based functional electrical stimulation system for upper-limb stroke rehabilitation”, Ph.D. dissertation, UNIVERSITY OF SOUTHAMPTON, Jun. 29, 2017. [Online]. Available: [https://eprints.soton.ac.uk/417274/1/final thesis.pdf](https://eprints.soton.ac.uk/417274/1/final%20thesis.pdf).
- [40] D. Popovic and T. Sinkjaer, *Control of movement for the physically disabled: Control for rehabilitation technology*. London, England: Springer, 2012, ISBN: 978-1-4471-1141-2.
- [41] S. Luo, H. Xu, Y. Zuo, X. Liu, and A. H. All, “A review of functional electrical stimulation treatment in spinal cord injury”, *Neuromolecular Med.*, vol. 22, no. 4, pp. 447–463, 2020, ISSN: 1535-1084. DOI: 10.1007/s12017-019-08589-9.
- [42] M. Descollonges, P. Marmier, M. Marillier, E. Jafari, J. V. Brugniaux, and G. Deley, “Effect of electrical muscle stimulation on cerebrovascular function and cognitive performance”, *Am. J. Physiol. Heart Circ. Physiol.*, 2024, ISSN: 0363-6135. DOI: 10.1152/ajpheart.00032.2024.

- [43] B. M. Doucet, A. Lam, and L. Griffin, “Neuromuscular electrical stimulation for skeletal muscle function”, *Yale J. Biol. Med.*, vol. 85, no. 2, pp. 201–215, 2012, ISSN: 0044-0086.
- [44] M. Gobbo, N. A. Maffioletti, C. Orizio, and M. A. Minetto, “Muscle motor point identification is essential for optimizing neuromuscular electrical stimulation use”, *J. Neuroeng. Rehabil.*, vol. 11, no. 1, p. 17, 2014, ISSN: 1743-0003. DOI: 10.1186/1743-0003-11-17.
- [45] C. D. Mørch, K. Hennings, and O. K. Andersen, “Estimating nerve excitation thresholds to cutaneous electrical stimulation by finite element modeling combined with a stochastic branching nerve fiber model”, *Med. Biol. Eng. Comput.*, vol. 49, no. 4, pp. 385–395, 2011, ISSN: 0140-0118. DOI: 10.1007/s11517-010-0725-8.
- [46] K. Masani and M. R. Popovic, “Functional electrical stimulation in rehabilitation and neurorehabilitation”, in *Springer Handbook of Medical Technology*, Berlin, Heidelberg: Springer Berlin Heidelberg, 2011, pp. 877–896, ISBN: 978-3-540-74657-7. DOI: 10.1007/978-3-540-74658-4_44.
- [47] J. S. Petrofsky, C. A. Phillips, R. M. Glaser, and H. H. Heaton III, “System and method for treating paralyzed persons”, pat. 4 499 900, Publication Title: US Patent, Feb. 19, 1985. [Online]. Available: <https://patents.google.com/patent/US4499900A/en> (visited on 02/02/2024).
- [48] P. Kajganic, “Optimization of functional electrical stimulation (FES) parameters for FES cycling”, Ph.D. dissertation, Ecole normale supérieure de lyon - ENS LYON, 2023. [Online]. Available: <https://theses.hal.science/tel-04352325v1/document>.
- [49] A. E. Aksöz, “Optimising performance in paraplegic FES-cycling by modulating stimulation parameters”, Ph.D. dissertation, ETH Zurich, 2018. DOI: 10.3929/ethz-b-000339907.

- [50] E. Ambrosini, S. Ferrante, A. Pedrocchi, G. Ferrigno, and F. Molteni, “Cycling induced by electrical stimulation improves motor recovery in postacute hemiparetic patients: A randomized controlled trial”, en, *Stroke*, vol. 42, no. 4, pp. 1068–1073, 2011.
- [51] E. Ambrosini, S. Ferrante, G. Ferrigno, F. Molteni, and A. Pedrocchi, “Cycling induced by electrical stimulation improves muscle activation and symmetry during pedaling in hemiparetic patients”, *IEEE Trans. Neural Syst. Rehabil. Eng.*, vol. 20, no. 3, pp. 320–330, 2012.
- [52] J. W. van der Scheer, V. L. Goosey-Tolfrey, S. E. Valentino, G. M. Davis, and C. H. Ho, “Functional electrical stimulation cycling exercise after spinal cord injury: A systematic review of health and fitness-related outcomes”, *J. Neuroeng. Rehabil.*, vol. 18, no. 1, 2021, ISSN: 1743-0003. DOI: 10.1186/s12984-021-00882-8.
- [53] G. M. Davis, N. A. Hamzaid, and C. Fornusek, “Cardiorespiratory, metabolic, and biomechanical responses during functional electrical stimulation leg exercise: Health and fitness benefits”, *Artif. Organs*, vol. 32, no. 8, pp. 625–629, 2008, ISSN: 0160-564X. DOI: 10.1111/j.1525-1594.2008.00622.x.
- [54] M. Laubacher, E. A. Aksöz, I. Bersch, and K. J. Hunt, “The road to cybathlon 2016 - functional electrical stimulation cycling team IRPT/SPZ”, *Eur. J. Transl. Myol.*, vol. 27, no. 4, 2017, ISSN: 2037-7452. DOI: 10.4081/ejtm.2017.7086.
- [55] N. A. Hakansson and M. L. Hull, “Muscle stimulation waveform timing patterns for upper and lower leg muscle groups to increase muscular endurance in functional electrical stimulation pedaling using a forward dynamic model”, *IEEE Trans. Biomed. Eng.*, vol. 56, no. 9, pp. 2263–2270, 2009, ISSN: 0018-9294. DOI: 10.1109/tbme.2009.2020175.
- [56] C. A. Cousin, C. A. Rouse, and W. E. Dixon, “Split-crank functional electrical stimulation cycling: An adapting admitting rehabilitation robot”, *IEEE Trans. Con-*

- trol Syst. Technol.*, vol. 29, no. 5, pp. 2153–2165, 2021, ISSN: 1063-6536. DOI: 10.1109/tcst.2020.3032474.
- [57] W. T. Liberson, H. J. Holmquest, D. Scot, and M. Dow, “Functional electrotherapy: Stimulation of the peroneal nerve synchronized with the swing phase of the gait of hemiplegic patients”, *Arch. Phys. Med. Rehabil.*, vol. 42, pp. 101–105, 1961, ISSN: 0003-9993.
- [58] L. Malisoux, C. Jamart, K. Delplace, H. Nielens, M. Francaux, and D. Theisen, “Effect of long-term muscle paralysis on human single fiber mechanics”, *J. Appl. Physiol.*, vol. 102, no. 1, pp. 340–349, 2007, ISSN: 8750-7587. DOI: 10.1152/japplphysiol.00609.2006.
- [59] K. J. Hunt, J. Fang, J. Saengsuwan, M. Grob, and M. Laubacher, “On the efficiency of FES cycling: A framework and systematic review”, *Technol. Health Care*, vol. 20, no. 5, pp. 395–422, 2012, ISSN: 0928-7329. DOI: 10.3233/thc-2012-0689.
- [60] K. S. Park, “Electrical stimulation of nerves and muscles”, in *Humans and Electricity*, Cham: Springer International Publishing, 2023, pp. 351–376, ISBN: 978-3-031-20783-9. DOI: 10.1007/978-3-031-20784-6_15.
- [61] M. Stoppa and A. Chiolerio, “Wearable electronics and smart textiles: A critical review”, *Sensors (Basel)*, vol. 14, no. 7, pp. 11 957–11 992, 2014, ISSN: 1424-8220. DOI: 10.3390/s140711957.
- [62] A. A. Simegnaw, B. Malengier, G. Rotich, M. G. Tadesse, and L. Van Langenhove, “Review on the integration of microelectronics for e-textile”, *Materials (Basel)*, vol. 14, no. 17, p. 5113, 2021, ISSN: 1996-1944. DOI: 10.3390/ma14175113.
- [63] E. Sazonov, Ed., *Wearable sensors: Fundamentals, implementation and applications*, San Diego, CA: Academic Press, 2021, ISBN: 978-0-12-819246-7. DOI: 10.1016/c2018-0-01225-6.

- [64] H. Wu, Y. Huang, F. Xu, Y. Duan, and Z. Yin, “Energy harvesters for wearable and stretchable electronics: From flexibility to stretchability”, *Adv. Mater.*, vol. 28, no. 45, pp. 9881–9919, 2016, ISSN: 0935-9648. DOI: 10.1002/adma.201602251.
- [65] A. Fleury, M. Sugar, and T. Chau, “E-textiles in clinical rehabilitation: A scoping review”, *Electronics (Basel)*, vol. 4, no. 1, pp. 173–203, 2015, ISSN: 2079-9292. DOI: 10.3390/electronics4010173.
- [66] S. u. Zaman, X. Tao, C. Cochrane, and V. Koncar, “Smart e-textile systems: A review for healthcare applications”, *Electronics (Basel)*, vol. 11, no. 1, p. 99, 2021, ISSN: 2079-9292. DOI: 10.3390/electronics11010099.
- [67] A. Patnaik and S. Patnaik, Eds., *Fibres to smart textiles: Advances in manufacturing, technologies, and applications*, London, England: CRC Press, 2019, ISBN: 978-1-138-33251-5.
- [68] A. Ankhili, X. Tao, C. Cochrane, V. Koncar, D. Coulon, and J.-M. Tarlet, “Ambulatory evaluation of ECG signals obtained using washable textile-based electrodes made with chemically modified PEDOT:PSS”, *Sensors (Basel)*, vol. 19, no. 2, p. 416, 2019, ISSN: 1424-8220. DOI: 10.3390/s19020416.
- [69] L. Popović-Maneski, M. D. Ivanović, V. Atanasoski, *et al.*, “Properties of different types of dry electrodes for wearable smart monitoring devices”, *Biomed. Tech. (Berl.)*, vol. 65, no. 4, pp. 405–415, 2020, ISSN: 0013-5585. DOI: 10.1515/bmt-2019-0167.
- [70] S. Kim, S. Lee, and W. Jeong, “EMG measurement with textile-based electrodes in different electrode sizes and clothing pressures for smart clothing design optimization”, *Polymers (Basel)*, vol. 12, no. 10, p. 2406, 2020, ISSN: 2073-4360. DOI: 10.3390/polym12102406.
- [71] H. Jin, N. Matsuhisa, S. Lee, M. Abbas, T. Yokota, and T. Someya, “Enhancing the performance of stretchable conductors for e-textiles by controlled ink permeation”,

- Adv. Mater.*, vol. 29, no. 21, p. 1605848, 2017, ISSN: 0935-9648. DOI: 10.1002/adma.201605848.
- [72] G. B. Tseghai, B. Malengier, K. A. Fante, and L. Van Langenhove, “The status of textile-based dry EEG electrodes”, *AUTEX Res. J.*, vol. 21, no. 1, pp. 63–70, 2021, ISSN: 1470-9589. DOI: 10.2478/aut-2019-0071.
- [73] D. Erdem, S. Yesilpinar, Y. Senol, D. Karadibak, and T. Akkan, “Design of TENS electrodes using conductive yarn”, *Int. J. Cloth. Sci. Technol.*, vol. 28, no. 3, pp. 311–318, 2016, ISSN: 0955-6222. DOI: 10.1108/ijcst-03-2016-0030.
- [74] L. Euler, L. Guo, and N.-K. Persson, “A review of textile-based electrodes developed for electrostimulation”, *Text. Res. J.*, vol. 92, no. 7, pp. 1300–1320, 2022, ISSN: 0040-5175. DOI: 10.1177/00405175211051949.
- [75] P. Kajganic, V. Bergeron, and A. Metani, “ICEP: An instrumented cycling ergometer platform for the assessment of advanced FES strategies”, *Sensors (Basel)*, vol. 23, no. 7, 2023, ISSN: 1424-8220. DOI: 10.3390/s23073522.
- [76] E. Jafari and A. Erfanian, “A distributed automatic control framework for simultaneous control of torque and cadence in functional electrical stimulation cycling”, *IEEE Trans. Neural Syst. Rehabil. Eng.*, vol. 30, pp. 1908–1919, 2022, ISSN: 1534-4320. DOI: 10.1109/TNSRE.2022.3188735.
- [77] E. Jafari, E. A. Aksoez, P. Kajganic, A. Metani, L. Popovic-Maneski, and V. Bergeron, “Optimization of seating position and stimulation pattern in functional electrical stimulation cycling: Simulation study”, *Annu. Int. Conf. IEEE Eng. Med. Biol. Soc.*, vol. 2022, pp. 725–731, 2022, ISSN: 2375-7477. DOI: 10.1109/EMBC48229.2022.9871339.
- [78] L. Z. P. Maneski, N. M. Malešević, A. M. Savić, T. Keller, and D. B. Popović, “Surface-distributed low-frequency asynchronous stimulation delays fatigue of stimulated muscles”, *Muscle Nerve*, vol. 48, no. 6, pp. 930–937, 2013, ISSN: 0148-639X. DOI: 10.1002/mus.23840.

- [79] N. M. Malešević, L. Z. Popović Maneski, V. Ilić, *et al.*, “A multi-pad electrode based functional electrical stimulation system for restoration of grasp”, *J. Neuroeng. Rehabil.*, vol. 9, no. 1, p. 66, 2012, ISSN: 1743-0003. DOI: 10.1186/1743-0003-9-66.
- [80] M. R. Ely and J. A. Taylor, “The practical utility of functional electrical stimulation exercise for cardiovascular health in individuals with spinal cord injury”, *Curr. Phys. Med. Rehabil. Rep.*, vol. 9, no. 3, pp. 154–162, 2021, ISSN: 2167-4833. DOI: 10.1007/s40141-021-00315-6.
- [81] H. E. Shin, M. Kim, D. Lee, *et al.*, “Therapeutic effects of functional electrical stimulation on physical performance and muscle strength in post-stroke older adults: A review”, *Ann. Geriatr. Med. Res.*, vol. 26, no. 1, pp. 16–24, 2022, ISSN: 2508-4798. DOI: 10.4235/agmr.22.0006.
- [82] D. R. Dolbow, A. S. Gorgey, J. A. Daniels, R. A. Adler, J. R. Moore, and D. R. Gater Jr, “The effects of spinal cord injury and exercise on bone mass: A literature review”, *NeuroRehabilitation*, vol. 29, no. 3, pp. 261–269, 2011, ISSN: 1053-8135. DOI: 10.3233/NRE-2011-0702.
- [83] L. Q. Liu, J. Moody, M. Traynor, S. Dyson, and A. Gall, “A systematic review of electrical stimulation for pressure ulcer prevention and treatment in people with spinal cord injuries”, *J. Spinal Cord Med.*, vol. 37, no. 6, pp. 703–718, 2014, ISSN: 1079-0268. DOI: 10.1179/2045772314Y.0000000226.
- [84] L. C. Burgess, L. Venugopalan, J. Badger, *et al.*, “Effect of neuromuscular electrical stimulation on the recovery of people with COVID-19 admitted to the intensive care unit: A narrative review”, *J. Rehabil. Med.*, vol. 53, no. 3, jrm00164, 2021, ISSN: 1650-1977. DOI: 10.2340/16501977-2805.
- [85] T. Keller and A. Kuhn, “Electrodes for transcutaneous (surface) electrical stimulation”, *J. Autom. Contr.*, vol. 18, no. 2, pp. 35–45, 2008, ISSN: 1450-9903. DOI: 10.2298/jac0802035k.

- [86] G. Cooper, A. T. Barker, B. W. Heller, T. Good, L. P. J. Kenney, and D. Howard, “The use of hydrogel as an electrode-skin interface for electrode array FES applications”, *Med. Eng. Phys.*, vol. 33, no. 8, pp. 967–972, 2011, ISSN: 1350-4533. DOI: 10.1016/j.medengphy.2011.03.008.
- [87] H. Zhou, Y. Lu, W. Chen, *et al.*, “Stimulating the comfort of textile electrodes in wearable neuromuscular electrical stimulation”, *Sensors (Basel)*, vol. 15, no. 7, pp. 17 241–17 257, 2015, ISSN: 1424-8220. DOI: 10.3390/s150717241.
- [88] G. Acar, O. Ozturk, A. J. Golparvar, T. A. Elboshra, K. Böhringer, and M. K. Yapici, “Wearable and flexible textile electrodes for biopotential signal monitoring: A review”, *Electronics (Basel)*, vol. 8, no. 5, p. 479, 2019, ISSN: 2079-9292. DOI: 10.3390/electronics8050479.
- [89] B. Moineau, C. Marquez-Chin, M. Alizadeh-Meghrazi, and M. R. Popovic, “Garments for functional electrical stimulation: Design and proofs of concept”, *J. Rehabil. Assist. Technol. Eng.*, vol. 6, p. 2 055 668 319 854 340, 2019, ISSN: 2055-6683. DOI: 10.1177/2055668319854340.
- [90] A. Ali, V. Baheti, J. Militky, and Z. Khan, “Utility of silver-coated fabrics as electrodes in electrotherapy applications”, *J. Appl. Polym. Sci.*, vol. 135, no. 23, p. 46 357, 2018, ISSN: 0021-8995. DOI: 10.1002/app.46357.
- [91] A. J. Golparvar and M. Kaya Yapici, “Wearable graphene textile-enabled EOG sensing”, presented at the 2017 IEEE SENSORS, IEEE, 2017. DOI: 10.1109/icsens.2017.8234242.
- [92] J. Zieba, M. Frydrysiak, L. Tesiorowski, and M. Tokarska, “Textronic matrix of electrode system to electrostimulation”, presented at the 2012 IEEE International Symposium on Medical Measurements and Applications Proceedings, IEEE, 2012. DOI: 10.1109/memea.2012.6226645.

- [93] K. Gniotek, M. Frydrysiak, J. Zieba, M. Tokarska, and Z. Stempien, “Innovative textile electrodes for muscles electrostimulation”, presented at the 2011 IEEE International Symposium on Medical Measurements and Applications, IEEE, 2011. DOI: 10.1109/memea.2011.5966678.
- [94] Y. Merhi, P. F. Betancur, T. S. Ripolles, *et al.*, “Printed dry electrode for neuromuscular electrical stimulation (NMES) for e-textile”, *Nanoscale*, vol. 15, no. 11, pp. 5337–5344, 2023, ISSN: 2040-3364. DOI: 10.1039/d2nr06008f.
- [95] K. Yang, C. Freeman, R. Torah, S. Beeby, and J. Tudor, “Screen printed fabric electrode array for wearable functional electrical stimulation”, *Sens. Actuators A Phys.*, vol. 213, pp. 108–115, 2014, ISSN: 0924-4247. DOI: 10.1016/j.sna.2014.03.025.
- [96] L. Popović-Maneski, M. Kostić, G. Bijelić, *et al.*, “Multi-pad electrode for effective grasping: Design”, *IEEE Trans. Neural Syst. Rehabil. Eng.*, vol. 21, no. 4, pp. 648–654, 2013, ISSN: 1534-4320. DOI: 10.1109/TNSRE.2013.2239662.
- [97] M. Papaiordanidou, S. Takamatsu, S. Rezaei-Mazinani, T. Lonjaret, A. Martin, and E. Ismailova, “Cutaneous recording and stimulation of muscles using organic electronic textiles”, *Adv. Healthc. Mater.*, vol. 5, no. 16, pp. 2001–2006, 2016, ISSN: 2192-2640. DOI: 10.1002/adhm.201600299.
- [98] E. Gunnarsson, K. Rödbj, and F. Seoane, “Seamlessly integrated textile electrodes and conductive routing in a garment for electrostimulation: Design, manufacturing and evaluation”, *Sci. Rep.*, vol. 13, no. 1, p. 17 408, 2023, ISSN: 2045-2322. DOI: 10.1038/s41598-023-44622-5.
- [99] L. Euler, L. Guo, and N.-K. Persson, “Textile electrodes: Influence of knitting construction and pressure on the contact impedance”, *Sensors (Basel)*, vol. 21, no. 5, p. 1578, 2021, ISSN: 1424-8220. DOI: 10.3390/s21051578.

- [100] M. Liu, T. Ward, D. Young, *et al.*, “Electronic textiles based wearable electrotherapy for pain relief”, *Sens. Actuators A Phys.*, vol. 303, no. 111701, p. 111 701, 2020, ISSN: 0924-4247. DOI: 10.1016/j.sna.2019.111701.
- [101] S. Park, H. Kim, and S. Lee, “Changes in characteristics of silver conductive fabrics owing to perspiration and washing”, *RSC Adv.*, vol. 13, no. 41, pp. 28 444–28 461, 2023, ISSN: 2046-2069. DOI: 10.1039/d3ra04276f.
- [102] A. Hunold, D. Ortega, K. Schellhorn, and J. Haueisen, “Novel flexible cap for application of transcranial electrical stimulation: A usability study”, *Biomed. Eng. Online*, vol. 19, no. 1, p. 50, 2020, ISSN: 1475-925X. DOI: 10.1186/s12938-020-00792-1.
- [103] R. L. Sakugawa, L. B. R. Orssatto, L. T. Sampaio, H. de Brito Fontana, and F. Diefenthaler, “Pressure on the electrode to reduce discomfort during neuromuscular electrical stimulation in individuals with different subcutaneous-fat thickness: Is the procedure effective and reliable?”, *IEEE Trans. Neural Syst. Rehabil. Eng.*, vol. 30, pp. 1–7, 2022, ISSN: 1534-4320. DOI: 10.1109/TNSRE.2021.3138202.
- [104] A. Botter, G. Oprandi, F. Lanfranco, S. Allasia, N. A. Maffiuletti, and M. A. Minetto, “Atlas of the muscle motor points for the lower limb: Implications for electrical stimulation procedures and electrode positioning”, *Eur. J. Appl. Physiol.*, vol. 111, no. 10, pp. 2461–2471, 2011, ISSN: 1439-6319. DOI: 10.1007/s00421-011-2093-y.
- [105] L. Popović-Maneski and S. Mateo, “MotiMove: Multi-purpose transcutaneous functional electrical stimulator”, *Artif. Organs*, vol. 46, no. 10, pp. 1970–1979, 2022, ISSN: 0160-564X. DOI: 10.1111/aor.14379.
- [106] M. Pournizam, B. J. Andrews, R. H. Baxendale, G. F. Phillips, and J. P. Paul, “Reduction of muscle fatigue in man by cyclical stimulation”, *J. Biomed. Eng.*, vol. 10, no. 2, pp. 196–200, 1988, ISSN: 0141-5425. DOI: 10.1016/0141-5425(88)90100-8.

- [107] L. Z. Popovic and N. M. Malešević, “Muscle fatigue of quadriceps in paraplegics: Comparison between single vs. multi-pad electrode surface stimulation”, presented at the 2009 Annual International Conference of the IEEE Engineering in Medicine and Biology Society, IEEE, 2009. DOI: 10.1109/iembs.2009.5333983.
- [108] N. M. Malešević, L. Z. Popović, L. Schwirtlich, and D. B. Popović, “Distributed low-frequency functional electrical stimulation delays muscle fatigue compared to conventional stimulation”, *Muscle Nerve*, vol. 42, no. 4, pp. 556–562, 2010, ISSN: 0148-639X. DOI: 10.1002/mus.21736.
- [109] M. J. Decker, L. Griffin, L. D. Abraham, and L. Brandt, “Alternating stimulation of synergistic muscles during functional electrical stimulation cycling improves endurance in persons with spinal cord injury”, *J. Electromyogr. Kinesiol.*, vol. 20, no. 6, pp. 1163–1169, 2010, ISSN: 1050-6411. DOI: 10.1016/j.jelekin.2010.07.015.
- [110] R. Nguyen, K. Masani, S. Micera, M. Morari, and M. R. Popovic, “Spatially distributed sequential stimulation reduces fatigue in paralyzed triceps surae muscles: A case study: Thoughts and progress”, *Artif. Organs*, vol. 35, no. 12, pp. 1174–1180, 2011, ISSN: 0160-564X. DOI: 10.1111/j.1525-1594.2010.01195.x.
- [111] D. G. Sayenko, M. R. Popovic, and K. Masani, “Spatially distributed sequential stimulation reduces muscle fatigue during neuromuscular electrical stimulation”, presented at the 2013 35th Annual International Conference of the IEEE Engineering in Medicine and Biology Society (EMBC), IEEE, 2013. DOI: 10.1109/embc.2013.6610325.
- [112] R. J. Downey, M. J. Bellman, H. Kawai, C. M. Gregory, and W. E. Dixon, “Comparing the induced muscle fatigue between asynchronous and synchronous electrical stimulation in able-bodied and spinal cord injured populations”, *IEEE Trans. Neural Syst. Rehabil. Eng.*, vol. 23, no. 6, pp. 964–972, 2015, ISSN: 1534-4320. DOI: 10.1109/tnsre.2014.2364735.

- [113] D. G. Sayenko, R. Nguyen, M. R. Popovic, and K. Masani, “Reducing muscle fatigue during transcutaneous neuromuscular electrical stimulation by spatially and sequentially distributing electrical stimulation sources”, *Eur. J. Appl. Physiol.*, vol. 114, no. 4, pp. 793–804, 2014, ISSN: 1439-6319. DOI: 10.1007/s00421-013-2807-4.
- [114] M. Laubacher, E. A. Aksöz, S. Binder-Macleod, and K. J. Hunt, “Comparison of proximally versus distally placed spatially distributed sequential stimulation electrodes in a dynamic knee extension task”, *Eur. J. Transl. Myol.*, vol. 26, no. 2, 2016, ISSN: 2037-7452. DOI: 10.4081/ejtm.2016.6016.
- [115] M. Laubacher, A. E. Aksöz, R. Riener, S. Binder-Macleod, and K. J. Hunt, “Power output and fatigue properties using spatially distributed sequential stimulation in a dynamic knee extension task”, *Eur. J. Appl. Physiol.*, vol. 117, no. 9, pp. 1787–1798, 2017, ISSN: 1439-6319. DOI: 10.1007/s00421-017-3675-0.
- [116] A. J. Bergquist, V. Babbar, S. Ali, M. R. Popovic, and K. Masani, “Fatigue reduction during aggregated and distributed sequential stimulation: Sequential stimulation”, *Muscle Nerve*, vol. 56, no. 2, pp. 271–281, 2017, ISSN: 0148-639X. DOI: 10.1002/mus.25465.
- [117] M. J. Wiest, A. J. Bergquist, M. G. Heffernan, M. Popovic, and K. Masani, “Fatigue and discomfort during spatially distributed sequential stimulation of tibialis anterior”, *IEEE Trans. Neural Syst. Rehabil. Eng.*, vol. 27, no. 8, pp. 1566–1573, 2019, ISSN: 1534-4320. DOI: 10.1109/tnsre.2019.2923117.
- [118] M. Laubacher, E. A. Aksoez, A. K. Brust, *et al.*, “Stimulation of paralysed quadriceps muscles with sequentially and spatially distributed electrodes during dynamic knee extension”, *J. Neuroeng. Rehabil.*, vol. 16, no. 1, 2019, ISSN: 1743-0003. DOI: 10.1186/s12984-018-0471-y.
- [119] L. De Macedo Pinheiro, A. C. C. De Sousa, and A. P. L. Bo, “Comparing spatially distributed and single electrode stimulation on individuals with spinal cord

- injury”, presented at the 2020 42nd Annual International Conference of the IEEE Engineering in Medicine & Biology Society (EMBC), IEEE, 2020. DOI: 10.1109/embc44109.2020.9176616.
- [120] R. S. Baptista, M. C. C. Moreira, L. D. M. Pinheiro, *et al.*, “User-centered design and spatially-distributed sequential electrical stimulation in cycling for individuals with paraplegia”, *J. Neuroeng. Rehabil.*, vol. 19, no. 1, 2022, ISSN: 1743-0003. DOI: 10.1186/s12984-022-01014-6.
- [121] M. Schmoll, R. Le Guillou, D. Lobato Borges, C. Fattal, E. Fachin-Martins, and C. Azevedo Coste, “Standardizing fatigue-resistance testing during electrical stimulation of paralysed human quadriceps muscles, a practical approach”, *J. Neuroeng. Rehabil.*, vol. 18, no. 1, 2021, ISSN: 1743-0003. DOI: 10.1186/s12984-021-00805-7.
- [122] I. Ceroni, S. Ferrante, F. Conti, *et al.*, “Comparing fatigue reducing stimulation strategies during cycling induced by functional electrical stimulation: A case study with one spinal cord injured subject”, presented at the 2021 43rd Annual International Conference of the IEEE Engineering in Medicine & Biology Society (EMBC), IEEE, 2021. DOI: 10.1109/embc46164.2021.9630197.
- [123] S. Agotici, K. Masani, and P. B. Yoo, “Computational study on spatially distributed sequential stimulation for fatigue resistant neuromuscular electrical stimulation”, *IEEE Trans. Neural Syst. Rehabil. Eng.*, vol. 29, pp. 2578–2586, 2021, ISSN: 1534-4320. DOI: 10.1109/TNSRE.2021.3133508.
- [124] D. G. Sayenko, R. Nguyen, T. Hirabayashi, M. R. Popovic, and K. Masani, “Method to reduce muscle fatigue during transcutaneous neuromuscular electrical stimulation in major knee and ankle muscle groups”, *Neurorehabil. Neural Repair*, vol. 29, no. 8, pp. 722–733, 2015, ISSN: 1545-9683. DOI: 10.1177/1545968314565463.

- [125] G. Ye, P. Theventhiran, and K. Masani, “Effect of spatially distributed sequential stimulation on fatigue in functional electrical stimulation rowing”, *IEEE Trans. Neural Syst. Rehabil. Eng.*, vol. 30, pp. 999–1008, 2022, ISSN: 1534-4320. DOI: 10.1109/tnsre.2022.3166710.
- [126] L. M. Schutte, M. M. Rodgers, F. E. Zajac, and R. M. Glaser, “Improving the efficacy of electrical stimulation-induced leg cycle ergometry: An analysis based on a dynamic musculoskeletal model”, *IEEE Trans. Rehabil. Eng.*, vol. 1, no. 2, pp. 109–125, 1993, ISSN: 1063-6528. DOI: 10.1109/86.242425.
- [127] S. C. Abdulla, O. Sayidmarie, and M. O. Tokhi, “Functional electrical stimulation-based cycling assisted by flywheel and electrical clutch mechanism: A feasibility simulation study”, *Rob. Auton. Syst.*, vol. 62, no. 2, pp. 188–199, 2014, ISSN: 0921-8890. DOI: 10.1016/j.robot.2013.10.005.
- [128] T. Angeli, M. Gföhler, T. Eberharter, P. Lugner, L. Rinder, and H. Kern, “Optimization of the pedal path for cycling powered by lower extremity muscles activated by functional electrical stimulation”, *Computer Methods in Biomechanics and Biomedical Engineering-3. Gordon and Breach*, 2001.
- [129] J. Rasmussen, S. T. Christensen, M. Gföhler, M. Damsgaard, and T. Angeli, “Design optimization of a pedaling mechanism for paraplegics”, *Struct. Multidiscipl. Optim.*, vol. 26, no. 1, pp. 132–138, 2004, ISSN: 1615-147X. DOI: 10.1007/s00158-003-0324-5.
- [130] J. J. Chen, N. Y. Yu, D. G. Huang, B. T. Ann, and G. C. Chang, “Applying fuzzy logic to control cycling movement induced by functional electrical stimulation”, *IEEE Trans. Rehabil. Eng.*, vol. 5, no. 2, pp. 158–169, 1997, ISSN: 1063-6528. DOI: 10.1109/86.593285.
- [131] M. J. Bellman, T.-H. Cheng, R. J. Downey, C. J. Hass, and W. E. Dixon, “Switched control of cadence during stationary cycling induced by functional electrical stim-

- ulation”, *IEEE Trans. Neural Syst. Rehabil. Eng.*, vol. 24, no. 12, pp. 1373–1383, 2016, ISSN: 1534-4320. DOI: 10.1109/tnsre.2015.2500180.
- [132] M. Gföhler and P. Lugner, “Cycling by means of functional electrical stimulation”, *IEEE Trans. Rehabil. Eng.*, vol. 8, no. 2, pp. 233–243, 2000, ISSN: 1063-6528. DOI: 10.1109/86.847825.
- [133] M. Gföhler and P. Lugner, “Dynamic simulation of FES-cycling: Influence of individual parameters”, *IEEE Trans. Neural Syst. Rehabil. Eng.*, vol. 12, no. 4, pp. 398–405, 2004, ISSN: 1534-4320. DOI: 10.1109/TNSRE.2004.836778.
- [134] J. J. Abbas and H. J. Chizeck, “Neural network control of functional neuromuscular stimulation systems: Computer simulation studies”, *IEEE Trans. Biomed. Eng.*, vol. 42, no. 11, pp. 1117–1127, 1995, ISSN: 0018-9294. DOI: 10.1109/10.469379.
- [135] F. E. Zajac, “Muscle and tendon: Properties, models, scaling, and application to biomechanics and motor control”, *Crit. Rev. Biomed. Eng.*, vol. 17, no. 4, pp. 359–411, 1989, ISSN: 0278-940X.
- [136] W. K. Durfee and K. I. Palmer, “Estimation of force-activation, force-length, and force-velocity properties in isolated, electrically stimulated muscle”, *IEEE Trans. Biomed. Eng.*, vol. 41, no. 3, pp. 205–216, 1994, ISSN: 0018-9294. DOI: 10.1109/10.284939.
- [137] A. M. Gordon, A. F. Huxley, and F. J. Julian, “The variation in isometric tension with sarcomere length in vertebrate muscle fibres”, *J. Physiol.*, vol. 184, no. 1, pp. 170–192, 1966, ISSN: 0022-3751. DOI: 10.1113/jphysiol.1966.sp007909.
- [138] D. A. Winter, *Biomechanics and motor control of human movement*. Hoboken, NJ, USA: John Wiley & Sons, Inc., 2009, ISBN: 978-0-470-54914-8. DOI: 10.1002/9780470549148.

- [139] D. E. Anderson, M. L. Madigan, and M. A. Nussbaum, “Maximum voluntary joint torque as a function of joint angle and angular velocity: Model development and application to the lower limb”, *J. Biomech.*, vol. 40, no. 14, pp. 3105–3113, 2007, ISSN: 0021-9290. DOI: 10.1016/j.jbiomech.2007.03.022.
- [140] M. Bellman, “Control of cycling induced by functional electrical stimulation: A switched systems theory approach”, *Ph. D. dissertation*, 2015.
- [141] S. Einar, “Development of a mathematical model of a rider-tricycle system”, Technical report, Department of Engineering Cybernetics, NTNU, 1–7, Tech. Rep., 2002.
- [142] E. Ambrosini, J. Zajc, S. Ferrante, *et al.*, “A hybrid robotic system for arm training of stroke survivors: Concept and first evaluation”, *IEEE Trans. Biomed. Eng.*, vol. 66, no. 12, pp. 3290–3300, 2019.